

Copyright Undertaking

This thesis is protected by copyright, with all rights reserved.

By reading and using the thesis, the reader understands and agrees to the following terms:

1. The reader will abide by the rules and legal ordinances governing copyright regarding the use of the thesis.
2. The reader will use the thesis for the purpose of research or private study only and not for distribution or further reproduction or any other purpose.
3. The reader agrees to indemnify and hold the University harmless from and against any loss, damage, cost, liability or expenses arising from copyright infringement or unauthorized usage.

IMPORTANT

If you have reasons to believe that any materials in this thesis are deemed not suitable to be distributed in this form, or a copyright owner having difficulty with the material being included in our database, please contact lbsys@polyu.edu.hk providing details. The Library will look into your claim and consider taking remedial action upon receipt of the written requests.

**STUDY OF KNIT-BASED COMFORTABLE AND
SCALABLE SENSORS FOR HUMAN MOTION
MONITORING**

DONG SHANSHAN

PhD

The Hong Kong Polytechnic University

2025

The Hong Kong Polytechnic University

School of Fashion and Textiles

Study of Knit-based Comfortable and Scalable Sensors for
Human Motion Monitoring

DONG Shanshan

A thesis submitted in partial fulfilment of the requirements for
the degree of Doctor of Philosophy

December 2024

Certificate of Originality

I hereby declare that this thesis is my own work and that, to the best of my knowledge and belief, it reproduces no material previously published or written, nor material that has been accepted for the award of any other degree or diploma, except where due acknowledgement has been made in the text.

(Signed)

DONG Shanshan

(Name of student)

Abstract

In the current era, human motion monitoring is a crucial research area with profound implications, playing significant roles in healthcare, sports, and daily life. In healthcare, it facilitates disease diagnosis and rehabilitation progress monitoring by assessing patients' physical activity levels. In sports, it optimizes training regimens through analyzing athletes' movements. In daily life, it oversees individuals' well-being and activity patterns. Given its importance, there has been a remarkable increase in research on flexible sensors, aiming to overcome the limitations of traditional rigid sensors like poor adaptability to body contours and user discomfort. To address these issues, researchers are utilizing innovative materials and designs that can easily adapt to body movements and contours. Textile-based sensors, in particular, hold a prominent position in human motion sensing, mainly due to their comfort-oriented characteristics. However, there are still many challenges in current research. For example, the production process is often complex, there exists a persistent contradiction between achieving high sensitivity and maintaining comfort, and the associated costs remain relatively high. To address these hurdles, the present thesis focuses on leveraging knitting technology for the development of human motion sensors. Firstly, the knitted structure imparts the sensor with remarkable flexibility and softness. Concurrently, it not only facilitates direct customization but also enables seamless integration, thereby significantly enhancing the practicality and comfort levels of the sensor. Additionally, advanced knitting machines are capable of realizing intricate sensor structures by integrating yarns possessing diverse functions in multifarious ways. This, in turn, augments the diversity and flexibility in the design process. Furthermore, the well-established knitting technology plays a pivotal role in promoting the scale expansion of flexible sensors as well as in reducing their production costs. Collectively, these distinctive characteristics firmly establish the importance and necessity of developing knitted-based sensors. In this research, three distinct types of knitted-based sensors have been successfully developed.

First, a soft, warm, and mass-producible triboelectric carpet fabric is developed for motion posture monitoring and user recognition. A specially prepared conductive chenille yarn consisting of core-Ag-coated nylon filaments and shell-acrylic staple fibers is used as the main raw material. And knitting weft insertion technology is employed to bundle conductive chenille yarns in 1×1 rib courses formed by nylon elastic yarns to make the chenille TENG carpet fabric. The chenille TENG fabric, which exhibits flexibility, warmth, low cost, ease of manufacturing, and compatibility with the living environment, has demonstrated a maximum power density of approximately $2942\text{ }\mu\text{W}/\text{m}^2$ in the contact-separation mode. Through simple circuit management for energy harvesting, it is capable of powering small electronic devices. Moreover, with the assistance of machine learning, the chenille TENG can be applied to behavior recognition and user identification. After training the time-current data, four distinct behaviors, namely slow walking, regular walking, jogging, and jumping, have been successfully classified, and four different subjects have been recognized. This carpet fabric thus shows significant potential in smart monitoring systems for home security, owing to its aforementioned properties and capabilities.

In the second work, an innovative method for efficiently manufacturing flexible sensing fabrics is proposed, leveraging three-thread fleecy knitting technology. This approach achieves a relatively high production rate of around $11.53\text{ m}^2/\text{h}$. The produced fleecy sensing fabric functions as a triboelectric nanogenerator, capable of generating electrical signals and attaining a peak power density of about $2446\text{ }\mu\text{W}/\text{m}^2$ upon rubbing against cotton fabric. Composed entirely of commercially available yarn materials, the fabric possesses outstanding flexibility, plumpness, and breathability. Remarkably, it maintains stable output performance even after undergoing multiple machine wash cycles. This fabric can be freely cut and tailored into self-powered flexible sensors for various applications, including insoles for movement pattern monitoring and carpets for movement posture tracking. With the reinforcement of machine learning algorithms,

the fleecy sensing fabric exhibits strong recognition capabilities. The combination of these features creates opportunities for the development of flexible sensors that are cost-efficient, comfortable, and widely applicable, thus expanding their potential for practical use in a wide range of scenarios.

The third work introduces a novel auxetic braided strain yarn sensor (ABSYS) capable of achieving industrialized automatic production. The highly stretchable ABSYS is constructed by wrapping rigid conductive multifilament and highly elastic nylon/spandex-covered yarn around an elastic core yarn in a mesh pattern using a circular braiding machine. It exhibits a pronounced auxetic effect and exceptional sensing performance, including good structural stability, a wide working range, and high sensitivity. Based on the developed ABSYS, a highly stretchable sensing fabric is created by seamlessly integrating it into rib fabric using knitting technology. The fabric demonstrates a broad working range of 2% to 60%, a rapid response time of 0.018 s, and dependable stability, effectively addressing the majority of human motion sensing requirements. This type of sensor enables effective motion monitoring through reliable bending detection at various joints, all while maintaining wearing comfort and aesthetics. This work offers a promising new approach for strain-sensing fibers and fabrics in wearable applications.

List of Publications

Related Journal Publications

1. **Dong S**, Ju Z, Yao P, Liu Y, Xu B, Hu H. Flexible and Freely Cuttable Fleecy Triboelectric Fabrics for Ultra-High Scalability in Self-Powered Sensing Applications. *Applied Materials Today*, 2025, 42, 102569.
2. **Dong S**, Yao P, Ju Z, Sheng Y, Xu B, Liu Y, Hu H. Conductive chenille yarn-based triboelectric carpet fabrics with enhanced flexibility and comfort for smart home monitoring. *Materials Today Energy*, 2024, 41, 101527.
3. Tian X, **Dong S**, Yang M, Ng H, Liu Y, Hu H, Hua T. Textile-Based Triboelectric Nanogenerators for Smart Wearable Systems: Comfort, Integration, and Application. *Advanced Materials Technologies*, 2023, 8(8), 2201294.

Other Journal Publications

1. **Dong S**, Hu H. Sensors based on auxetic materials and structures: A review. *Materials*, 2023, 16(9), 3603.
2. Ju Z, **Dong S**, Lau W, Liu Y, Hu H. Comfort properties of PLA/cotton multilayered quilted fabrics. *Textile Research Journal*, 2024, 00405175241282033.
3. Tian X, Niu B, Hua T, Yang M, Yang Y, **Dong S**. Continuous Fabrication of a Highly Integrated, User-Friendly, and Low-Cost Triboelectric Yarn/Fabric for Diverse Sensing Applications. *ACS Sustainable Chemistry & Engineering*, 2023, 11(45), 16087-16097.

Paper in Preparation

Dong S, Ju Z, Liu Y, Xu B, Hu H. Highly Stretchable and Structurally Stable Auxetic Braided Strain Yarn Sensor for Wearable Motion Monitoring.

Conference Presentations

Oral presentation

Shanshan Dong, Hong Hu, “The value of traditional knitting technology in intelligent wearable system”, **The competition for the Outstanding Study Award of International Conference on Intelligent Wearable Systems (ICIWS 2022)**, June 22, 2022, The Hong Kong Polytechnic University, Hong Kong SAR, China.

Poster presentation

1. **Shanshan Dong**, Pengpeng Yao, Zixin Ju, Yanping Liu, Hong Hu, “Self-powered Chenille Carpet for Smart Home Monitoring and Security Systems”, **PAIR Conference 2023: Research Excellence for Societal Impacts**, May 10, 2023, The Hong Kong Polytechnic University, Hong Kong SAR, China.
2. **Shanshan Dong**, Pengpeng Yao, Zixin Ju, Yilan Sheng, Yanping Liu, Hong Hu, “Comfortable, Warm and Appearance Compatible Triboelectric Chenille Carpet for Smart Home Monitoring and Security Systems”, **2024 European Materials Research Society (E-MRS) Spring Meeting**, May 27, 2024, Convention and Exhibition Centre of Strasbourg, France.

Acknowledgements

As my doctoral journey nears its end, when I look back on the past, my heart is filled with profound gratitude.

First and foremost, I would like to express my heartfelt appreciation to my supervisor, Professor Hu Hong. Over the past three years, Professor Hu Hong consistently provided me with unwavering support, profound inspiration, and tremendous encouragement. Under his meticulous guidance, I have not only acquired a broader range of scientific knowledge and rich research experience but also gained invaluable growth in aspects such as planning, thinking, communication, and self-adjustment. These assets will benefit me throughout my life.

Simultaneously, I am deeply grateful to my co-supervisors, Professor Liu Yanping and Professor Xu Bingang. They offered me substantial support and supervision during the research process, helping me progress steadily. Additionally, Professor Hua Tao provided me with strong support in research equipment, laying a solid foundation for my research work. I hereby express my sincere gratitude to him.

I also want to thank the members of Professor Hu's research group, Ms. Ju Zixin, Dr. Chang Yuping, Dr. Zhang Minglonghai, Mr. Li Keda, Mr. Li Zhenyu, Mr. Tu Yuecheng, as well as my collaborators, Dr. Yao Pengpeng, Dr. Tian Xiao, Dr. Yang Mengyan, and Miss Sheng Yilan. During my doctoral studies, they assisted me a lot in both my life and research.

Furthermore, I would like to extend my sincere thanks to all the research technicians and administrative staff at the School of Fashion and Textiles and the UMF - Materials Research Centre of The Hong Kong Polytechnic University. The help they provided has created an excellent environment for my study and research.

Most importantly, I want to convey my deepest gratitude to my family. They have always given me unconditional love and support, serving as the most solid backing on my journey. At the same time, I am thankful to my friends. Their companionship and care have brought me endless joy and warmth during my postgraduate years.

Table of Contents

Certificate of Originality	I
Abstract.....	II
List of Publications	V
Acknowledgements	VII
List of Figures.....	XIII
List of Tables	XX
List of Abbreviations	XXI
Chapter 1: Introduction	1
1.1 Background and Challenges.....	1
1.2 Research Objectives	2
1.3 Research Methodology.....	3
1.4 Research Significance	5
1.5 Outline of the Thesis	6
Chapter 2: Literature Review.....	8
2.1 Comfortability of Textiles.....	8
2.1.1 Sensorial and tactile comfort and evaluation methods	9
2.1.2 Fit comfort and evaluation methods	10
2.1.3 Heat-moisture comfort and evaluation methods.....	12
2.1.4 Aesthetics.....	13
2.2 Textile-based Flexible Sensors	14
2.2.1 Textile-based triboelectric sensor.....	15
2.2.2 Textile-based resistive sensor	24

2.2.3 Textile-based piezoelectric sensor	28
2.2.4 Textile-based capacitive sensor	32
2.2.5 Textile-based hybrid mode sensor	35
2.3 Application of Textile-based Sensors	36
2.3.1 Intelligent sports sensors	36
2.3.2 Motion capture in VR/AR	38
2.3.3 Biomonitoring sensors	39
2.4 Conclusion.....	42
References	43
Chapter 3: Conductive Chenille Yarn-based Triboelectric Carpet Fabrics for Smart Home Monitoring	57
3.1 Introduction	57
3.2 Experimental Section	58
3.2.1 Materials	58
3.2.2 Fabrication methods	59
3.2.3 Physical and electrical characterization.....	60
3.3 Results and Discussion.....	60
3.3.1 Design and fabrication of the C-TENG carpet fabric.....	60
3.3.2 Comfort performance of the C-TENG fabric	62
3.3.3 Working mechanism of the C-TENG fabric.....	65
3.3.4 Electrical performance of the C-TENG fabric	66
3.3.5 Sensing carpet for home security systems	69
3.4 Conclusion.....	73
References	75

Chapter 4: Flexible and Freely Cuttable Fleecy Triboelectric Fabrics for Ultra-High Scalability in Self-Powered Sensing Applications79

4.1 Introduction	79
4.2 Experimental Section	81
4.2.1 Materials	81
4.2.2 Fabrication methods	81
4.2.3 Characterization and testing	81
4.3 Results and Discussion.....	82
4.3.1 Structural features and fabrication process of the fleecy TENG fabric.....	82
4.3.2 Basic parameters and physical properties.....	84
4.3.3 Working mechanism of the fleecy TENG fabric.....	88
4.3.4 Output performance of the fleecy TENG fabric	89
4.3.5 Applications of the fleecy TENG fabric.....	93
4.4 Conclusion.....	95
References	97

Chapter 5: Highly Stretchable and Structurally Stable Auxetic Braided Yarn based Sensor for Motion Monitoring102

5.1 Introduction	102
5.2 Experimental Section	104
5.2.1 Materials	104
5.2.2 Fabrication methods	104
5.2.3 Characterization and testing	105
5.3 Results and Discussion.....	105
5.3.1 Structure design and working mechanism of the ABSYS.....	105
5.3.2 Fabrication of the ABSYS	107

5.3.3 Auxetic performance of ABSYSs.....	112
5.3.4 Strain sensing capabilities of ABSYSs.....	115
5.3.5 Fabrication and characterization of ABSYS-based knitted sensors	117
5.3.6 Application demonstration of motion monitoring	120
5.4 Conclusion.....	121
References	123
Chapter 6: Conclusions and Outlook.....	127
6.1 Conclusions	127
6.1 Outlook.....	129

List of Figures

Figure 1.1 Flowchart of the overall methodology.....	3
Figure 2.1 Schematic illustration of the human microclimate.	13
Figure 2.2 Working mechanism of the t-TENG sensor. (a) Triboelectric propensity of some common textile materials. (b) Working principle of the contact-separation mode TENG. (c) The output signal curve under cyclic compression-release.	16
Figure 2.3 Various typical St-TENGs. (a) A yarn-based TENG strain sensor with multigradient hierarchical structure and (b) its high elasticity and flexibility. (c) Structural design of a coaxial fiber optic sensor and (d) its high stretchability. (e) High-performance wearable t-TENG with oblique microrod array structure. (f) Hydrophobic layered composite t-TENG. (g) Topologically optimized droplet energy harvesting fabric. (h) TENG based on 3D weft-knitted spacer fabric. (i) Enhanced 3D spacer fabric-based TENG with many pyramids on the surface...	19
Figure 2.4 Various typical Pt-TENGs. (a) Core-shell yarn consisting of a conductive fiber core and a standard textile fiber sheath and (b) flexible TENG textiles made from such core-shell yarns. (c) Energy-harvesting textiles made by weaving or embroidering TENG core-shell yarns and (d) various patterns achieved by this technology. (e) Tubular TENG fabric made from braided core-shell yarns and (f) knitted pants with seamless integration of this sensing fabric.	21
Figure 2.5 TENG sensing fabrics realized by special fabric structures. (a) TENG based on knitted spacer fabric structure. (b) Triboelectric all-textile sensor array (TATSA) formed by full cardigan stitch. (c) TATSA samples in various colors. (d) TATSA integrated into clothing to monitor pulse and breathing signals. (e) TENG fabric realized by knitting plating technique and (f) its excellent flexibility.....	23
Figure 2.6 Fiber/yarn-based resistive sensors. (a) A MXene/PU composite fiber sensor prepared by scalable wet spinning technology and (b) a coaxial wet spinning method for manufacturing sheath/core fibers composed of pure PU fiber core wrapped with MXene shell. (c) A strain sensor developed by coating CNT ink onto	

PU yarn using expansion and ultrasonic processes. (d) A flexible strain sensor made by uniformly adhering graphene to the surface of polyurethane multifilament using polyvinyl alcohol. (e) Full-fiber auxetic-interlaced yarn sensor (AIYS) and its (f) obvious auxetic effect. (g) AIYS used to recognize 26 letters.	26
Figure 2.7 Fabric-based resistive sensors. (a) Fabrication of a stretchable resistive sensor by high temperature carbonization of silk fabric. (b) 3D spacer fabrics for improving the sensitivity of carbonized fabric sensors. (c) A method for producing scalable, highly conductive and elastic PU/PEDOT: PSS composite fibers. (d) A flexible strain sensor formed by embedding acrylic/copper double-coated conductive yarns into the rib fabric.	27
Figure 2.8 Working principle of t-PENG.	29
Figure 2.9 Fiber/yarn-based PENGs. (a) PENG composite yarn created using simple wrapping and coating techniques. (b) PVDF-TrFE electrospun strips twisted into highly stretchable yarn sensors. (c) PENG yarn developed using electrospinning and braiding techniques and (d) such yarn used in clothing to detect human motion.	30
Figure 2.10 Fabric-based PENGs. (a) Graphene/PVDF coated fabric and (b) its sensing performance. (c) 3D spacer fabric for improving the piezoelectric properties of PVDF film. (d) A new method for producing multiple bundles of PVDF nanofibers simultaneously using 50 nozzles and the subsequent development process of PVDF yarn and fabrics.....	32
Figure 2.11 Textile-based capacitive sensors. (a) A flexible plate capacitor with an internal surface structure using fabric as substrate, conductive rubber as electrode layer, and PDMS as dielectric layer and (b) the state of the sensor when compressed. (c) Fabric capacitive sensor prepared using thermal bonding electrical connection method and (d) laser cutting process for customizing individual sensors. (e) A capacitive pressure sensor designed by interweaving core conductive core-spun yarn and (f) its photo. (g) A helical auxetic yarn capacitive sensor.....	34
Figure 2.12 Textile-based hybrid mode sensors. (a) Preparation process of copper core	

PENG yarn and spring core TENG yarn and (b) 3D interlocking parallel structure of hybrid triboelectric/piezoelectric fabric. (c) All-textile capacitive pressure sensor made of piezoelectric P (VDF-TrFE) nanofiber membrane as dielectric layer and conductive fabric as electrode. (d) Preparation process and structure of a three-layer core-sheath structured resistive/capacitive hybrid response optical fiber.36

Figure 2.13 Textile-based sensors for sports monitoring. (a) Smart sensing insole and (b) its gait monitoring curves. (c) Schematic illustration of a t-TENG and piezoelectric chip hybrid sensing sock. (d) Resistive and capacitive fabric sensor array for monitoring Taekwondo movements.37

Figure 2.14 Textile-based sensors for VR/AR applications. (a) Schematic diagram of the structure of a coated superhydrophobic triboelectric textile and (b) the CNN model used for training and (c) its application in virtual pitching. (d) Schematic diagram of the gesture recognition gloves and (e) the sign language recognition and communication demonstration in virtual space. (f) Auxetic strain sensing yarn for sign language recognition.39

Figure 2.15 Textile-based sensors for vital signs monitoring. (a) PEDOT-TPU composite fiber used to measure skin temperature and (b) its sensitivity performance. (b) Schematic structure of the multilayered t-TENG and the picture of using a mobile phone to display pulse monitoring data in real time. (c) Schematic illustration of the enlarged view of the knitted sensor and its application to monitor pulse and respiratory signals in real time.40

Figure 3.1 Preparation of the conductive chenille yarn and C-TENG. (a) Schematic diagram of the fabrication process. (b) Picture of the chenille spinning machine. (c) Schematic diagram of the blade device. SEM images of (d) Ag-plated nylon yarn, (e) acrylic yarn, and (f) elastic nylon yarn. (g) Enlarged photo of the conductive chenille yarn. (h) Photo of the C-TENG carpet fabric being knitted on the flat knitting machine. (i) Side view and (j) top view of the C-TENG fabric. (k) Enlarged photo of the fabric surface.61

Figure 3.2 Photos of three conventional carpet fabrics. (a) Coral velvet fabric. (b) Striped felt fabric. (c) Tufted fabric.	63
Figure 3.3 Comparison of the hand feel properties of four fabrics. (a) Softness, fluffiness, and fullness. (b) Warp surface characteristics. (c) Weft surface characteristics.....	65
Figure 3.4 Working mechanism of the C-TENG.	66
Figure 3.5 Electrical Output of the C-TENG rubbed against a PE fabric. (a) Output voltage and (b) current at different frequencies under the force of 200N. (c) Output voltage and (d) current with different forces at a frequency of 3 Hz.....	67
Figure 3.6 Electrical performance of the C-TENG. (a) Output voltage and power density of the C-TENG under different external resistances under 200N and 3 Hz. (b) Output voltage of the C-TENG with different contact materials under 200N and 3Hz.	68
Figure 3.7 Stability and durability of the C-TENG. (a) Long-term current output of the C-TENG under 200 N and 3 Hz. (b) Output voltage of the C-TENG under 200N and 3 Hz after washing.	69
Figure 3.8 The C-TENG carpet fabric and its output under different motions and subjects. (a) Photos of the carpet fabric being rolled and folded. (b) Electrical signals produced when walking on the carpet. (c) Characteristics of the current signals under four behaviors (slow walking, walking, jogging, and jumping). (d) Photos of four subjects standing on the carpet and the current signals generated by them. (e) Photos of soles and socks made of different materials and the current signals they generate.	70
Figure 3.9 Motion behavior recognition and individual identification. (a) Schematic flowchart of the machine learning method. (b) Classification results of motion behavior recognition. (c) Classification results of individual identification. (d) Classification results for different sole and sock materials.	72
Figure 3.10 Applications of the C-TENG carpet in smart home security systems.	73
Figure 4.1 Fabrication of the fleecy TENG fabric. (a) Schematic diagram of the fleecy	

<p>fabric structure. (b) Photos of the three-thread fleecy machine and its knitting work area. (c) Enlarged photo of the fleecy side. SEM images of (d) acrylic yarn and (e) single fiber. Enlarged photos of (f) substrate side surface and (g) cross side. (h) SEM image of Ag-plated nylon multifilament.....</p>	84
<p>Figure 4.2 Photos of three fleecy fabrics. (a) Fleecy TENG fabric. (b) Commercial fabric 1. (c) Commercial fabric.....</p>	85
<p>Figure 4.3 Results of KES compression and bending tests. (a) Wale bending curves and (b) course bending curves. (c) Load-displacement curves under compression. (d) Capability comparison radar chart of the hand-feel attributes of the three fabrics.</p>	87
<p>Figure 4.4 Working mechanism of the fleecy TENG fabric. (I) Initial Contact. (II) Separation in Progress. (III) Equilibrium State of Separation. (IV) Reapproaching Phase.</p>	88
<p>Figure 4.5 Electrical output of the fleecy TENG fabric rubbed against a cotton fabric. (a) Output voltage and (b) current at different frequencies under a compression force of 200 N. (c) Output voltage and (d) current under different compression forces at a frequency of 3 Hz.</p>	90
<p>Figure 4.6 Electrical performance of the fleecy TENG fabric. (a) Output voltage and power density under different external resistances under 200 N and 3 Hz. (b) Output voltage with different contact materials under 200 N and 3Hz.</p>	91
<p>Figure 4.7 Photos of different knitted fabrics used for rubbing against the fleecy TENG fabric. (a) Polyethylene fabric. (b) Cotton fabric. (c) Nylon fabric. (d) Polyester fabric.</p>	91
<p>Figure 4.8 Stability and durability of the fleecy TENG fabric. (a) Current output under 10,000 contact-separation cycles at 200 N and 3 Hz. (b) Output voltage under 200 N and 3 Hz after different washing times.</p>	92
<p>Figure 4.9 SEM images of fleecy TENG fabric before and after washing. (a) Unwashed. (b) Washed once. (c) Washed three times.</p>	93
<p>Figure 4.10 Application demonstration of the fleecy TENG fabric. (a) Circuit diagram</p>	

for charging a capacitor. (b) Curves for charging commercial capacitors of various specifications. (c) A pair of insoles made from fleecy TENG fabric and (d) sports shoes with smart insoles placed. (e) Differential signals output under three motions: tiptoeing, walking, and jumping. (f) Recognition and classification results of three motions based on deep learning.	95
Figure 5.1 Structure of the ABSYS and cross-section of the conductive multifilament: (a) at the initial state; (b) under extrusion in the first stage; (c) under extension in the second stage.	107
Figure 5.2 Fabrication process of the ABSYS. (a) Yarn configuration on the circular braiding machine. (b) Schematic diagram of the mechanism responsible for forming the braided structure.	108
Figure 5.3 Tensile properties of three component yarns. (a) Stress-strain curves of conductive yarn and wrap yarn. (b) Stress-strain curves of elastic core yarns with different diameters.	110
Figure 5.4 Photos of a sample at different strains during stretching.	113
Figure 5.5 Tensile Poisson's ratio of all samples at different strains. (a) Strain-Poisson's ratio curves of ABSYS samples with one conductive yarn. (b) Comparison with ABSYS samples with two conductive yarns. (c) Comparison with samples without wrap network.	114
Figure 5.6 $\Delta R/R_0$ -strain curves of all samples within a large strain range of 60%. (a) ABSYS samples with one conductive yarn. (b) Comparison with ABSYS samples with two conductive yarns. (c) Comparison with samples without wrap network.	115
Figure 5.7 Sensing Performance of the C3-A Sample. (a) Gauge factor at different strains. (b) $\Delta R/R_0$ -time curves at 2%, 5%, 10% strains with 200 mm/min tensile speed. (c) $\Delta R/R_0$ -time curves at 20%, 40%, 60% strains with 200 mm/min tensile speed. (d) $\Delta R/R_0$ -time curves at different tensile speeds with 40% strain.	117
Figure 5.8 Sensing Performance of the ABSYS-based knitted sensor. (a) Photograph of the knitted sensor. (b) $\Delta R/R_0$ -time curves for the knitted sensor under strain	

levels of 1%, 2%, 5%, and 10% at a tensile speed of 200 mm/min. (c) $\Delta R/R_0$ -time curves for the knitted sensor under strain levels of 20%, 40%, and 60% at a tensile speed of 200 mm/min.....	118
Figure 5.9 Response time measurement of the ABSYS-based knitted sensor.	119
Figure 5.10 Durability of the ABSYS-based knitted sensor. (a) Comparison of the resistance response of the knitted sensor at 1% strain before and after washing. (b) Comparison of the resistance response at 60% strain before and after washing. (c) Resistance response at 40% strain over 3000 stretch-recovery cycles.	120
Figure 5.11 Elbow and finger sleeves responding to various joint bending movements. (a) Photograph of the elbow sleeve. (b) Resistance response signals of the elbow joint at different bending degrees. (c) Photograph of the finger sleeve. (d) Resistance response signals of the finger at different bending degrees. (e) Resistance response signals of the elbow joint at varying bending speeds. (f) Resistance response signals of the finger at varying bending speeds.	121

List of Tables

Table 3.1 Basic parameters and physical properties of the C-TENG fabric and three conventional carpet fabrics.	63
Table 3.2 Comparison of comfort parameters of four fabrics.	64
Table 3.3 Information about four subjects involved in individual identification.	71
Table 4.1 Basic parameters and breathability properties of three fabrics.	85
Table 4.2 Comparison of comfort parameters of three fabrics.	87
Table 5.1 Details of three composing yarns.	109
Table 5.2 Details of various ABSYS samples.	111

List of Abbreviations

3D	Three-dimensional
KES	Kawabata evaluation system
TENG	Triboelectric nanogenerator
t-TENG	Textile-based TENG
St-TENG	Semi-textile structure TENG
Pt-TENG	Pure textile structure TENG
PU	Polyurethane
PDMS	Polydimethylsiloxane
PNG	Fiber nanogenerator
AgNW	Silver nanowire
PTFE	Polytetrafluoroethylene
PET	Polyethylene terephthalate
EHT	Energy harvesting textile
TATSA	Triboelectric all-textile sensor array
1D	One-dimensional
GF	Gauge factor
CNT	Carbon nanotube
AIYS	Auxetic-interlaced yarn sensor
PEDOT	Poly(3,4-ethylenedioxythiophene)
PSS	Poly(styrene sulfonate)
PENG	Piezoelectric nanogenerator
PVDF	Polyvinylidene fluoride
TrFE	Trifluoroethylene
VR	Virtual reality
AR	Augmented reality
TPU	Thermoplastic urethane
Ag-plated	Silver-plated

C-TENG	Chenille TENG
PE	Polyethylene
PET	Polyester
ABSYS	Auxetic braided strain yarn sensor

Chapter 1: Introduction

1.1 Background and Challenges

In recent years, the rapid development and integration of new material technologies, Internet technology, and artificial intelligence have sparked a surge in research on various smart products, including smart wearable devices, smart interactive devices, and simulation robots. As developers and users of these smart products, humans are increasingly prioritizing the portability and comfort of these products, leading to a growing demand for flexible smart products. Consequently, the development of flexible sensors widely applied in smart products has emerged as a key research focus. Flexible sensors, made of materials with good flexibility, ductility, and fit, have garnered attention due to their versatility in various usage scenarios. For instance, flexible fiber strain sensors can be integrated into clothing for health monitoring by capturing body movements, breathing, and pulse, and can also be incorporated into gloves for gesture recognition in sign language interaction. When combined with signal transmission, intelligent analysis, and display equipment, flexible sensors enable the creation of remote, efficient, and precise intelligent monitoring or interactive systems. In summary, flexible sensors play a crucial role in sports health, medical monitoring, artificial intelligence, human-computer interaction, and other fields.

A large number of bendable, stretchable, and even implantable flexible sensing devices have been reported for smart wearable applications. The preparation of flexible sensors typically involves the addition of conductive functional materials onto flexible substrates through coating, adhesion, chemical deposition, and other methods. Conductive fibers, carbon-based materials, and metal particles are commonly used as conductive materials, while polymer films, foams, gels, and textiles are the primary substrates for flexible sensing devices. Among them, textile-based flexible sensors stand out in the wearable field due to the natural properties of textiles such as softness,

breathability, stretchability, washability, and wear resistance. They can be integrated into clothing, home textiles, and medical rehabilitation products for application.

However, the main challenges at present are simple and efficient expansion methods and solving the contradiction between high comfort and sensitivity. Most sensors involve raw material preparation and equipment integration processes in the laboratory stage, which are cumbersome and costly and are not suitable for commercial expansion. In addition, the functional materials used to improve sensitivity usually affect the wearing comfort of the device.

Considering the above, an economical and efficient method is highly desired to develop comfortable and highly sensitive textile sensors. This goal can be achieved through the cooperation of material selection, structural design and preparation process. Knitting technology can transform a yarn into a piece of fabric, which is simple, efficient, and versatile compared to weaving technology. Moreover, with the development of advanced knitting machines, three-dimensional (3D) fabrics of various structures have been easily realized. Knitting technology shows great potential in the development of flexible or wearable sensors. This study will develop flexible sensors based on knitting technology for human motion monitoring.

1.2 Research Objectives

To address the challenges mentioned, this study focuses on developing scalable sensors with excellent flexibility and comfort for human motion monitoring by utilizing pure fiber materials and convenient knitting technology. Given the inherent complexity and diversity of human kinematics, we will design and develop three complementary sensors to accommodate distinct motion patterns and application scenarios. The specific objectives of this research are as follows:

1. To develop flexible chenille carpet-based sensors through innovative fancy spinning and weft inlay techniques, enabling continuous ground-contact motion monitoring while preserving intrinsic tactile comfort and aesthetic appeal of conventional floor coverings.
2. To develop cost-effective fleecy fabric sensors by leveraging commercially available yarn materials and industrialized three-thread fleecy knitting technology, achieving the monitoring of multimodal human motion involving contact interfaces.
3. To develop high-performance strain-sensing fabrics through scalable braiding and precise weft inlay integration, creating wearable systems with wide strain-range capability, enhanced sensitivity, and exceptional stability for monitoring complex joint motions during dynamic activities including gait and gesture.

1.3 Research Methodology

To accomplish the research objectives, this study will develop three distinct knit-based sensors utilizing different yarn materials and fabrication techniques, each optimized for specific human motion monitoring applications. The experimental methodology is systematically outlined in the flowchart presented in Figure 1.1.

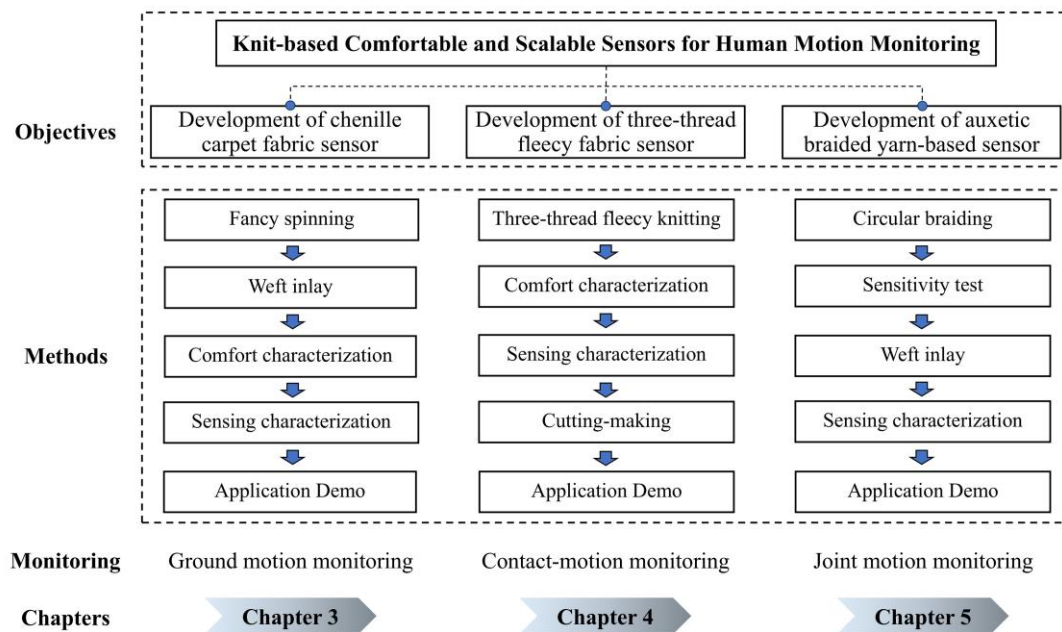


Figure 1.1 Flowchart of the overall methodology.

M1. Design and Preparation of Triboelectric Chenille Carpet Fabrics: Initially, fancy spinning technology will be used to produce core conductive chenille yarns, where the conductive core will serve as the electrode and the outer pile will act as the primary triboelectric material. Subsequently, the fabric will be created by integrating the chenille yarn with a knitted elastic ribbed base, enhancing its application potential while maintaining flexibility and comfort.

M2. Design and Preparation of Fleecy Triboelectric Fabrics: This will involve using three-thread fleecy knitting technology to develop triboelectric fabrics, with the three yarns designated for the top friction layer, the middle electrode layer, and the bottom substrate layer, respectively. The use of commercially available yarns will facilitate ultra-high production efficiency and comfort comparable to traditional fabrics. The fabric will be further adapted for multiple uses through free cutting and potential subsequent processing.

M3. Design and Preparation of Resistive Auxetic Strain Sensing Yarns and Sensing Fabrics: A sensing yarn with an auxetic structure will be developed using circular braiding technology. This structure will include three components: an elastic core yarn with excellent stretch and recovery properties, a conductive multifilament for resistance sensing, and a braided layer formed by fine elastic wrap yarns for high structural stability. The auxetic sensing yarns will be seamlessly embedded into fabrics through advanced knitting technology to form fabric sensors.

M4. Characterization and Applications of Prepared Sensing Yarns and Fabrics: Initially, the physical properties and comfort of the prepared sensing textiles will be assessed through mechanical tests. Subsequently, the sensing performance of all sensors, including their sensitivity and stability, will be tested. Furthermore, machine learning or deep learning technology will be employed to facilitate monitoring and recognition

functions across various application scenarios.

1.4 Research Significance

This study explores the feasibility of creating comfortable and cost-effective textile-based sensors using various commercial textile raw materials and knitting technology. It opens new avenues for smart textiles, enabling the production of sensing fabrics that are both comfortable and functional. The three sensors developed in this research demonstrate versatile application capabilities across different scenarios.

Firstly, these sensors are constructed from pure commercial yarns without the need for additional chemical treatments or rigid components. By utilizing readily available textile materials, the sensors maintain a high level of comfort, safety, and durability. The absence of chemical treatments not only reduces potential health risks but also aligns with environmentally sustainable practices. Moreover, the use of flexible textile yarns ensures that these sensors can be seamlessly integrated into existing textile products without compromising their inherent properties. This integration capability is crucial for the development of smart textiles, as it allows for the creation of multifunctional fabrics that retain the look and feel of traditional textiles while providing advanced sensing capabilities. The ease of integration also facilitates the adoption of these sensors in a wide range of applications, from health monitoring and sportswear to industrial safety and beyond.

Secondly, the manufacturing process employs well-established textile industrial technologies, particularly knitting. Knitting technology allows for the creation of fabrics with complex structures and diverse patterns, providing significant flexibility in sensor design. This flexibility enables customization to meet a wide range of application needs, and the performance of textile sensors can be enhanced through innovative structural designs. Additionally, knitting technology excels at integrating multiple functions within a single fabric. It facilitates the incorporation of conductive fibers,

sensing elements, and other smart materials seamlessly. The entire preparation process is scalable and continuous, eliminating the need for complex processing steps. Knitting technology is already widely used in the textile industry, and its application in producing textile sensors can significantly reduce the costs associated with developing and manufacturing motion monitoring sensors. This cost reduction not only makes large-scale production economically feasible but also promotes the widespread adoption and use of these sensors.

This study further advances the field by integrating various knitted sensors with machine learning techniques to achieve reliable human motion recognition. Owing to the simplified and broadly applicable raw materials and preparation processes, this knit-based approach shows great promise for the future development of smart textile devices and smart sensing systems.

1.5 Outline of the Thesis

This thesis is organized as follows:

Chapter 1 provides an overview of the research background on flexible sensors, highlighting the benefits of textile-based sensors and identifying current challenges in the field. It outlines the study's objectives, methodologies, and the specific issues it aims to address.

Chapter 2 reviews recent advancements in textile-based sensors, categorizing them into types including triboelectric, resistive, piezoelectric, capacitive, and hybrid, and discusses their various applications.

Chapter 3 elaborates on the fabrication process of chenille triboelectric nanogenerator carpet fabric. Initially, core conductive chenille yarn is produced using advanced fancy spinning technique. This yarn is subsequently employed as weft inlay yarn to create

carpet fabric through knitting technology, specifically designed for monitoring human motion. This carpet fabric not only generates energy to power small electronic devices through straightforward circuit management but also facilitates behavior recognition and user identification with the assistance of machine learning. Moreover, the carpet fabric is characterized by its softness, warmth, cost-effectiveness, and mass-producibility, as well as its compatibility with living environments, making it exceptionally well-suited for home security smart monitoring systems.

In Chapter 4, the emphasis is placed on attaining an ultra-high production efficiency of flexible sensing fabrics via the utilization of three-thread fleecy knitting technology. The fabric, which is wholly fabricated from commercially obtainable yarn materials, demonstrates outstanding pliability, plumpness, and air permeability. It sustains stable performance even subsequent to undergoing multiple machine wash cycles. This fabric can be conveniently cut and tailored to form self-powered flexible sensors for a variety of applications, for instance, being used as insoles for the surveillance of motion patterns and as carpets for tracing motion postures.

Chapter 5 introduces the development of a novel all-fiber auxetic braided strain yarn sensor and a sensing fabric based on it, which are suitable for industrialization and automation. The sensing fabric demonstrates excellent sensing capabilities without compromising comfort. It can be seamlessly integrated into clothing for motion monitoring using advanced knitting technology, offering a new approach to strain sensing in wearable applications.

Chapter 6 concludes the research project by summarizing the findings, acknowledging existing limitations, and discussing future directions for knit-based flexible sensors.

Chapter 2: Literature Review

Textile-based sensors have received extensive attention in recent years, especially in the fields of wearable devices and smart textiles. They are expected to have the comfort of textiles, including softness, breathability, lightness, and stretchability, as well as durability such as washability. Many different types of textile-based sensors have been developed, but most of them focus on sensing performance, and the indicators and evaluation methods for comfort are still unclear. Here, the comfort evaluation of textiles is briefly summarized and the status of mainstream textile-based sensors in recent years is introduced.

2.1 Comfortability of Textiles

As electronic and information technologies continue to advance and societal perceptions of these technologies evolve, wearable electronics and smart textiles with capabilities for communication, energy conversion, and electrical conduction have garnered significant interest. In today's fast-paced world, integrating the internet and artificial intelligence with wearable technology holds transformative potential, significantly enhancing efficiency and convenience in daily life [1,2]. Textiles have increasingly gained attention in energy and sensing applications due to their distinct advantages, such as being lightweight, breathable, flexible, and washable. Comfort is derived from a complex interplay of physical, sensory, and psychological experiences [3,4]. It heavily relies on individual subjective assessments and is influenced by various factors, including environmental conditions, personal state, and clothing attributes [5]. Numerous indicators assess clothing comfort, with evaluation methods categorized into subjective assessments and objective measurements. A comprehensive approach to evaluating fabric comfort combines both subjective and objective techniques [6]. Generally, the fundamental comfort attributes of clothing fabrics encompass sensory and tactile comfort, fit comfort, thermal and moisture comfort, and aesthetic appearance

[7-9].

2.1.1 Sensorial and tactile comfort and evaluation methods

Sensorial and tactile comfort in fabrics refers to the absence of discomfort or health risks from skin contact or prolonged exposure [10]. Fabric handle, a crucial measure of tactile comfort, includes attributes like thickness, stiffness, fluffiness, and smoothness, which are influenced by raw material specifications and manufacturing parameters [10,11]. Long-term exposure safety is also vital, with the clothing industry enforcing strict standards for skin contact and harmful substance content in fabrics [12,13].

Traditional fabrics are primarily produced through weaving or knitting technology, while nonwoven fabrics serve as fillers or composites not in direct skin contact. Yarn, the raw material for fabrics, significantly affects fabric handle [14]. For instance, thick yarns impart a heavy feel. Yarn properties, such as fiber type, fineness, and twist, complicate evaluations of fabric handle. Yarns are categorized into staple, continuous filament, and hybrid types based on fiber composition [15,16]. Staple yarns are spun from short fibers using various processes like ring or air spinning [15]. Continuous filaments include natural silk and artificial chemical filaments, with variations based on twist or elasticity [16]. Hybrid yarns mix short fibers and long filaments, such as common cotton-spandex core-spun yarn [15]. Generally, filament yarns, especially untwisted ones, produce smoother fabrics than spun staple yarns. High-twist yarns can create a wrinkled texture, often used for specific fabric styles [17]. Fabrics with elastic filaments or spandex-hybrid yarns tend to be softer and drape better.

Manufacturing processes also impact the hand feel of fabrics. Knitted fabrics, with loop structures, offer more stretch and flexibility than woven fabrics, which interlace warp and weft yarns. Parameters like density and texture significantly influence fabric handle [14]. High density typically results in tighter, stiffer fabrics. However, fabric textures

are varied and complex, lacking uniform rules. Improving sensory and tactile comfort depends on effectively designing and matching raw materials with manufacturing processes.

The Kawabata Evaluation System for Fabrics (KES-F) is the primary method for assessing fabric handle [18,19]. It includes instruments like tensile and shear tester, compression tester, bending tester, and friction tester to measure various indices [20]. The system evaluates primary handle attributes such as stiffness and fullness by testing mechanical and surface properties, then assesses comprehensive handle to reflect overall wearing comfort. The KES system categorizes fabric handle evaluation into measured mechanical properties, inferred primary handle, and systematically analyzed comprehensive handle. Additionally, fabric stiffness, bending length, and flexural rigidity are assessed using ASTM D1388 and BS 3356 standards.

The production of textile-based sensors involves conductive and electrical materials, such as nanoparticles, hard wires or threads, and thin films. The integration method of these materials with traditional fabrics is crucial for wearing comfort. By selecting appropriate materials, structural parameters, and production processes, the sensor's sensory comfort can be further improved.

2.1.2 Fit comfort and evaluation methods

Fit comfort in clothing pertains to the mechanical interaction between the fabric and human body, including skin pressure comfort and the adaptability of the fabric to the limbs during exercise [21,22]. The goal is to avoid restricting the wearer's normal movement. Clothing pressure is the perpendicular stress exerted by the fabric on the skin when worn, arising from the fabric's weight, tightness due to insufficient garment size, and interaction during joint movements [23]. Undersized garments or body movements can deform the fabric, increasing pressure. Thus, fabric extensibility is

crucial for pressure comfort during activity [24,25]. Weft knitted fabrics typically offer superior elasticity, making them ideal for intimate apparel to enhance comfort. Additionally, elastic yarns like spandex are often used in sportswear to improve fit comfort. While elastic fabrics enhance fit comfort, especially in sportswear, excessive extensibility is not always beneficial. Fabrics should have good elastic recovery and reliable durability, and provide stable pressure on the skin, which is beneficial to health [26]. Besides extensibility, clothing looseness-the space between fabric and skin-also affects fit comfort [27]. The body's three-dimensional shape requires varying looseness for different areas, influenced by fabric cut and garment design. High-quality clothing focuses on fit, while systems allowing consumer participation in 3D design can cater to diverse needs [28]. Fabric extensibility and looseness are complementary; as one increases, the other can decrease [22,29]. For instance, yoga clothes or sports tights require less looseness due to high fabric extensibility, while everyday garments like shirts and trousers need less extensibility and more looseness to maintain style and comfort.

Fit comfort evaluation involves subjective assessments and objective measurements [30]. Subjective evaluation involves participants rating comfort attributes like itching and compression, though results can be influenced by personal conditions and habits, making the data less directly usable. Objective measurements test the pressure garments exert on the skin in real-time, using methods like strain gauge sensors, air pressure measurement, pressure dummy testing, and virtual modeling [21,25,31-33]. A comprehensive fit comfort assessment combines both subjective and objective methods for reliable results.

For textile-based sensors, incorporating flexible, stretchable structures into apparel, especially sportswear, can maximize fit comfort.

2.1.3 Heat-moisture comfort and evaluation methods

Thermal comfort and humidity comfort are often assessed together due to their interrelated nature. Heat-moisture comfort is highly related to the microclimate (a thin air layer close to the skin within the garment, as shown in Figure 2.1), encompassing both thermal and humidity aspects [34]. This comfort results from a complex interplay of physical, mental, and sensory perceptions, heavily influenced by individual subjective feelings [35]. Factors such as environmental conditions (temperature, wind speed, and humidity), heat production of body, and clothing characteristics affect this comfort [36]. Clothing's primary role is to maintain heat and moisture balance in the microclimate across changing environments and activities to enhance comfort [37,38].

Thermal comfort is the state of feeling neither hot nor cold, achieved by maintaining the body's thermal balance. Heat transfer in the microclimate occurs through radiation, conduction, convection, and evaporation [39]. Body heat transfers to clothing and then to the environment. Fabrics, being porous, have complex heat transfer processes influenced by fiber structure, air content, porosity, moisture, and other factors [40-42]. Higher porosity aids heat transfer, while thicker fabrics reduce heat loss [41]. Thus, summer fabrics are typically light and porous for cooling, while winter fabrics often include air layers for insulation [43,44]. Thermal comfort is evaluated through indicators like thermal conductivity, insulation rate, and thermal resistance, with instruments such as thermal conductivity testers and thermal manikins [45-47]. ASTM-F1868 is used for assessing thermal resistance.

Moisture transfer in fabrics, crucial for thermal comfort, especially during sweating, involves several processes: water vapor diffusion, adsorption and condensation on fabric surfaces and fiber capillaries, liquid water absorption and transport, and evaporation [48,49]. Fabric moisture transfer varies with fiber types, production techniques, and structures [50,51]. For instance, cotton absorbs moisture well but dries

slowly, while polyester dries quickly but lacks hygroscopicity due to its molecular structure. Developing moisture-wicking and quick-drying fabrics focuses on altering fiber cross-sections, designing new multicomponent fibers, and creating special fabric structures [52-54]. Humidity comfort is assessed through air permeability, moisture resistance, and moisture permeability using instruments like air permeability testers and sweating fabric manikins [55-59]. Standards such as ASTM D737, ISO 9237, and GB/T 24218.15 evaluate air permeability, while GB/T 12704.1 or ASTM E96 assess water-vapor transmission. Absorption and quick-drying properties are evaluated by GB/T 21655.

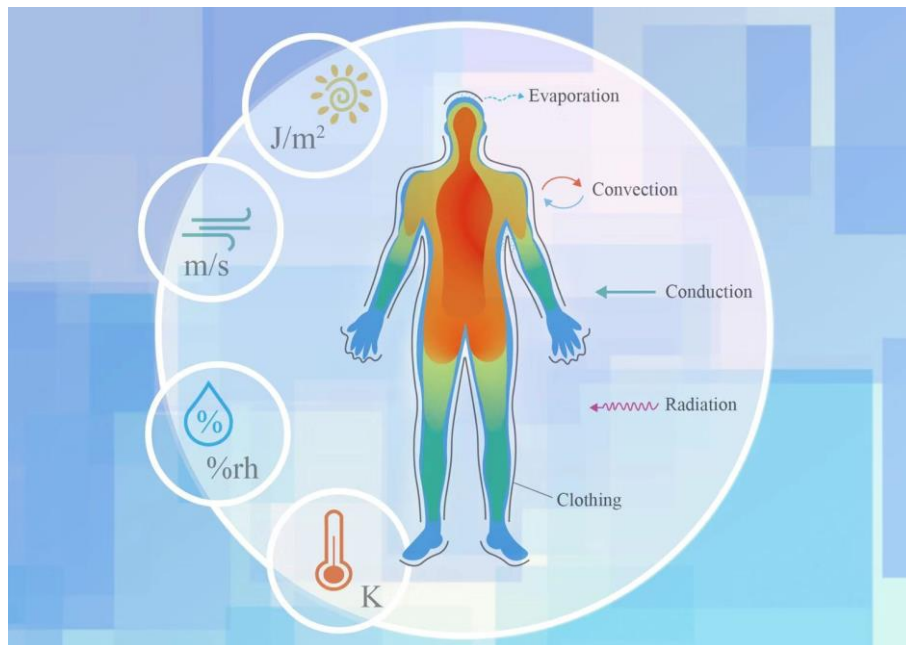


Figure 2.1 Schematic illustration of the human microclimate.

2.1.4 Aesthetics

With evolving lifestyles and mindsets, clothing appearance significantly influences consumer choices [60]. The most immediate and striking aesthetic element is the use of vibrant colors and patterns. Generally, colorful fabrics are created in three ways. First, solid colors or patterns are applied to semi-bleached (natural or white) fabrics through techniques like dyeing and printing [61,62]. Second, dyed yarns are used to produce

patterned fabrics directly through jacquard knitting and weaving [63]. Third, intricate patterns are crafted on embroidery machines or through hand embroidery [64].

The second element of visual aesthetics involves the texture and geometric structure on the surface of fabric. Variations in yarn structure and manufacturing parameters yield diverse textures. For instance, filament yarns tend to create a transparent and glossy look, while twisted yarns can introduce slight surface wrinkles. Fabric texture is further enhanced through stitch and structural design. Weft-knitted fabrics can achieve various textured surfaces, such as pique, cable, and cardigan stitches, through combinations of floats, loops, and tucks [65]. Woven fabrics, like plain, twill, and satin, are formed by arranging warp and weft yarns [66]. Combining different weaves and yarns results in more variations. For instance, satin fabric, made from fine filaments like silk or shiny viscose have a smooth, lustrous surface, conveying luxury and comfort [67]. Pleated fabrics can be created by incorporating elastic yarns [68]. Additional processes can also add texture, such as sanding or brushing for plush surfaces [69,70], salt shrinking for bubble-like textures [71], and embossing for large folds [72].

The third element of visual aesthetics is the garment's style and shape. Unique or exaggerated accessories and shapes enhance the clothing's aesthetics and distinctiveness, often seen in necklines, sleeves, and waist areas [73,74].

When integrating textile-based sensors into clothing, their impact on visual aesthetics must be considered, ensuring sensors are seamlessly incorporated into the textile without compromising appearance.

2.2 Textile-based Flexible Sensors

Textile-based sensors can be classified in different ways. According to the structure, they can be divided into fiber type, two-dimensional fabric type, and three-dimensional

fabric type. According to the working principle, they can be divided into triboelectric sensor, resistive sensor, piezoelectric sensor, capacitive sensor, etc.

2.2.1 Textile-based triboelectric sensor

Triboelectric nanogenerator (TENG) is a new type of energy device that converts static charges into flowing current through a simple dielectric-electrode combination structure, which can be used to power electronics [75]. With the advantages of sustainability, simple structure, and simple fabrication, TENGs have received extensive attention in recent years. TENGs have different output responses to diverse forms of mechanical motion, so they are excellent self-powered sensors in addition to providing power service. Especially, textile-based TENGs (t-TENGs) can be used as wearable sensors for monitoring human activities due to their properties of softness, breathability, stretchability, and washability.

TENGs work based on triboelectric electrification, which involves contact and friction between two different materials. Various materials differ in their ability to gain or lose electrons after rubbing, and Figure 2.2a shows the triboelectric propensity of some common textile materials [76]. Positive materials tend to lose electrons to form positive charges after friction, while negative materials are more likely to gain electrons. The composition of a TENG includes triboelectric layers that can generate static charges after rubbing and one or more electrodes that induce and transfer electrons to form the current.

There are four basic TENG modes until now, including contact-separation mode, sliding mode, single-electrode mode, and freestanding triboelectric-layer mode [77]. The working principle of the first mode is shown in Figure 2.2b. When pressed and rubbed in contact, the surfaces of the two triboelectric layers will generate equal static charges with opposite polarities. After releasing the pressure, the up and down layers

separate gradually, resulting in an increased potential difference between the two surfaces. The potential difference will drive the induced electrons to flow from one electrode to another through the external circuit until it is balanced when the maximum separation is reached, thereby forming the current. Likewise, a reverse flow of electrons will occur due to the reduction of the potential difference when the two layers are compressed again. The other modes work similarly, just differ in the form of contact. During periodic compression-release cycles, the TENG will generate regular AC outputs, as shown in Figure 2.2c. The sensing mechanism of TENGs is that in a single cycle, parameters such as the magnitude, frequency, and speed of the mechanical force will be reflected in the maximum value (distance between the peak and the trough), width, and climbing (or descending) slope of the output signal, so the mechanical motion data will be transformed into visualized curves for subsequent analysis.

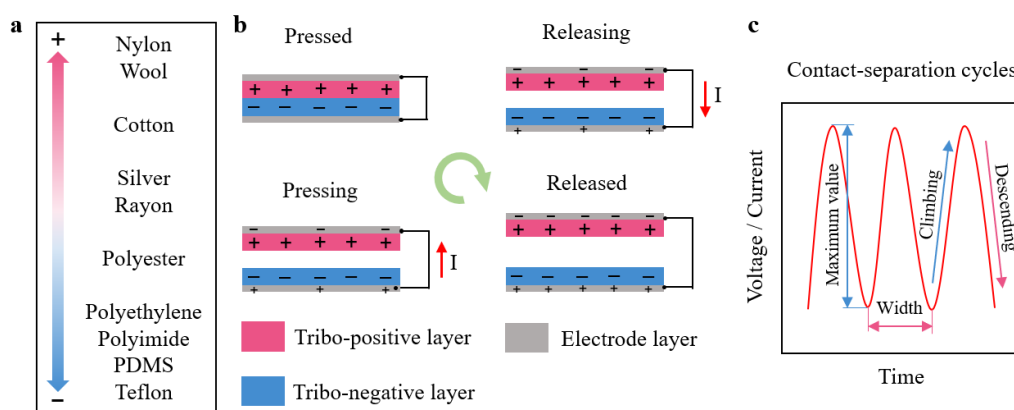


Figure 2.2 Working mechanism of the t-TENG sensor. (a) Triboelectric propensity of some common textile materials. (b) Working principle of the contact-separation mode TENG. (c) The output signal curve under cyclic compression-release.

There are mainly two ways to fabricate t-TENGs, one is to add triboelectric and electrode layers on common textile substrates by using chemical or physical methods, which form a semi-textile structure (St-TENG). Methods such as thin film lamination, coating, printing, and injection molding are commonly used to fabricate St-TENGs [78]. The other one is to employ dielectric and conductive yarns and fabricate them into t-TENGs through traditional textile techniques such as knitting, weaving, and braiding,

which form a pure textile structure (Pt-TENG).

St-TENGs offer a broad range of options for triboelectric layer materials, while electrode layer materials are typically composed of metal- and carbon-based substances. Textile substrates come in various forms, with elastic fibers and yarns frequently used in tensile strain sensors, and 3D spacer fabrics, known for their excellent compression resilience, commonly employed in contact-separation modes. The primary advantage of St-TENGs lies in their ability to form various shapes of protruding micro-nano structures or particles on the surface of the triboelectric layer through chemical or physical modification. This increases the effective contact area, resulting in a high voltage output, often exceeding 100 V. However, the use of dense films or coatings may reduce comfort by affecting breathability, and the laboratory preparation methods used are not suitable for large-scale production. A straightforward strategy involved creating a 1D tensile strain TENG sensor by applying conductive materials onto elastic fiber or yarn substrates. Common elastic substrates included polyurethane (PU), polydimethylsiloxane (PDMS), silicone rubber, and elastomeric poly(methyl acrylate). For example, Chen et al. developed a highly stretchable yarn TENG using a multigradient hierarchical structure composed of highly stretchable PU and ultraflexible silicone rubber (Figure 2.3a) [79]. The process began with wrapping a conductive electrode around the stretchable PU to create the initial helical layer, serving as the inner electrode. This was followed by encapsulating the layer with ultraflexible silicone rubber to facilitate electrification and charge generation. Finally, copper wires were wound around the silicone rubber, acting as the outer electrode and an additional triboelectrification layer. This hierarchical helical yarn exhibited remarkable flexibility and operated effectively within a strain range of 60% to 120% (Figure 2.3b). Similarly, Cheng's group developed a stretchable fiber nanogenerator (FNG) capable of capturing various mechanical energies, including strains from 0% to 50%, as well as pressing, twisting, and bending [80]. This coaxial fiber design featured a core fiber with a PU-silver nanowire (AgNW)-polytetrafluoroethylene (PTFE) layer and a sheath electrode

with a PDMS-AgNW layer (Figure 2.3c). The resulting FNG was highly stretchable, allowing it to adapt to surfaces with arbitrary curvature, as depicted in Figure 2.3d. This type of 1D sensor was characterized by its flexible structure and ease of integration into wearable products. Two-dimensional and 3D St-TENGs enhanced their functionality through strategic material pairing and physical or chemical modifications. For instance, Zhang et al. created a high-performance wearable t-TENG with an oblique microrod array structure, achieving a peak power density of $211.7 \mu\text{W}/\text{cm}^2$. This t-TENG was designed to be worn on the elbow, enabling continuous energy harvesting from human motion, serving as a sustainable power source or sensor (Figure 2.3e) [81]. Additionally, a hydrophobic layer composite enabled the collection of energy from water droplets. An all-textile TENG with hydrophobic and breathable properties was created, incorporating triboelectric nanoparticles on its surface to effectively harness energy from raindrops, resulting in an output voltage of 22 V (Figure 2.3f). This innovation can be incorporated into rainwear and other types of wearable rain gear [82]. Liang and colleagues developed a droplet energy harvesting fabric optimized for topology, which offers high flexibility and breathability (Figure 2.3g). Utilizing this fabric, they constructed a self-powered wireless wearable prototype capable of successfully detecting key droplet characteristics, including temperature, salinity, and pH [83]. 3D spacer fabrics were frequently used as substrate materials for St-TENGs due to their excellent compression recovery properties. Zhu et al. developed a friction nanogenerator using a 3D weft-knitted spacer fabric, consisting of two outer layers made of spandex/nylon multifilaments and a spacer layer of polyester monofilaments (Figure 2.3h). The nylon fibers exhibited a positive friction polarity, while the lower layer was coated with PTFE, which had a negative friction polarity. The polyester spacer layer provided elasticity, and graphene ink was applied to the upper nylon layer for charge collection [84]. Similarly, Liu et al. prepared a friction nanogenerator using a commercially available 3D spacer fabric as a template (Figure 2.3i). This fabric was woven from polyethylene terephthalate (PET) fibers and coated with a thin PDMS layer via dip coating. The surface featured numerous pyramids, ensuring effective friction

with the PET fiber layer under pressure [85]. While these TENGs typically exhibit strong electrical output due to high-density metal and polymer coatings, these coatings compromise the softness and breathability of the fabric, reducing comfort when used in wearable electronic devices.

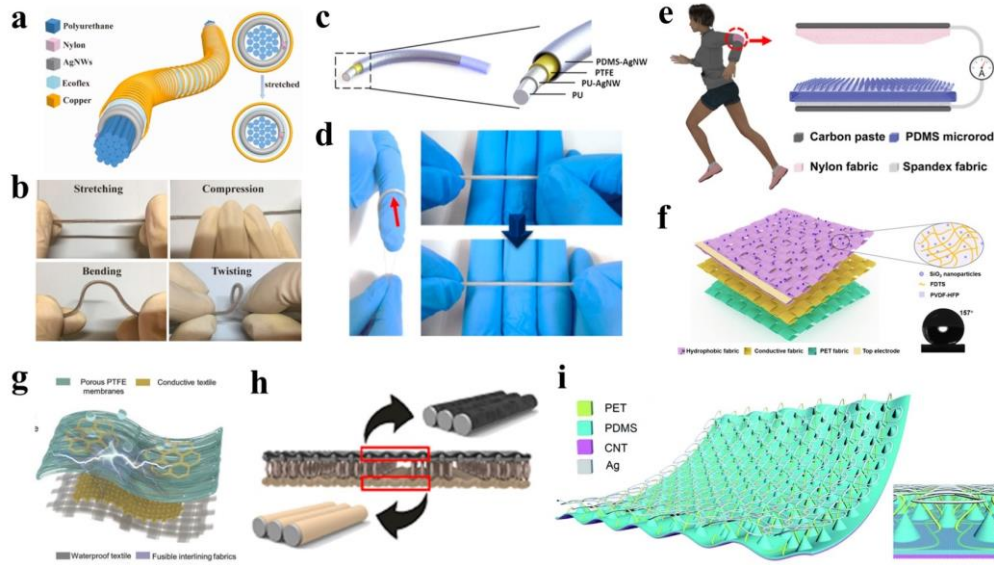


Figure 2.3 Various typical St-TENGs. (a) A yarn-based TENG strain sensor with multigradient hierarchical structure and (b) its high elasticity and flexibility [79]. (c) Structural design of a coaxial fiber optic sensor and (d) its high stretchability [80]. (e) High-performance wearable t-TENG with oblique microrod array structure [81]. (f) Hydrophobic layered composite t-TENG [82]. (g) Topologically optimized droplet energy harvesting fabric [83]. (h) TENG based on 3D weft-knitted spacer fabric [84]. (i) Enhanced 3D spacer fabric-based TENG with many pyramids on the surface [85].

Pt-TENGs are typically produced using conventional textile techniques such as knitting, weaving, and braiding. To meet textile manufacturing requirements and optimize triboelectric properties, materials are selected based on their triboelectric characteristics. Soft, highly positive materials like nylon yarn are commonly used to create the positive triboelectric layer, while highly negative materials such as Teflon and polyethylene yarns are used for the negative triboelectric layer. Electrode yarns often consist of steel

composite yarns, silver-plated yarns, and carbon fiber yarns. A common approach involves creating core-shell yarns with conductive cores, which are then incorporated into t-TENGs using traditional textile methods [86-95]. As illustrated in Figure 2.4a, Yu et al. innovatively crafted a comfortable and flexible TENG textile by weaving or knitting core-shell yarns, which consist of a conductive fiber core encased in a sheath of standard textile fibers [86]. In this design, the inner conductive fibers act as electrodes, while the outer fibers serve as a triboelectric dielectric material. These TENG textiles (Figure 2.4b) retain the advantageous properties of apparel fabrics, such as being flexible, lightweight, and allowing for diverse fiber material choices. Similarly, as shown in Figure 2.4c, Ye et al. developed an energy harvesting textile (EHT) by weaving or embroidering TENG yarn. This yarn was made with a stainless steel fiber core and a shell of natural silk fiber combined with PTFE fiber, using a shuttle loom or embroidery machine [95]. By carefully selecting materials and designing the structure, the EHT's overall performance was improved, including its output performance, mechanical strength, flexibility, and wearability. As shown in Figure 2.4d, the core-shell yarns can be crafted into any desired pattern using an automatic embroidery machine. Dong et al. used a circular braiding method to prepare conductive core-shell yarns and employed weft knitting technology to create a tubular TENG capable of operating in both tension and compression modes (Figure 2.4e) [96]. This fabric can be seamlessly integrated into knitted trousers for motion monitoring using intarsia technique (Figure 2.4f).

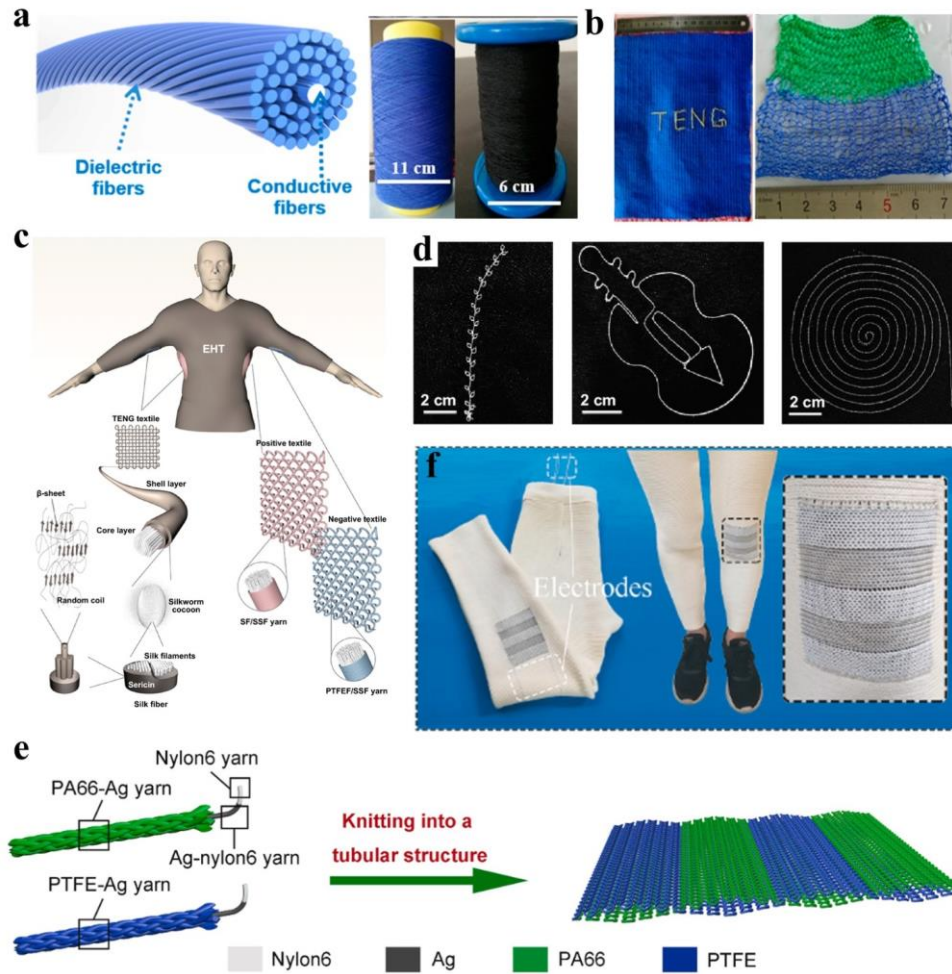


Figure 2.4 Various typical Pt-TENGs. (a) Core-shell yarn consisting of a conductive fiber core and a standard textile fiber sheath and (b) flexible TENG textiles made from such core-shell yarns [86]. (c) Energy-harvesting textiles made by weaving or embroidering TENG core-shell yarns and (d) various patterns achieved by this technology [95]. (e) Tubular TENG fabric made from braided core-shell yarns and (f) knitted pants with seamless integration of this sensing fabric [96].

Another strategy involves combining different functional yarn materials to create a TENG through the fabric's structure itself. For instance, a sandwich-structured TENG was created utilizing a knitted spacer fabric. In this design, the top and bottom layers were composed of conductive silver-plated nylon fibers and dielectric polyacrylonitrile fibers, respectively. Cotton fibers, which had neutral triboelectric properties, were used to connect these layers (Figure 2.5a) [92]. The fabricated t-TENG was ultrathin,

lightweight, and flexible, making it suitable for scrolling, folding, and kneading. A triboelectric all-textile sensor array (TATSA) was knitted using a full cardigan stitch, incorporating conductive yarns, nylon yarns, and ordinary threads (Figure 2.5b) [91]. Thanks to the variety of commercial nylon yarns available, TATSAs were produced in a range of colors to meet aesthetic and fashion requirements, as shown in Figure 2.5c. This TATSA design could be seamlessly incorporated into various sections of clothing to enhance visual appeal and was employed for monitoring respiratory and pulse signals (Figure 2.5d). The plating technique (Figure 2.5e) allowed for a physical parallel overlapping arrangement of the conductive and friction layers while preserving the original breathable pore structure and flexible texture of the knitted fabric (Figure 2.5f) [97].

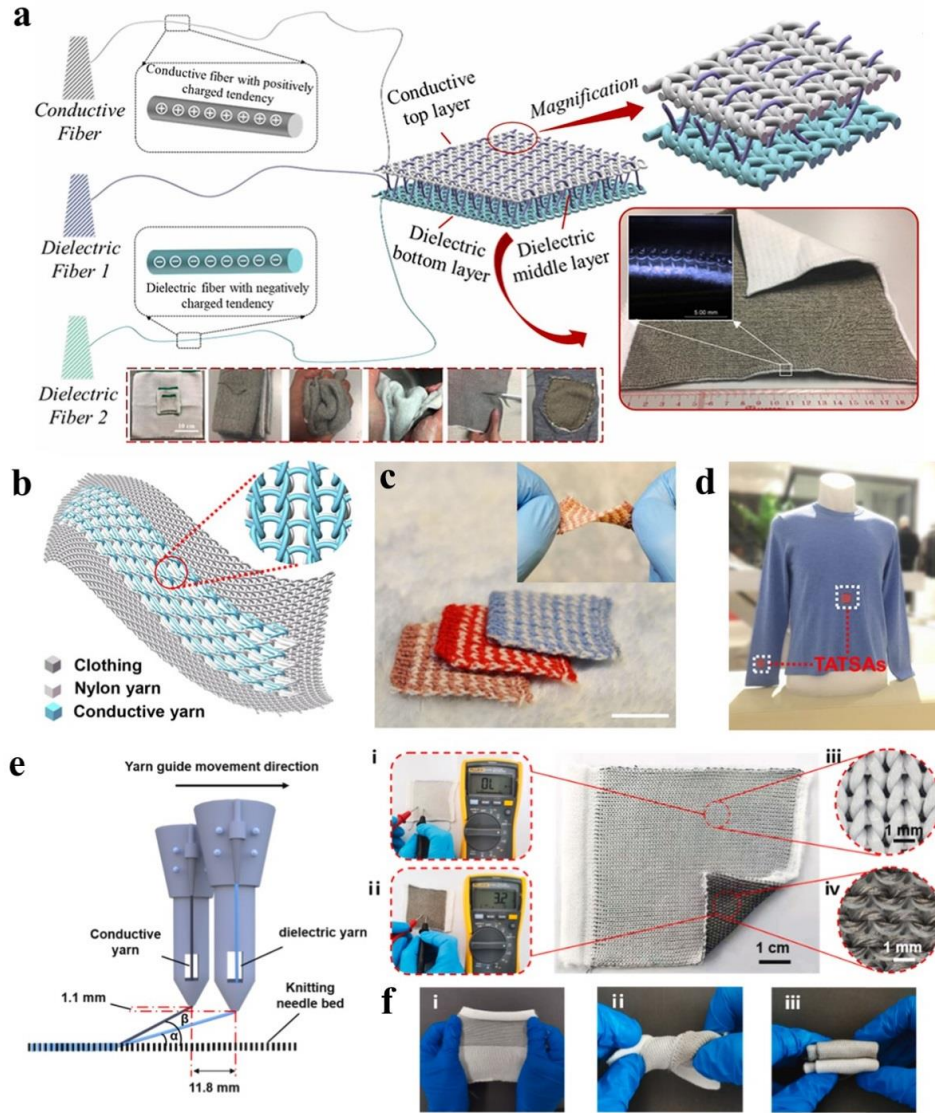


Figure 2.5 TENG sensing fabrics realized by special fabric structures. (a) TENG based on knitted spacer fabric structure [92]. (b) Triboelectric all-textile sensor array (TATSA) formed by full cardigan stitch. (c) TATSA samples in various colors. (d) TATSA integrated into clothing to monitor pulse and breathing signals [91]. (e) TENG fabric realized by knitting plating technique and (f) its excellent flexibility [97].

These methods can enhance the comfort of self-powered sensing fabrics and are well-suited for mass production. However, the output of Pt-TENGs is generally low because of the limited surface modification techniques available.

2.2.2 Textile-based resistive sensor

The working mechanism of resistive sensors is to reflect the magnitude of strain or force (a few reflect changes in temperature or humidity) through the change in resistance of conductive materials, which are widely used in various fields due to their simple working principle and structures. Textile-based resistive sensors combine the softness and comfort of textiles and have more advantages in wearable sensing. They are mainly divided into fiber/yarn-based sensors and fabric-based sensors.

Fiber/yarn-based resistive sensors, characterized by their one-dimensional (1D) linear structure, are predominantly utilized for tensile strain sensing. Their flexible architecture allows for seamless integration into clothing and other textile products. The primary components of these 1D resistive strain sensors include conductive and elastic elements. Conductive components are responsible for sensing resistance changes, with their conductive properties significantly influencing the sensor's sensitivity and stability. Common materials used for these components include conductive polymers [98], carbon-based materials [99,100], and metals [101,102]. The elastic component, on the other hand, provides an appropriate working range for tensile strain, necessitating different elastic materials for various applications. Typical materials include PU and elastic polyester. There are two main methods for preparing fiber/yarn-based resistive sensors. The first involves directly creating stretchable conductive fiber sensors through specialized spinning techniques. This method begins at the source by mixing conductive materials with elastic matrix materials or spatially positioning them, followed by extrusion through a spinneret into a coagulation bath to form composite fibers. For example, scalable wet spinning technology was able to produce MXene/PU composite fibers that were both conductive and highly stretchable (Figure 2.6a). These fibers could sense strains up to approximately 152% and exhibited a high gauge factor (GF) of about 12,900 [98]. Additionally, a coaxial wet spinning method was developed, which resulted in sheath/core fibers consisting of a pure PU fiber core enveloped by an

MXene shell (Figure 2.6b). These fibers demonstrated enhanced stability when subjected to cyclic stretch-release deformation across various applied strains [98]. The second method is simpler, integrating the conductor and elastomer through physical or chemical processes. For example, Sun et al. developed a strain sensor by coating conductive carbon nanotube (CNT) ink onto PU yarn using expansion and ultrasonic treatment processes (Figure 2.6c). This sensor, with high tensile strength, sensitivity, and wear resistance, achieves an ultra-low detection limit of less than 0.1% strain through a crack structure, enabling quick and accurate detection of subtle human movements such as pulse, vocalization, inhalation, and facial micro-expressions [99]. Similarly, Li et al. utilized polyvinyl alcohol as a binder to evenly adhere graphene to the surface of polyurethane multifilament, creating a flexible strain sensor (Figure 2.6d). They investigated the effects of graphene concentration and coating number on sensor performance, including sensitivity, linearity, repeatability, hysteresis, and thermal stability [100]. Recent advancements have also led to the development of yarn strain sensors with negative Poisson structures. A full-fiber auxetic-interlaced yarn sensor (AIYS) was created using mass-producible spinning technology. This sensor, as depicted in Figure 2.6e, features two conductive silver-plated polyamide yarns interlaced with a core PU yarn at high speed along the winding direction, forming a sensing yarn that exhibits a pronounced auxetic effect (Figure 2.6f). The sensing mechanism relies on the contact resistance between the helical units of the sheath yarn and the fiber bundle during stretching. Sixteen sensing yarns are embedded in key joints of knitted gloves, enabling the recognition of 26 letters through machine learning (Figure 2.6g) [101]. Building on this structure, Zhang et al. explored the impact of the number of core yarns and spiral conductive yarns on the auxetic and sensing performance of the sensor, ultimately developing a strain sensor suitable for monitoring large human body movements [102].

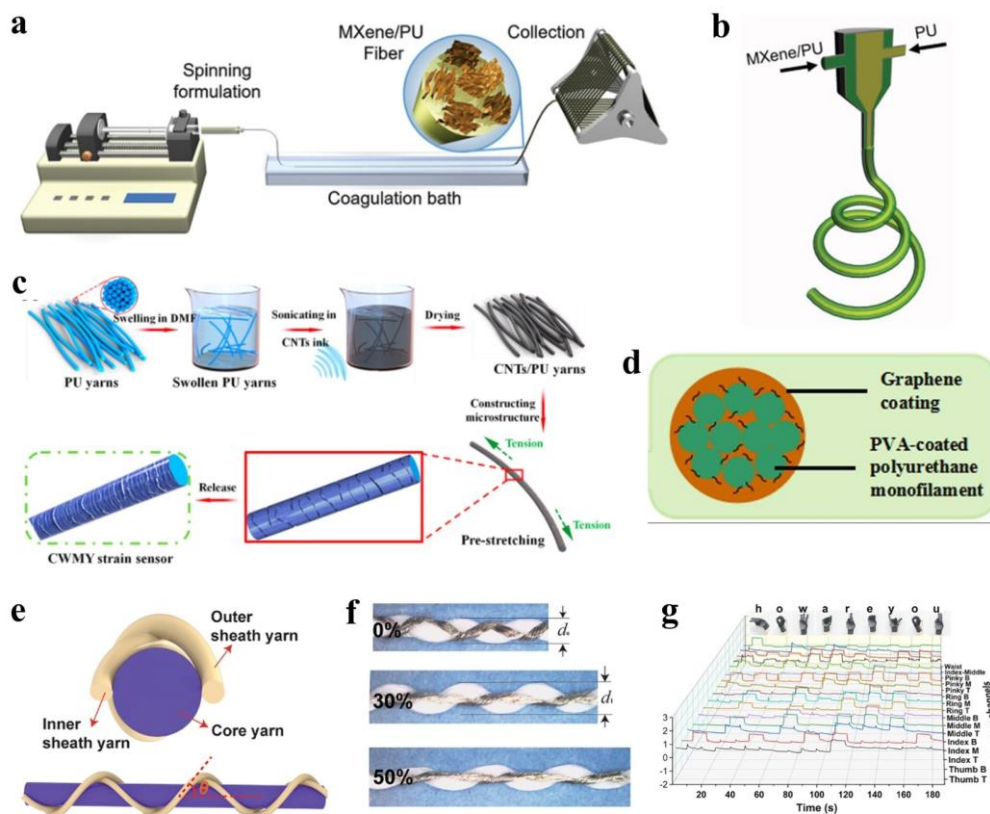


Figure 2.6 Fiber/yarn-based resistive sensors. (a) A MXene/PU composite fiber sensor prepared by scalable wet spinning technology and (b) a coaxial wet spinning method for manufacturing sheath/core fibers composed of pure PU fiber core wrapped with MXene shell [98]. (c) A strain sensor developed by coating CNT ink onto PU yarn using expansion and ultrasonic processes [99]. (d) A flexible strain sensor made by uniformly adhering graphene to the surface of polyurethane multifilament using polyvinyl alcohol [100]. (e) Full-fiber auxetic-interlaced yarn sensor (AIYS) and its (f) obvious auxetic effect. (g) AIYS used to recognize 26 letters [101].

To effectively develop fabric-based resistive sensors, it is imperative to integrate resistive-responsive conductive materials into fabric substrates. A fundamental approach to achieving this involves incorporating conductive substances into conventional fabrics through physical or chemical methods. For instance, CNTs and poly(3,4-ethylenedioxythiophene): poly(styrene sulfonate) (PEDOT:PSS) inks were inkjet printed onto fabric substrates to fabricate resistive-responsive temperature

sensors [103]. Moreover, carbonization of natural biomaterials has emerged as an effective strategy to engineer conductive networks for enhanced resistive sensing textiles. For example, silk fabrics that underwent high-temperature carbonization in an inert atmosphere (Figure 2.7a) were directly utilized as stretchable resistive sensors, exhibiting exceptional flexibility, high sensitivity, and a broad operational strain range [104]. This technique enabled the detection of human activities and biological signals from multiple directions and was also applicable to other fabrics, such as cotton [105]. Choi et al. improved the sensitivity of carbonized fabric sensors by employing 3D spacer fabrics, as illustrated in Figure 2.7b [106]. Another effective strategy involved integrating conductive or resistive sensing yarns into fabrics using traditional textile manufacturing techniques. For instance, conductive yarns were embroidered into fire-resistant clothing to develop temperature sensors [107]. As shown in Figure 2.7c, Seyedin's team devised a scalable production method for highly conductive and elastic PU/PEDOT:PSS composite fibers [108], which were combined with spandex in a circular weft knitting machine to produce knitted fabrics with significant strain sensing properties [109]. Fan et al. created acrylic/copper double-coated conductive yarns and embedded them into highly elastic rib fabrics using weft inlay technology to form flexible strain sensors, as illustrated in Figure 2.7d [110]. These sensing fabrics could be seamlessly integrated into garments for the purpose of monitoring human motion.

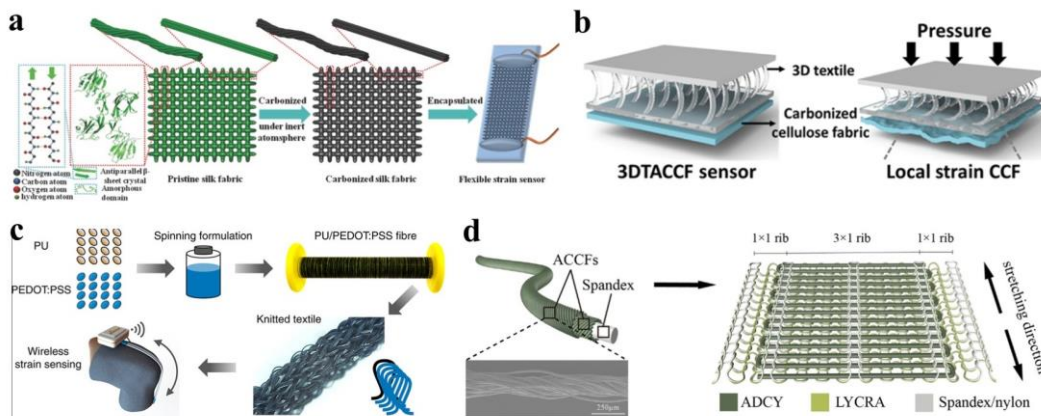


Figure 2.7 Fabric-based resistive sensors. (a) Fabrication of a stretchable resistive sensor by high temperature carbonization of silk fabric [104]. (b) 3D spacer fabrics for improving the sensitivity of carbonized fabric sensors [106]. (c) A method for

producing scalable, highly conductive and elastic PU/PEDOT: PSS composite fibers [108]. (d) A flexible strain sensor formed by embedding acrylic/copper double-coated conductive yarns into the rib fabric [110].

2.2.3 Textile-based piezoelectric sensor

First proposed in 2006, the piezoelectric nanogenerator (PENG) is one of the two primary types of nanogenerators [111], along with the TENG. PENGs exploit the piezoelectric effect to transform mechanical energy into electrical energy. Typically composed of nanoscale piezoelectric materials, these devices generate voltage by inducing charge separation when subjected to mechanical stresses like bending, stretching, or compression. Common piezoelectric materials encompass piezoelectric crystals (single crystals) [112,113], piezoelectric ceramics (polycrystalline semiconductors) [114-116], and polymer-based piezoelectric materials [117,118]. With the advent of smart wearable technology, flexible piezoelectric materials, such as electrospun polyvinylidene fluoride (PVDF) fiber membranes, have gained significant popularity. Similar to TENG, PENGs can detect and measure physical quantities like pressure, acceleration, vibration, force, and sound waves by analyzing the generated electrical signals, making them effective sensors. Textile-based PENGs (t-PENGs) offer enhanced flexibility and comfort, making them particularly suitable for wearable applications. Structurally, they can be categorized into fiber/yarn-based PENGs and fabric-based PENGs. The working principle of t-PENG is shown in Figure 2.8. In the initial state, the charge centers of the cations and anions coincide with each other, and there is no polarization inside the piezoelectric material (i). When pressure is applied, the deformation of the piezoelectric fabric results in negative strain and volume reduction. The charge centers separate to form an electric dipole, and the electric dipole moment changes, which results in the formation of a piezoelectric potential between the electrodes. If the electrode is connected to an external load, the piezoelectric potential will drive electrons through the external circuit and achieve a new equilibrium

state (ii), thereby generating electrical energy. The highest polarization density (iii) occurs when the two conductive fabric electrodes are in complete contact, that is, when the maximum pressing state is achieved. When the external force is released, electrons flow back to rebalance the charge caused by the released strain under short-circuit conditions (iv). By applying reciprocating strain, a steady pulse of current will flow through the external circuit. When the measurement system is connected in reverse, the output voltage and current signals are reversed [119].

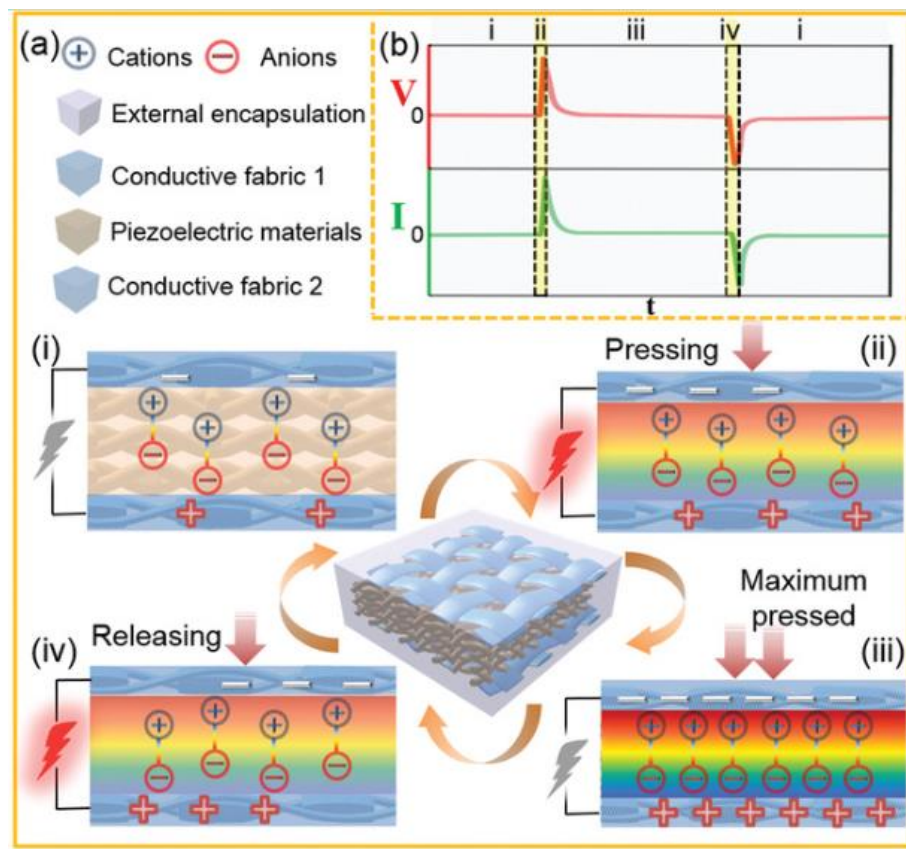


Figure 2.8 Working principle of t-PENG [119].

Fiber/yarn-based PENGs are easily integrated into clothing and wearable products, but their structure is more complex than fiber/yarn-based resistive sensors due to the necessity of both piezoelectric and electrode materials. A typical fabrication method involves embedding piezoelectric materials between internal and external conductive electrodes. For instance, as illustrated in Figure 2.9a, a highly flexible PENG composite

yarn can be created using simple wrapping and coating techniques. An electrospun PVDF-trifluoroethylene (PVDF-TrFE) film is hand-wound onto silver-coated nylon yarn and then covered with conductive CNTs. The assembly is dip-coated in the elastomer styrene-ethylene-butylene-styrene for mechanical protection and electrical insulation [120]. The resulting PENG yarn can be curled, knotted, sewn, and woven without damage, and a 1 cm segment can produce a voltage output of up to 2.6 V when compressed transversely. Additionally, PVDF-TrFE electrospun strips can be twisted into highly stretchable yarns, as shown in Figure 2.9b, achieving a tensile strain capacity of approximately 740%, which generates alternating electrical potentials during stretching and shrinking [121]. Xue et al. developed a more comfortable and durable PENG yarn using electrospinning and braiding technologies. As depicted in Figure 2.9c, PVDF nanofibers are continuously and evenly wound onto a conductive core yarn via electrospinning, followed by the application of a conductive braiding network using circular braiding technology to form a three-layer PENG yarn. Fabrics made from this yarn can be incorporated into clothing to detect human motion (Figure 2.9d) [122].

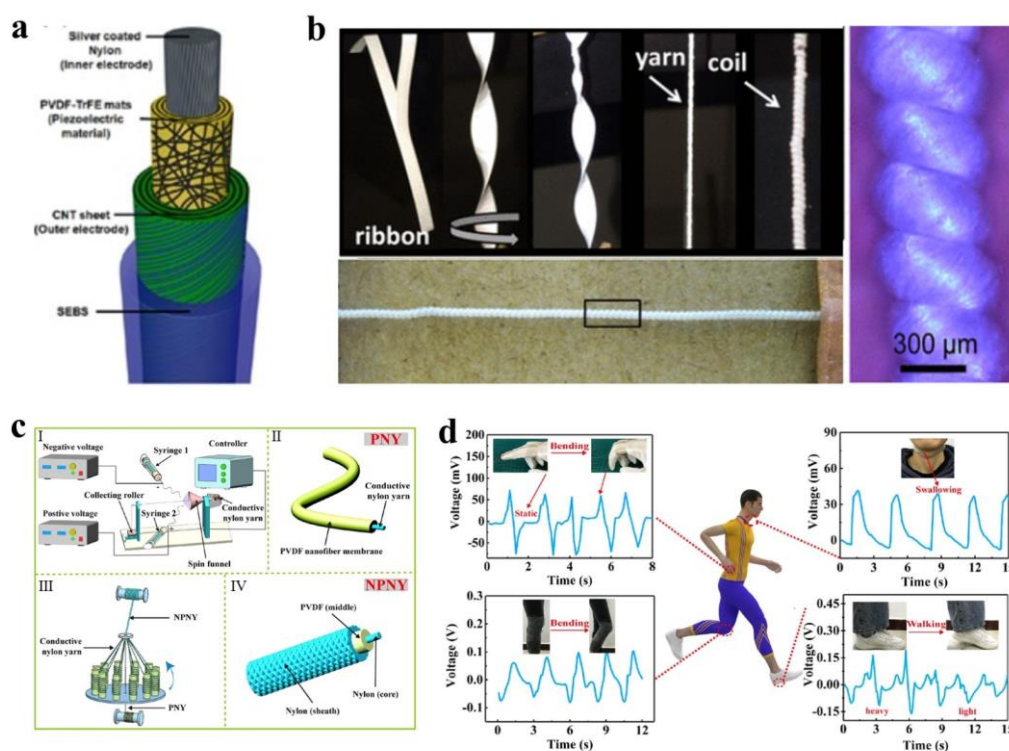


Figure 2.9 Fiber/yarn-based PENGs. (a) PENG composite yarn created using simple

wrapping and coating techniques [120]. (b) PVDF-TrFE electrospun strips twisted into highly stretchable yarn sensors [121]. (c) PENG yarn developed using electrospinning and braiding techniques and (d) such yarn used in clothing to detect human motion [122].

Fabric-based PENGs typically incorporate piezoelectric materials into fabric substrates through methods such as coating and dipping. For instance, as illustrated in Figure 2.10a, Huang et al. immersed polyester fabric in a graphene/PVDF solution, followed by drying to produce a graphene/PVDF-coated fabric. This coated fabric was then integrated with AI foil electrodes to create a piezoelectric sensor. The performance of this sensor, based on graphene/PVDF-coated fabric, is significantly enhanced compared to sensors made from pure PVDF film and PVDF-coated polyester, as shown in Figure 2.10b [123]. 3D spacer fabrics, a popular choice for textile substrates in pressure sensors, were employed to improve the piezoelectric properties of PVDF films. As depicted in Figure 2.10c, a piezoelectric sensor was constructed by sandwiching electrodes and a PVDF film between two layers of spacer fabric. The prestrained monofilaments in the spacer fabric enhanced the piezoelectric output by inducing multiple local strains on the PVDF film when external force was applied. This configuration showed significant potential for detecting biological signals such as sound waves, breathing, and pulse, as well as movement signals like fingertip pressure, sole pressure, and knee bending [124]. In addition, transforming piezoelectric materials into yarns offers a more stable and efficient production strategy for piezoelectric sensors. Kim et al. employed an innovative electrospinning technique, utilizing 50 nozzles to simultaneously produce multiple bundles of PVDF nanofibers. These fibers were then processed into PVDF yarns through stretching and twisting. Subsequently, the PVDF yarns were used as weft yarns to weave various fabric structures, as shown in Figure 2.10d. The resulting fabric was placed between conductive fabrics to form pressure sensors, which demonstrated excellent sensing performance and were suitable for gesture and motion recognition applications [125].

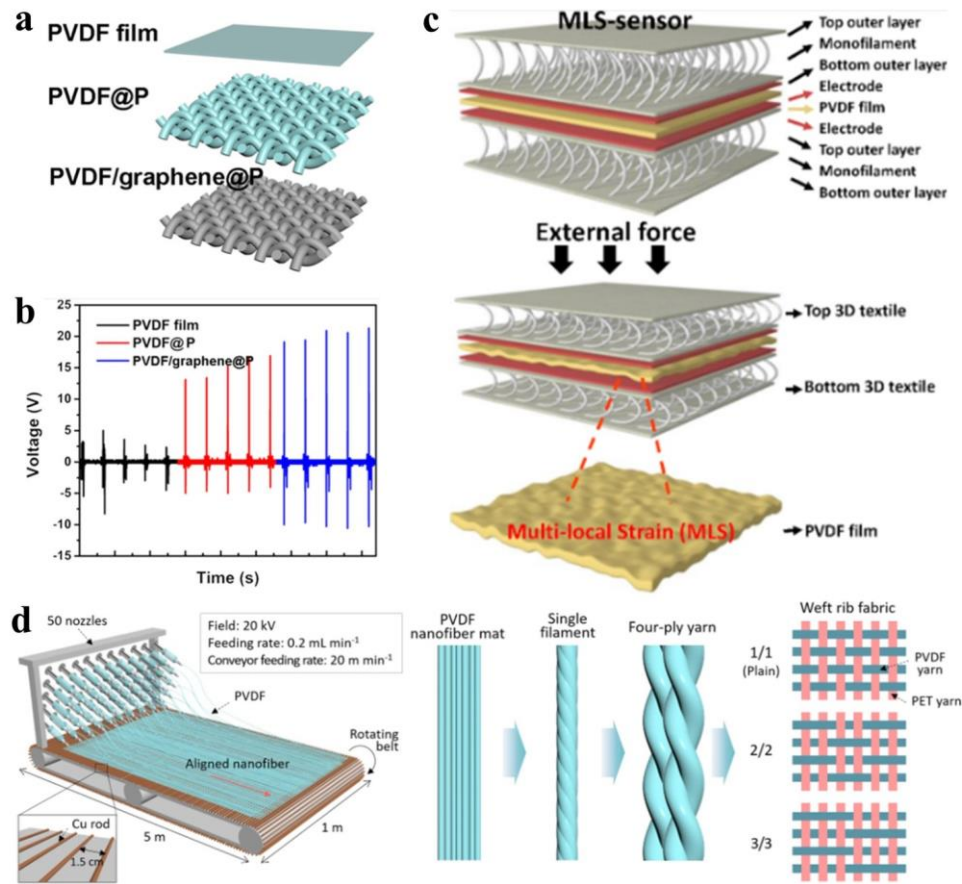


Figure 2.10 Fabric-based PENGs. (a) Graphene/PVDF coated fabric and (b) its sensing performance [123]. (c) 3D spacer fabric for improving the piezoelectric properties of PVDF film [124]. (d) A new method for producing multiple bundles of PVDF nanofibers simultaneously using 50 nozzles and the subsequent development process of PVDF yarn and fabrics [125].

2.2.4 Textile-based capacitive sensor

Capacitive sensors are devices that translate physical or mechanical quantities into changes in capacitance, making them ideal for measuring displacement, vibration, speed, and pressure. Textile-based capacitive sensors typically employ a parallel plate configuration, consisting of a dielectric layer positioned between two conductive textile layers. Compared to other textile sensors, they offer a stable structure, rapid response, and high linearity. The capacitance CC is determined by the following formula [126]:

$$C = \frac{\varepsilon_0 \varepsilon_r A}{d} \quad \text{Equation 2.1}$$

In the formula, ε_0 represents the vacuum dielectric constant, ε_r is the relative dielectric constant of the dielectric layer, A denotes the effective area of the electrodes, and d is the distance between the electrode plates. When an external force is applied, the material of the capacitive sensor deforms, potentially altering ε_r , A , or d , which in turn changes the capacitance C . By establishing a relationship between the capacitance and the deformation or force through testing, the sensor can effectively detect changes.

The silicon-based sensor serves as a representative example of textile-based capacitive sensors, featuring a silicon-based elastic medium positioned between two textile-based conductive plates. For instance, Gao et al. employed a fabric structure as a substrate, utilizing nickel-plated carbon fiber-filled conductive rubber for the electrode layer and PDMS as the dielectric layer to construct a flexible plate capacitor with an internal surface structure, as depicted in Figure 2.11a. This sensor is highly responsive to human movement, water droplets, and finger touch, owing to the strain response of the dielectric, as illustrated in Figure 2.11b [127]. The Walsh team advanced the field by developing a sensor sheet suitable for mass production. They used a flexible thermal bonding electrical connection method to securely attach a silicone elastomer between two conductive knitted fabrics (Figure 2.11c). Furthermore, individual sensors can be customized through a laser cutting process (Figure 2.11d). This sensor sheet exhibits a sensitive capacitance change in response to tension or compression, providing the flexibility and comfort necessary for monitoring human movement [128].

Moving beyond the conventional monolithic flat plate structure, researchers have progressively developed array capacitive sensors using interwoven fabrics. For example, Zhang et al. designed a capacitive pressure sensor by interweaving core-conductive core-spun yarns, as shown in Figure 2.11e and f. Capacitance changes occur at the intersections of these yarns. When external pressure is applied, the distance between adjacent yarns decreases, resulting in an increase in capacitance. This system

has a detection limit of approximately 3.6 Pa, enabling the sensor array to reliably detect the loading and unloading of individual soybeans (approximately 200 mg) [129]. The sensitivity of capacitive sensors has traditionally been limited by their structural and operational principles. Conventional materials exhibit a positive Poisson's ratio, which restricts the area expansion of the capacitor element to less than the applied strain, thereby preventing the sensor from achieving a GF greater than 1. Cuthbert et al. addressed this limitation by developing a helical auxetic yarn capacitive sensor, as shown in Figure 2.11g. This sensor achieved a GF of up to 4 due to the auxetic effect, which allows for a greater increase in electrode area relative to the applied strain [130].

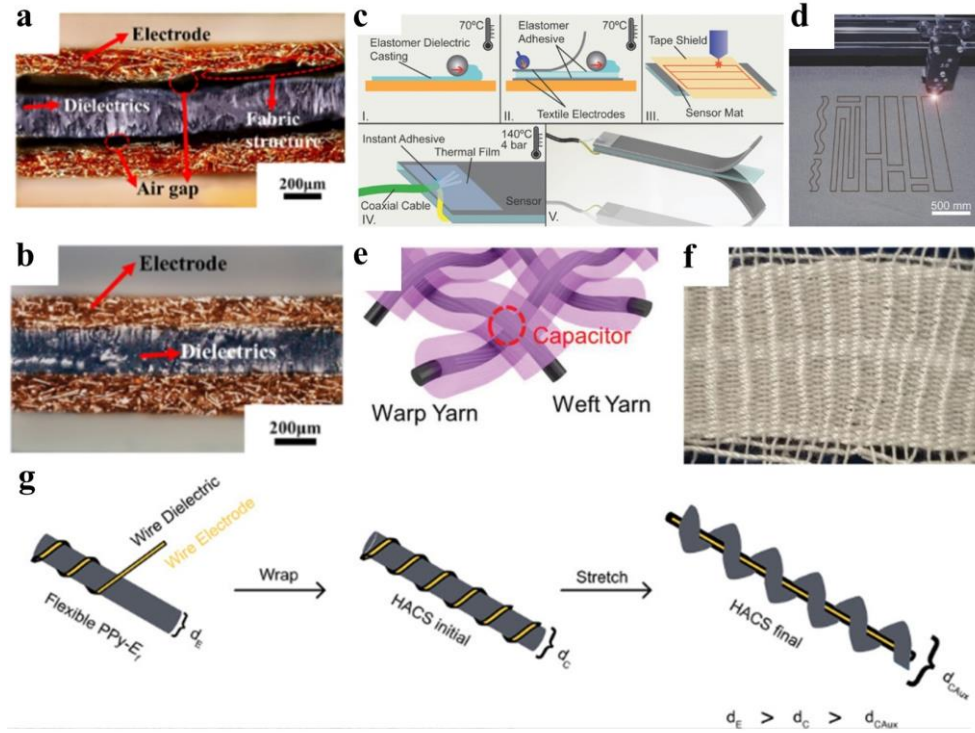


Figure 2.11 Textile-based capacitive sensors. (a) A flexible plate capacitor with an internal surface structure using fabric as substrate, conductive rubber as electrode layer, and PDMS as dielectric layer and (b) the state of the sensor when compressed [127]. (c) Fabric capacitive sensor prepared using thermal bonding electrical connection method and (d) laser cutting process for customizing individual sensors [128]. (e) A capacitive pressure sensor designed by interweaving core conductive core-spun yarn and (f) its photo [129]. (g) A helical auxetic yarn capacitive sensor [130].

2.2.5 Textile-based hybrid mode sensor

In addition to the aforementioned textile-based sensors that operate on a single mechanism, there exist hybrid mode sensors that combine multiple working principles. By integrating different modes, the sensitivity of these sensors can be significantly enhanced. Common mode combinations include triboelectric/piezoelectric [131,132], piezoelectric/capacitive [133,134], and resistive/capacitive [135,136]. For instance, a hybrid triboelectric/piezoelectric 3D fabric was developed. As illustrated in Figure 2.12a, a copper wire and a spring served as electrodes, while piezoelectric materials (BaTiO₃/PDMS) and triboelectric materials (AgNW/PDMS) were applied to create the PENG yarn and the TENG yarn as warp yarns, respectively. Subsequently, the PTFE yarn was used as weft yarn to construct a 3D interlocking parallel structure hybrid nanogenerator (Figure 2.12b). Due to the coupling effect, the triboelectric and piezoelectric effects synergistically operated under pressure, resulting in a nanogenerator textile with outstanding output performance. This textile functioned as a self-powered motion detector capable of identifying various bending and stretching movements, including finger, wrist, elbow, and knee motions, as well as arm swings and footsteps [131]. Su et al. fabricated a fully textile capacitive pressure sensor using a piezoelectric P(VDF-TrFE) nanofiber membrane as the dielectric layer and conductive fabrics as the electrodes, as depicted in Figure 2.12c. The piezoelectric properties of the P(VDF-TrFE) nanofibers generated a potential difference under pressure, thereby amplifying the sensor's sensitivity [134]. Additionally, a resistive/capacitive hybrid response optical fiber pressure sensor with a three-layer core-sheath structure was developed. The preparation process and structure are shown in Figure 2.12d. The inner layer consisted of PU elastic electrodes with high CNT content, the middle layer comprised PU piezoresistive composite materials with low CNT content, and the outer layer was made of insulating materials. Experimental results demonstrated that the hybrid response significantly enhanced sensitivity [135].

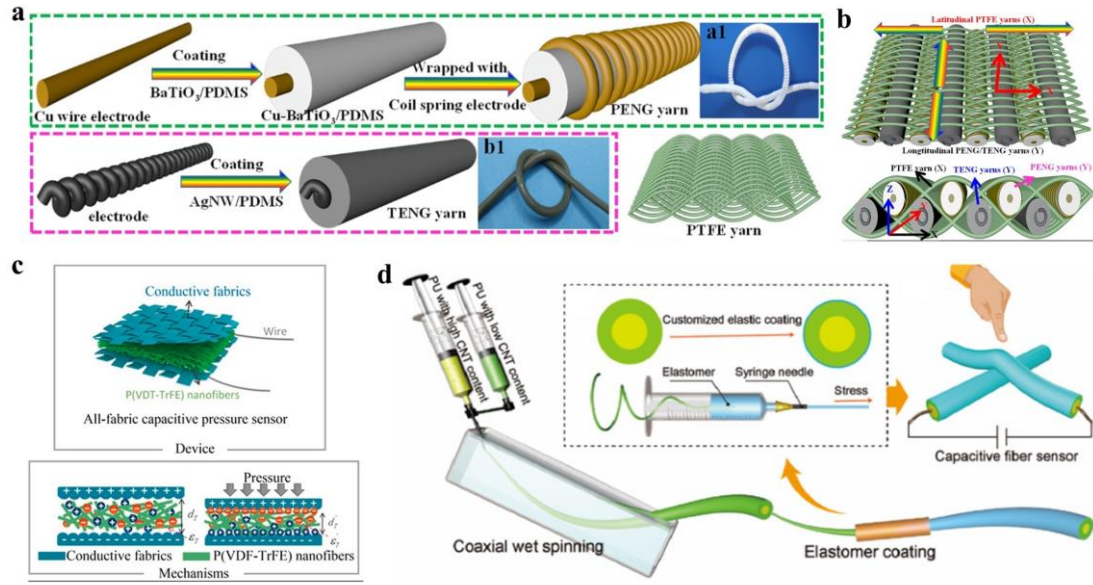


Figure 2.12 Textile-based hybrid mode sensors. (a) Preparation process of copper core PENG yarn and spring core TENG yarn and (b) 3D interlocking parallel structure of hybrid triboelectric/piezoelectric fabric [131]. (c) All-textile capacitive pressure sensor made of piezoelectric P (VDF-TrFE) nanofiber membrane as dielectric layer and conductive fabric as electrode [134]. (d) Preparation process and structure of a three-layer core-sheath structured resistive/capacitive hybrid response optical fiber [135].

2.3 Application of Textile-based Sensors

Textile-based sensors offer numerous advantages, particularly in wearable applications, owing to the inherent properties of textiles. These sensors can be seamlessly integrated into clothing to monitor the movements of various parts of the human body. With the help of advanced machine learning or deep learning, the detected signals can be accurately classified, allowing textile-based sensors to be applied in a wide range of fields, including the monitoring of sports performance, the capture of gestures or postures in virtual reality (VR) and augmented reality (AR) environments, and vital signs detection within the healthcare sector.

2.3.1 Intelligent sports sensors

The idea of intelligent exercise is to assist in more professional, personalized and scientific fitness. Textile-based sensors equipped with sensing, recording, and feedback capabilities offer significant potential in sports monitoring by evaluating and guiding users' exercise or training routines, while having considerable wear comfort, having great application potential in sports monitoring. For example, Lin et al. developed a triboelectric sensing device embedded in an insole (Figure 2.13a), capable of accurately monitoring and distinguishing various gaits such as walking, running, jumping, and striding in real time by analyzing gravity-induced electrical outputs (Figure 2.13b). This innovative insole not only tracks gait data during physical activity to evaluate fitness outcomes but also aids in a sports fall alert system [137]. Zhu's team incorporated a t-TENG-piezo chip hybrid sensor into a sock for motion tracking and gait recognition. What's more, this hybrid sensor is capable of quickly assessing sweat levels by analyzing the output signal produced through direct mechanical contact (Figure 2.13c) [132]. A resistive and capacitive fabric sensor array was developed for monitoring Taekwondo movements, as shown in Figure 2.13d, which has dual responses to tactile and tension stimuli [138]. The above-mentioned textile-based sensors will play an important role in intelligent sports applications.

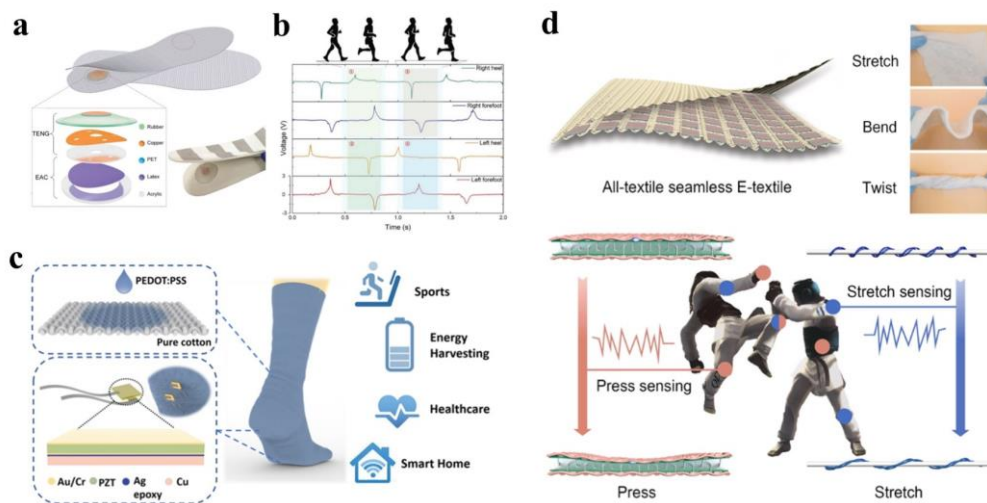


Figure 2.13 Textile-based sensors for sports monitoring. (a) Smart sensing insole and (b) its gait monitoring curves [137]. (c) Schematic illustration of a t-TENG and piezoelectric chip hybrid sensing sock [132]. (d) Resistive and capacitive fabric sensor

array for monitoring Taekwondo movements [138].

2.3.2 Motion capture in VR/AR

VR/AR technology integrates real and virtual worlds, allowing users to gain immersive perception in virtual scenes and interact with virtual props. This represents a profound form of human-computer interaction, with applications spanning education, entertainment, medical rehabilitation, and industrial design. A crucial aspect of VR/AR interaction involves collecting and interpreting user data, such as position, gestures, posture, and motion, which typically relies on bulky wearable sensors and advanced photographic equipment. Textile-based sensors offer a more cost-effective, portable, and comfortable alternative. Currently, gesture recognition is a primary focus in this field. For instance, Wen et al. developed a superhydrophobic triboelectric textile using a CNT/thermoplastic elastomer coating method, creating a self-powered gesture recognition glove (Figure 2.14a). By training a CNN model (Figure 2.14b), this glove achieved high-precision VR/AR gesture control, applicable to virtual activities like shooting and pitching (Figure 2.14c) [139]. Subsequently, Wen and his team devised a sign language recognition and communication system by integrating technologies such as a t-TENG gesture recognition glove (Figure 2.14d), AI modules, and VR interfaces. This system successfully recognized 50 words and 20 sentences in sign language, projecting the results into virtual space as audio or text, thus facilitating barrier-free communication between the hearing impaired and those with normal hearing (Figure 2.14e) [140]. The auxetic resistive strain sensing yarn was integrated into a glove and also achieved accurate sign language recognition, as shown in Figure 2.14f [101]. It is undeniable that textile-based sensors show great potential in virtual technology applications.

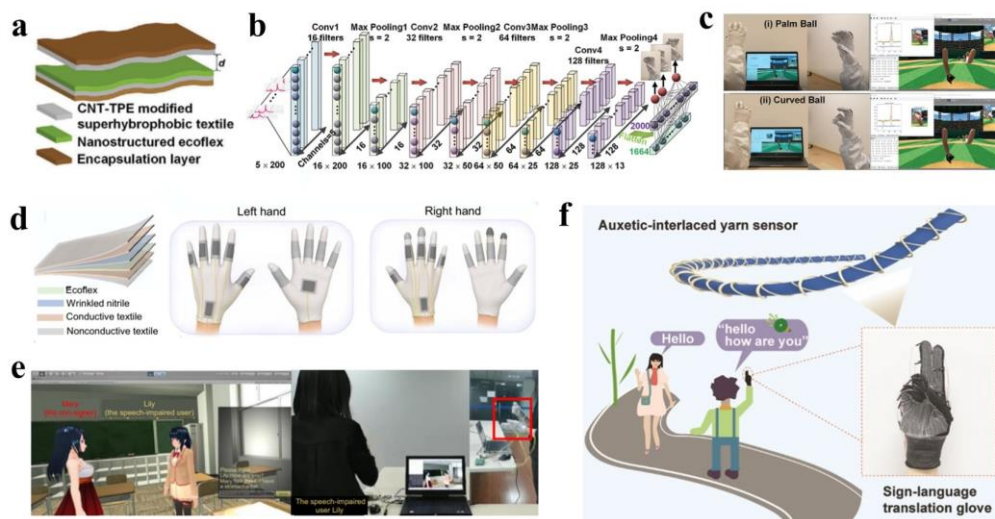


Figure 2.14 Textile-based sensors for VR/AR applications. (a) Schematic diagram of the structure of a coated superhydrophobic triboelectric textile and (b) the CNN model used for training and (c) its application in virtual pitching [139]. (d) Schematic diagram of the gesture recognition gloves and (e) the sign language recognition and communication demonstration in virtual space [140]. (f) Auxetic strain sensing yarn for sign language recognition [101].

2.3.3 Biomonitoring sensors

Biomonitoring is essential for medical rehabilitation and the care of patients or individuals in high-risk categories. Portable and wearable monitoring devices offer extensive capabilities for everyday health tracking. In recent years, textile-based sensors have shown great potential in human biomonitoring. These sensors primarily assess health conditions by monitoring vital signs, including heartbeat, respiration, blood flow, pulse, and skin temperature. This technology provides a promising foundation for effective and convenient monitoring and diagnosis of daily health. For instance, as shown in Figure 2.15a, a PEDOT-thermoplastic urethane (TPU) composite fiber prepared by in-situ polymerization showed high temperature sensitivity and ideal temperature resolution. When the fiber was sewn into textiles in an S-shape, the sensing performance was almost unaffected by tension (Figure 2.15b), which allows the sensor

to accurately measure skin temperature during daily activities [141]. Fang et al. introduced a multilayered t-TENG-based arterial pressure sensor that was both comfortable and waterproof, designed to measure blood pressure with the assistance of machine learning. By combining this sensor with a signal processing circuit, a Bluetooth transmission module, and a mobile app, it is possible to create a portable and user-friendly wireless cardiovascular monitoring system (Figure 2.15b) [142]. Fan et al. developed a triboelectric sensor with high sensitivity to skin micro-pressure capture by utilizing pure textile materials and weft knitting technology. This flexible sensing device was able to monitor pulse and respiration simultaneously and could be applied in cardiovascular disease and sleep apnea syndrome. What's more, this sensor can be seamlessly integrated into garments through knitting technique without compromising aesthetics and comfort (Figure 2.15c) [91].

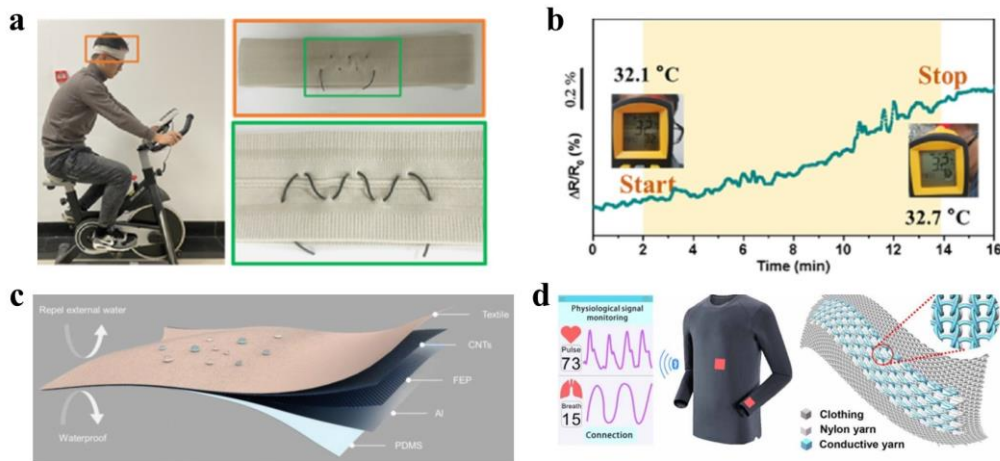


Figure 2.15 Textile-based sensors for vital signs monitoring. (a) PEDOT-TPU composite fiber used to measure skin temperature and (b) its sensitivity performance [141]. (b) Schematic structure of the multilayered t-TENG and the picture of using a mobile phone to display pulse monitoring data in real time [142]. (c) Schematic illustration of the enlarged view of the knitted sensor and its application to monitor pulse and respiratory signals in real time [91].

Although the above studies have reported the application of textile-based sensors in

multiple fields and achieved a series of successful demonstrations, there are still many challenges for their commercial applications.

1) Durability and stability. Although traditional textiles have good abrasion resistance, as functional materials, conductive particles and coatings are more easily damaged under continuous friction. In addition, due to the softness of textile fabrics, irreversible deformation will inevitably occur under long-term mechanical force, which will damage the sensitivity and accuracy of sensors, especially of those used to monitor tiny biological signals. What's more, factors such as stains and perspiration will affect the performance stability of sensors, which requires the development and introduction of comfortable and efficient packaging technology to solve this problem.

2) Oxidation of the electrode. Conductive metal-containing materials such as silver-coated yarns are often employed as electrodes. Metal materials exposed to the air are prone to oxidation and damage the electrical conductivity, thereby affecting the output signal. In future applications, electrode protection processes need to be developed to avoid this situation.

3) The contradiction between comfort and sensitivity. The comfort of textile-based sensors is close to that of ordinary clothing fabrics, however, the sensing performance of them has not been effectively improved. The dense coatings and films on the surface of textiles improve the sensitivity, but they will affect the hand feeling and breathability of the sensing fabrics. At present, no research can achieve the advantages of both, which is one of the main directions for future research.

4) Integration of intelligent sensing systems. Textile-based sensors are usually applied by integrating them in clothing or other textiles. The intarsia technique appears to be a promising strategy for integrating smart technology into knitted wearables. Nevertheless, the wide range of applications necessitates the development of other seamless integration methods. A wearable intelligent sensing system typically comprises modules like sensors, management circuits, and wireless transmission components. The challenges of connecting these functional modules and achieving comprehensive integration with the wearable substrate remain unresolved, calling for

collaborative efforts from researchers across multiple disciplines.

2.4 Conclusion

This chapter begins by outlining the concepts of comfort and evaluation methods for textiles. It then provides a detailed summary of the main classifications of textile-based sensors, including their working mechanisms, preparation methods, and recent research progress. The chapter concludes with a discussion on the primary applications of these sensors and the challenges that need to be addressed. Integrating textiles into sensors enhances their comfort by improving flexibility, breathability, aesthetics, and durability. Textile-based sensors show significant potential across various fields, particularly in smart wearables. However, they are still far from achieving widespread commercialization. Most research remains confined to laboratory settings, requiring cumbersome and complex preparation processes that are not conducive to large-scale industrial expansion. While adding a conductive layer through coating or deposition can improve sensor sensitivity, it often compromises the fabric's inherent comfort and wear resistance. Although established textile technologies such as knitting, weaving, and non-wovens support the large-scale production of textile-based sensors, the trade-off between sensitivity and comfort remains unresolved. Yarn-shaped sensors have demonstrated ease of integration into wearable products, yet they typically possess larger diameters and greater stiffness compared to traditional yarns. These sensors are often incorporated into clothing or other wearables through gluing or hand-stitching, which can negatively impact aesthetics and comfort. The remaining challenge is to combine textile technology with sensor development to create innovative methods for mass-producing flexible sensors that maintain stable sensitivity and comfort.

References

1. Q. Shi, B. Dong, T. He, Z. Sun, J. Zhu, Z. Zhang, C. Lee, Progress in wearable electronics/photronics—Moving toward the era of artificial intelligence and internet of things, *InfoMat.* 2 (2020) 1131-1162.
2. D. Nahavandi, R. Alizadehsani, A. Khosravi, R. Acharya, Application of artificial intelligence in wearable devices: Opportunities and challenges, *Comput. Methods Prog. Biomed.* 213 (2022) 106541.
3. Y. Li, The science of clothing comfort, *Text. Prog.* 31 (2001) 1.
4. E. Kamalha, Y. Zeng, J.I. Mwasiagi, S. Kyatuheire, The comfort dimension; a review of perception in clothing, *J. Sens. Stud.* 28 (2013) 423-444.
5. S. Kaplan, A. Okur, The meaning and importance of clothing comfort: A case study for Turkey, *J. Sens. Stud.* 23 (2008) 688-706.
6. K. Slater, Discussion paper the assessment of comfort, *J. Text. Inst.* 77 (1986) 157-171.
7. S. Kawabata, M. Niwa, Fabric performance in clothing and clothing manufacture, *J. Text. Inst.* 80 (1989) 19-50.
8. F.S. Kilinc-Balci, in *Improving comfort in clothing* (Ed: G. Song), Woodhead Publishing, Sawston, Cambridge 2011, Ch. 4.
9. L.L. Matté, A.C. Broega, M.E.B. Pinto, in *Textiles, Identity and Innovation: Design the Future* (Eds: G. Montagna, C. Carvalho), CRC Press, Boca Raton, FL 2018, Ch. 1.
10. A. Das, R. Alagirusamy, in *Improving Comfort in Clothing* (Ed: G. Song), Woodhead Publishing, Sawston, Cambridge 2011, Ch. 9.
11. B.C. Ellis, R.K. Garnsworthy, A review of techniques for the assessment of hand, *Text. Res. J.* 50 (1980) 231-238.
12. E. Priha, Are textile formaldehyde regulations reasonable? Experiences from the Finnish textile and clothing industries, *Regul. Toxicol. Pharmacol.* 22 (1995) 243-249.

13. M. Gobalakrishnan, S. Das, D. Saravanan, in *Chemical Management in Textiles and Fashion* (Ed: S. S. Muthu), Woodhead Publishing, Sawston, Cambridge 2021, Ch. 6.
14. S.A. Hosseini Ravandi, M. Valizadeh, in *Improving comfort in clothing* (Ed: G. Song), Woodhead Publishing, Sawston, Cambridge 2011, Ch. 2.
15. R. Chattopadhyay, in *Technical Textile Yarns* (Eds: R. Alagirusamy, A. Das), Woodhead Publishing, Sawston, Cambridge 2010, Ch. 1.
16. C. Lawrence, in *Textiles and fashion* (Ed: R. Sinclair), Woodhead Publishing, Sawston, Cambridge 2015, Ch. 10.
17. M. Matsudaira, K. Nakano, Y. Yamazaki, Y. Hayashi, O. Hayashi, Effects of weave density, yarn twist and yarn count on fabric handle of polyester woven fabrics by objective evaluation method, *J. Text. Inst.* 100 (2009) 265-274.
18. J. Kawamoto, Hand of Wool Fabrics and Its Control, *Sen'i Kikai Gakkaishi*. 32 (1979) 156-161.
19. M. Matsudaira, Fabric handle and its basic mechanical properties, *J. Text. Eng.* 52 (2006) 1-8.
20. O. Tokmak, O.B. Berkalp, J. Gersak, Investigation of the mechanics and performance of woven fabrics using objective evaluation techniques. Part I: the relationship between FAST, KES-F and Cusick's drape-meter parameters, *Fibres Text. East. Eur.* 18 (2010) 79.
21. J. Wang, Y. Li, Effect of Clothing Pressure on Exercise Fatigue Based on EEG, *AATCC J. Res.* 8 (2021) 40-45.
22. J. Geršak, in *Anthropometry, apparel sizing and design* (Eds: N. Zakaria, D. Gupta), Woodhead Publishing, Sawston, Cambridge 2014, Ch. 12.
23. Y.W. Kim, Y.J. Baek, Distribution of the Garment Pressure by Postures, *J. Korean Soc. Cloth. Text.* 33 (2009) 775-781.
24. W. Kirk Jr, S.M. Ibrahim, Fundamental relationship of fabric extensibility to anthropometric requirements and garment performance, *Text. Res. J.* 36 (1966) 37-47.

25. D. Chen, H. Liu, Q. Zhang, H. Wang, Effects of mechanical properties of fabrics on clothing pressure, *Prz. Elektrotech.* 89 (2013) 232-235.
26. M. Harumi, N. Miyuki, M. Hideo, K. Kiyokazu, Effects of clothing pressure exerted on a trunk on heart rate, blood pressure, skin blood flow and respiratory function, *Sen'i Kikai Gak kaishi.* 54 (2001) 57-62.
27. A. Beazley, Size and fit: The development of size charts for clothing-Part 3, *J. Fash. Mark. Manage.* 3 (1999) 66-84.
28. J. Wang, G. Lu, L. Chen, Y. Geng, W. Deng, Customer participating 3D garment design for mass personalization, *Text. Res. J.* 81 (2011) 187-204.
29. H. Liu, D. Chen, Q. Wei, R. Pan, A study of the relationship between clothing pressure and garment bust strain, and Young's modulus of fabric, based on a finite element model, *Text. Res. J.* 81 (2011) 1307-1319.
30. Y. Teyeme, B. Malengier, T. Tesfaye, I.C. Wrobel, A.B.H. Musa, L.V. Langenhove, A review of contemporary techniques for measuring ergonomic wear comfort of protective and sport clothing, *Autex Res. J.* 21 (2021) 32-44.
31. T. Mitsuno, A. Kai, Distribution of the preferred clothing pressure over the whole body, *Text. Res. J.* 89 (2019) 2187-2198.
32. H. Yoshirnura, K. Ishikawa, Some measurements of garment compression on the body, *Sen'i Kikai Gakkaishi.* 39 (1983) 525-531.
33. Y.L. Lin, M.J.J. Wang, The development of a clothing fit evaluation system under virtual environment, *Multimedia Tools Appl.* 75 (2016) 7575-7587.
34. N.J. Rosenberg, B.L. Blad, S.B. Verma, *Microclimate: the biological environment*, Wiley, NJ 1983.
35. S. Lenzholzer, J. Koh, Immersed in microclimatic space: Microclimate experience and perception of spatial configurations in Dutch squares, *Landscape Urban Plann.* 95 (2010) 1-15.
36. H. Ueda, Y. Inoue, M. Matsudaira, T. Araki, G. Havenith, Regional microclimate humidity of clothing during light work as a result of the interaction between local sweat production and ventilation, *Int. J. Clothing Sci. Technol.* 18 (2006) 225-234.

37. H. Sari, X. Berger, A new dynamic clothing model. Part 2: Parameters of the underclothing microclimate, *Int. J. Therm. Sci.* 39 (2000) 646-654.
38. G. Havenith, Interaction of clothing and thermoregulation, *Exog. Dermatol.* 1 (2002) 221-230.
39. Z. Sun, N. Pan, in *Therm. Moisture Transp. Fibrous Mater.* (Eds: N. Pan, P. Gibson), Woodhead Publishing, Sawston, Cambridge 2006, Ch. 7.
40. J.E. Werden, M.K. Fahnestock, R.L. Galbraith, Thermal Comfort of Clothing of Varying Fiber Content, *Text. Res. J.* 29 (1959) 640-651.
41. Y. Yang, X. Yu, L. Chen, P. Zhang, Effect of knitting structure and yarn composition on thermal comfort properties of bi-layer knitted fabrics, *Text. Res. J.* 91 (2021) 3-17.
42. F. Wang, W. Shi, Y. Lu, G. Song, R.M. Rossi, S. Anaheim, Effects of moisture content and clothing fit on clothing apparent 'wet' thermal insulation: a thermal manikin study, *Text. Res. J.* 86 (2016) 57-63.
43. V. Buzaitė, D. Mikucionienė, Effect of inner layer structures of weft-knitted spacer fabrics on thermal insulation and air permeability, *Text. Res. J.* 92 (2021) 2862-2872.
44. B.A. MacRae, R.M. Laing, C.A. Wilson, Importance of air spaces when comparing fabric thermal resistance, *Text. Res. J.* 81 (2011) 1963-1965.
45. X. Xu, T. P. Rioux, A. W. Potter, Fabric thermal resistance and ensemble thermal resistances are two different concepts. *J. Occup. Environ. Hyg.* 11 (2014) D187-D188.
46. M. Matusiak, Thermal comfort index as a method of assessing the thermal comfort of textile materials. *Fibres Text. East. Eur.* 18 (2010) 79.
47. Z. Lei, Review of application of thermal manikin in evaluation on thermal and moisture comfort of clothing, *J. Eng. Fibers Fabr.* 14 (2019) 1558925019841548.
48. B. Das, A. Das, V.K. Kothari, R. Figueiro, M. Araújo, Moisture transmission through textiles: Part II: Evaluation Methods and Mathematical Modelling, *Autex Res. J.* 7 (2007) 194-216.

49. X.Q. Dai, R. Imamura, G.L. Liu, F.P. Zhou, Effect of moisture transport on microclimate under T-shirts, *Eur. J. Appl. Physiol.* 104 (2008) 337-340.
50. B. Das, A. Das, V.K. Kothari, R. Figueiro, M. Araújo, Moisture transmission through textiles, *Autex Res. J.* 7 (2007) 100-110.
51. E. Onofrei, A.M. Rocha, A. Catarino, The influence of knitted fabrics' structure on the thermal and moisture management properties, *J. Eng. Fibers Fabr.* 6 (2011) 10-22.
52. F. Wang, X. Zhou, S. Wang, Development processes and property measurements of moisture absorption and quick dry fabrics, *Fibres Text. East. Eur.* 17 (2009) 46-49.
53. D. Chen, L. Tan, H. Liu, F. Tang, J. Hu, Y. Li, Fabrication of fast-absorbing and quick-drying wool fabrics with good washing durability, *ChemSusChem.* 3 (2010) 1031-1035.
54. Q. Chen, D. Shou, R. Zheng, J. Fan, X. Wan, B. Fu, P. Ma, The moisture management and drying properties of weft knitted plating fabrics, *Fibers Polym.* 21 (2020) 1347-1354.
55. P. Gibson, D. Rivin, C. Kendrick, H.S. Gibson, Humidity-dependent air permeability of textile materials¹, *Text. Res. J.* 69 (1999) 311-317.
56. P.W. Gibson, M. Charmchi, Modeling convection/diffusion processes in porous textiles with inclusion of humidity-dependent air permeability, *Int. Commun. Heat Mass Transfer.* 24 (1997) 709-724.
57. A.H. Woodcock, Moisture transfer in textile systems, Part I, *Text. Res. J.* 32 (1962) 628-633.
58. F. Kar, J. Fan, W. Yu, Comparison of different test methods for the measurement of fabric or garment moisture transfer properties, *Meas. Sci. Technol.* 18 (2007) 2033.
59. J. Fan, X. Qian, New functions and applications of Walter, the sweating fabric manikin, *Eur. J. Appl. Physiol.* 92 (2004) 641-644.
60. A. O'cass, Fashion clothing consumption: antecedents and consequences of

- fashion clothing involvement, *Eur. J. Mark.* 38 (2004) 869-882.
61. F.M.D. Chequer, G.A.R. Oliveira, E.R.A. Ferraz, J.C. Cardoso, M.V.B. Zanoni, D.P. Oliveira, Textile dyes: dyeing process and environmental impact, *Eco-Friendly Text. Dyeing Finish.* 6 (2013) 151-176.
 62. D.J. Tyler, Textile digital printing technologies, *Text. Prog.* 37 (2005) 1-65.
 63. D. Zheng, Y. Han, J.L. Hu, A new method for classification of woven structure for yarn-dyed fabric, *Text. Res. J.* 84 (2014) 78-95.
 64. D. Sofronova, R.A. Angelova, Classification of digital stitch lines in machine embroidery, *Ind. Text.* 72 (2021) 538-544.
 65. D.J. Spencer, *Knitting technology: a comprehensive handbook and practical guide*, Woodhead Publishing, NJ 2001.
 66. P. Irawan, PhD Thesis, Cornell University 2008.
 67. J.J. Kim, K.I. Shin, H.S. Ryu, E.A. Kim, M. Lee, K.W. Oh, Luster properties of polyester filament yarn woven fabrics, *Text. Res. J.* 74 (2004) 72-77.
 68. E.S. ElNashar, F. Kalaoglu, M. Hashem, presented at XIII International Workshop Physics of Fibrous Materials: Structure, Properties, Science Intensive Technologies and Materials, Russia, May 2010.
 69. M.E. Hall, Finishing of technical textiles, *Handb. Tech. Text.* 12 (2000) 152.
 70. M.A. Bueno, B. Durand, M. Renner, Optical characterization of the state of fabric surfaces, *Opt. Eng.* 39 (2000) 1697-1703.
 71. K. Wells, presented at 2nd Int. Text. and Costume Congr. Bangkok, Thailand, Oct. 2013.
 72. R.A. Herard, Yesterday's Finishing Techniques Applied To Today's Fabrics, *Text. Chem. Color.* 11 (1979) 24.
 73. A. Kennedy, E.B. Stoehrer, J. Calderin, *Fashion design, referenced: A visual guide to the history, language, and practice of fashion*, Rockport Pub, NJ 2013.
 74. L. Volpintesta, *The language of fashion design: 26 principles every fashion designer should know*, Rockport Pub, NJ 2014.
 75. F.R. Fan, Z.Q. Tian, Z.L. Wang, Flexible triboelectric generator, *Nano energy.* 1

- (2012) 328-334.
76. D.J. Lacks, R.M. Sankaran, Contact electrification of insulating materials, *J. Phys. D.* 44 (2011) 453001.
 77. S. Wang, L. Lin, Z.L. Wang, Triboelectric nanogenerators as self-powered active sensors, *Nano Energy.* 11 (2015) 436-462.
 78. K. Dong, X. Peng, Z.L. Wang, Fiber/fabric-based piezoelectric and triboelectric nanogenerators for flexible/stretchable and wearable electronics and artificial intelligence, *Adv. Mater.* 32 (2020) 1902549.
 79. J. Chen, X. Wen, X. Liu, J. Cao, Z. Ding, Z. Du, Flexible hierarchical helical yarn with broad strain range for self-powered motion signal monitoring and human-machine interactive, *Nano Energy.* 80 (2021) 105446.
 80. Y. Cheng, X. Lu, K.H. Chan, R. Wang, Z. Cao, J. Sun, G.W. Ho, A stretchable fiber nanogenerator for versatile mechanical energy harvesting and self-powered full-range personal healthcare monitoring, *Nano Energy.* 41 (2017) 511-518.
 81. L. Zhang, C. Su, L. Cheng, N. Cui, L. Gu, Y. Qin, R. Yang, F. Zhou, Enhancing the performance of textile triboelectric nanogenerators with oblique microrod arrays for wearable energy harvesting, *ACS Appl. Mater. Interfaces.* 11 (2019) 26824-26829.
 82. C. Ye, D. Liu, X. Peng, Y. Jiang, R. Cheng, C. Ning, F. Sheng, Y. Zhang, K. Dong, Z.L. Wang, A hydrophobic self-repairing power textile for effective water droplet energy harvesting, *ACS nano.* 15 (2021) 18172-18181.
 83. F. Liang, X. Chao, S. Yu, Y. Gu, X. Zhang, X. Wei, J. Fan, X. Tao, D. Shou, An All-Fabric Droplet-Based Energy Harvester with Topology Optimization, *Adv. Energy Mater.* 12 (2022) 2102991.
 84. M. Zhu, Y. Huang, W.S. Ng, J. Liu, Z. Wang, Z. Wang, H. Hu, C. Zhi, 3D spacer fabric based multifunctional triboelectric nanogenerator with great feasibility for mechanized large-scale production, *Nano Energy.* 27 (2016) 439-446.
 85. L. Liu, J. Pan, P. Chen, J. Zhang, X. Yu, X. Ding, B. Wang, X. Sun, H. Peng, A triboelectric textile templated by a three-dimensionally penetrated fabric, *J. Mater.*

- Chem. A. 4 (2016) 6077-6083.
86. A. Yu, X. Pu, R. Wen, M. Liu, T. Zhou, K. Zhang, Y. Zhang, J. Zhai, W. Hu, Z.L. Wang, Core-shell-yarn-based triboelectric nanogenerator textiles as power cloths, *ACS nano*. 11 (2017) 12764-12771.
 87. X. Tian, T. Hua, Antibacterial, scalable manufacturing, skin-attachable, and eco-friendly fabric triboelectric nanogenerators for self-powered sensing, *ACS Sustain. Chem. Eng.* 9 (2021) 13356-13366.
 88. H. Li, S. Zhao, X. Du, J. Wang, R. Cao, Y. Xing, C. Li, A Compound Yarn Based Wearable Triboelectric Nanogenerator for Self-Powered Wearable Electronics, *Adv. Mater. Technol.* 3 (2018) 1800065.
 89. M. Lou, I. Abdalla, M. Zhu, X. Wei, J. Yu, Z. Li, B. Ding, Highly wearable, breathable, and washable sensing textile for human motion and pulse monitoring, *ACS Appl. Mater. Interfaces*. 12 (2020) 19965-19973.
 90. Q. He, Y. Wu, Z. Feng, W. Fan, Z. Lin, C. Sun, Z. Zhou, K. Meng, W. Wu, J. Yang, An all-textile triboelectric sensor for wearable teleoperated human-machine interaction, *J. Mater. Chem. A*. 7 (2019) 26804-26811.
 91. W. Fan, Q. He, K. Meng, X. Tan, Z. Zhou, G. Zhang, J. Yang, Z.L. Wang, Machine-knitted washable sensor array textile for precise epidermal physiological signal monitoring, *Sci. Adv.* 6 (2020) eaay2840.
 92. J. Gong, B. Xu, X. Guan, Y. Chen, S. Li, J. Feng, Towards truly wearable energy harvesters with full structural integrity of fiber materials, *Nano Energy*. 58 (2019) 365-374.
 93. L. Ma, R. Wu, S. Liu, A. Patil, H. Gong, J. Yi, F. Sheng, Y. Zhang, J. Wang, J. Wang, W. Guo, Z.L. Wang, A machine-fabricated 3D honeycomb-structured flame-retardant triboelectric fabric for fire escape and rescue, *Adv. Mater.* 32 (2020) 2003897.
 94. L. Ma, R. Wu, A. Patil, J. Yi, D. Liu, X. Fan, F. Sheng, Y. Zhang, S. Liu, S. Shen, J. Wang, Z.L. Wang, Acid and alkali-resistant textile triboelectric nanogenerator as a smart protective suit for liquid energy harvesting and self-powered monitoring

- in high-risk environments, *Advanced Functional Materials*. 31 (2021) 2102963.
95. C. Ye, S. Dong, J. Ren, S. Ling, Ultrastable and high-performance silk energy harvesting textiles, *Nanomicro Lett.* 12 (2020) 1-15.
 96. S. Dong, F. Xu, Y. Sheng, Z. Guo, X. Pu, Y. Liu, Seamlessly knitted stretchable comfortable textile triboelectric nanogenerators for E-textile power sources, *Nano Energy*. 78 (2020) 105327.
 97. F. Xu, S. Dong, G. Liu, C. Pan, Z.H. Guo, W. Guo, L. Li, Y. Liu, C. Zhang, X. Pu, Z.L. Wang, Scalable fabrication of stretchable and washable textile triboelectric nanogenerators as constant power sources for wearable electronics, *Nano Energy*. 88 (2021) 106247.
 98. S. Seyedin, S. Uzun, A. Levitt, B. Anasori, G. Dion, Y. Gogotsi, J.M. Razal, MXene composite and coaxial fibers with high stretchability and conductivity for wearable strain sensing textiles, *Adv. Funct. Mater.* 30 (2020) 1910504.
 99. H. Sun, K. Dai, W. Zhai, Y. Zhou, J. Li, G. Zheng, B. Li, C. Liu, C. Shen, A highly sensitive and stretchable yarn strain sensor for human motion tracking utilizing a wrinkle-assisted crack structure, *ACS Appl. Mater. Interfaces*. 11 (2019) 36052-36062.
 100. X. Li, T. Hua, B. Xu, Electromechanical properties of a yarn strain sensor with graphene-sheath/polyurethane-core, *Carbon*. 118 (2017) 686-698.
 101. R. Wu, S. Seo, L. Ma, J. Bae, T. Kim, Full-Fiber Auxetic-Interlaced Yarn Sensor for Sign-Language Translation Glove Assisted by Artificial Neural Network, *Nanomicro Lett.* 14 (2022) 1-14.
 102. Z. Zhang, S. Liu, M. Wu, S. Liu, Shape-adaptable and wearable strain sensor based on braided auxetic yarns for monitoring large human motions, *Appl. Mater. Today*. 35 (2023) 101996.
 103. B.A. Kuzubasoglu, E. Sayar, S.K. Bahadir, Inkjet-printed CNT/PEDOT: PSS temperature sensor on a textile substrate for wearable intelligent systems, *IEEE Sens. J.* 21 (2021) 13090-13097.
 104. C. Wang, X. Li, E. Gao, M. Jian, K. Xia, Q. Wang, Z. Xu, T. Ren, Y. Zhang,

- Carbonized silk fabric for ultrastretchable, highly sensitive, and wearable strain sensors, *Adv. Mater.* 28 (2016) 6640-6648.
105. M. Zhang, C. Wang, H. Wang, M. Jian, X. Hao, Y. Zhang, Carbonized cotton fabric for high-performance wearable strain sensors, *Adv. Funct. Mater.* 27 (2017) 1604795.
 106. H. Choi, J. Sun, B. Ren, S. Cha, J. Lee, B.M. Lee, J.J. Park, J.H. Choi, J.J. Park, 3D textile structure-induced local strain for a highly amplified piezoresistive performance of carbonized cellulose fabric based pressure sensor for human healthcare monitoring, *Chem. Eng. J.* 450 (2022) 138193.
 107. R. Polanský, R. Soukup, J. Řeboun, J. Kalčík, D. Moravcová, L. Kupka, M. Švantner, P. Honnerová, A. Hamáček, A novel large-area embroidered temperature sensor based on an innovative hybrid resistive thread, *Sens. Actuator A-Phys.* 265 (2017) 111-119.
 108. M.Z. Seyedin, J.M. Razal, P.C. Innis, G.G. Wallace, Strain-responsive polyurethane/PEDOT: PSS elastomeric composite fibers with high electrical conductivity, *Adv. Funct. Mater.* 24 (2014) 2957-2966.
 109. S. Seyedin, J.M. Razal, P.C. Innis, A. Jeiranikhameneh, S. Beirne, G.G. Wallace, Knitted strain sensor textiles of highly conductive all-polymeric fibers, *ACS Appl. Mater. Interfaces.* 7 (2015) 21150-21158.
 110. C. Fan, Y. Liu, Y. Zhang, A Universal, Highly Sensitive and Seamlessly Integratable Textile Resistive Strain Sensor, *Adv. Fiber Mater.* 6 (2024) 1152-1161.
 111. Z.L. Wang, J. Song, Piezoelectric nanogenerators based on zinc oxide nanowire arrays, *Science.* 312 (2006) 242-246.
 112. J. Koruza, H. Liu, M. Höfling, M.H. Zhang, P. Veber, (K, Na) NbO₃-based piezoelectric single crystals: Growth methods, properties, and applications, *J. Mater. Res.* 35 (2020) 990-1016.
 113. M. Peddigari, G.Y. Kim, C.H. Park, Y. Min, J.W. Kim, C.W. Ahn, J.J. Choi, B.D. Hahn, J.H. Choi, D.S. Park, A comparison study of fatigue behavior of hard and soft piezoelectric single crystal macro-fiber composites for vibration energy

- harvesting, *Sensors*. 19 (2019) 2196.
114. J. Hao, W. Li, J. Zhai, H. Chen, Progress in high-strain perovskite piezoelectric ceramics, *Mater. Sci. Eng. R Rep.* 135 (2019) 1-57.
 115. H. Lifi, C. Ennawaoui, A. Hajjaji, S. Touhtouh, S. Laasri, M. Yessari, M. Benjelloun, Sensors and energy harvesters based on (1-x) PMN-xPT piezoelectric ceramics, *Eur. Phys. J. Appl. Phys.* 88 (2019) 10901.
 116. B.O. Chen, H. Li, W. Tian, C. Zhou, PZT based piezoelectric sensor for structural monitoring, *J. Electron. Mater.* 48 (2019) 2916-2923.
 117. W. Qian, K. Zhao, D. Zhang, C.R. Bowen, Y. Wang, Y. Yang, Piezoelectric material-polymer composite porous foam for efficient dye degradation via the piezo-catalytic effect, *ACS Appl. Mater. Interfaces*. 11 (2019) 27862-27869.
 118. S.D. Mahapatra, P.C. Mohapatra, A.I. Aria, G. Christie, Y.K. Mishra, S. Hofmann, V.K. Thakur, Piezoelectric materials for energy harvesting and sensing applications: Roadmap for future smart materials, *Adv. Sci.* 8 (2021) 2100864.
 119. K. Dong, X. Peng, Z.L. Wang, Fiber/fabric-based piezoelectric and triboelectric nanogenerators for flexible/stretchable and wearable electronics and artificial intelligence, *Adv. Mater.* 32 (2020) 1902549.
 120. H.J. Sim, C. Choi, C.J. Lee, Y.T. Kim, G.M. Spinks, M.D. Lima, R.H. Baughman, S.J. Kim, Flexible, stretchable and weavable piezoelectric fiber, *Adv Eng Mater.* 17 (2015) 1270-1275.
 121. M. Baniasadi, J. Huang, Z. Xu, S. Moreno, X. Yang, J. Chang, M.A.Q. Lopez, M. Naraghi, M.M. Jolandan, High-performance coils and yarns of polymeric piezoelectric nanofibers, *ACS Appl. Mater. Interfaces*. 7 (2015) 5358-5366.
 122. L. Xue, W. Fan, Y. Yu, K. Dong, C. Liu, Y. Sun, C. Zhang, W. Chen, R. Lei, K. Rong, Q. Wang, A novel strategy to fabricate core-sheath structure piezoelectric yarns for wearable energy harvesters, *Adv. Fiber Mater.* 3 (2021) 239-250.
 123. T. Huang, S. Yang, P. He, J. Sun, S. Zhang, D. Li, Y. Meng, J. Zhou, H. Tang, J. Liang, G. Ding, X. Xie, Phase-separation-induced PVDF/graphene coating on fabrics toward flexible piezoelectric sensors, *ACS Appl. Mater. Interfaces*. 10

(2018) 30732-30740.

124. S. Ahn, Y. Cho, S. Park, J. Kim, J. Sun, D. Ahn, M. Lee, D. Kim, T. Kim, K. Shin, J.J. Park, Wearable multimode sensors with amplified piezoelectricity due to the multi local strain using 3D textile structure for detecting human body signals, *Nano Energy*. 74 (2020) 104932.
125. D.B. Kim, J. Han, S.M. Sung, M.S. Kim, B.K. Choi, S.J. Park, H.R. Hong, H.J. Choi, B.K. Kim, C.H. Park, J.H. Paik, J.S. Lee, Y.S. Cho, Weave-pattern-dependent fabric piezoelectric pressure sensors based on polyvinylidene fluoride nanofibers electrospun with 50 nozzles, *npj Flex. Electron*. 6 (2022) 69.
126. J. Wang, J. Jiu, M. Nogi, T. Sugahara, S. Nagao, H. Koga, P. He, K. Suganuma, A highly sensitive and flexible pressure sensor with electrodes and elastomeric interlayer containing silver nanowires, *Nanoscale*. 7 (2015) 2926-2932.
127. M. Gao, Z. Xia, X. Wang, J. Wang, P. Huang, Fabrication of a flexible capacitor sensor with surface-fabric-structured conductive silicon rubber, *Sens. Actuators A-Phys*. 295 (2019) 141-150.
128. A. Atalay, V. Sanchez, O. Atalay, D.M. Vogt, F. Haufe, R.J. Wood, C.J. Walsh, Batch fabrication of customizable silicone-textile composite capacitive strain sensors for human motion tracking, *Adv. Mater. Technol*. 2 (2017) 1700136.
129. Q. Zhang, Y.L. Wang, Y. Xia, P.F. Zhang, T.V. Kirk, X.D. Chen, Textile-only capacitive sensors for facile fabric integration without compromise of wearability, *Adv. Mater. Technol*. 4 (2019) 1900485.
130. T.J. Cuthbert, B.C. Hannigan, P. Roberjot, A.V. Shokurov, C. Menon, HACS: Helical Auxetic Yarn Capacitive Strain Sensors with Sensitivity Beyond the Theoretical Limit, *Adv. Mater*. 35 (2023) 2209321.
131. L. Liu, Y. Li, M. Xu, R. Tao, Q. Zhong, X. Yang, S. Lan, J. Xie, G. Chen, Y. Mao, W. Hu, Hybrid tribo/piezoelectric nanogenerator textile derived from 3D interlocked parallel-arranged yarns for bio-motion energy harvesting and tactile sensing, *Chem. Eng. J*. 474 (2023) 145866.
132. M. Zhu, Q. Shi, T. He, Z. Yi, Y. Ma, B. Yang, T. Chen, C. Lee, Self-powered and

- self-functional cotton sock using piezoelectric and triboelectric hybrid mechanism for healthcare and sports monitoring, *ACS nano*. 13 (2019) 1940-1952.
133. G. Kaur, J.S. Meena, M. Jassal, A.K. Agrawal, Hybrid piezo-capacitive multimodal sensors based on polyurethane–poly (vinylidene fluoride) nanofibers for wearable E-textiles, *ACS Appl. Electron. Mater.* 5 (2023) 3298-3308.
 134. M. Su, J. Fu, Z. Liu, P. Li, G. Tai, P. Wang, L. Xie, X. Liu, X. He, D. Wei, J. Yang, All-Fabric Capacitive Pressure Sensors with Piezoelectric Nanofibers for Wearable Electronics and Robotic Sensing, *ACS Appl. Mater. Interfaces*. 15 (2023) 48683-48694.
 135. X. Qu, J. Li, Z. Han, Q. Liang, Z. Zhou, R. Xie, H. Wang, S. Chen, Highly sensitive fiber pressure sensors over a wide pressure range enabled by resistive-capacitive hybrid response, *ACS nano*. 17 (2023) 14904-14915.
 136. T.T.N. Truong, J. Kim, High-performance resistive/capacitive pressure sensor applied on smart insoles detecting abnormal activity, *J. Appl. Polym. Sci.* 141 (2024) e55768.
 137. Z. Lin, Z. Wu, B. Zhang, Y.C. Wang, H. Guo, G. Liu, C. Chen, Y. Chen, J. Yang, Z.L. Wang, A triboelectric nanogenerator-based smart insole for multifunctional gait monitoring, *Adv. Mater. Technol.* 4 (2019) 1800360.
 138. Y. Ma, J. Ouyang, T. Raza, P. Li, A. Jian, Z. Li, H. Liu, M. Chen, X. Zhang, L. Qu, M. Tian, G. Tao, Flexible all-textile dual tactile-tension sensors for monitoring athletic motion during taekwondo, *Nano Energy*. 85 (2021) 105941.
 139. F. Wen, Z. Sun, T. He, Q. Shi, M. Zhu, Z. Zhang, L. Li, T. Zhang, C. Lee, Machine Learning Glove Using Self-Powered Conductive Superhydrophobic Triboelectric Textile for Gesture Recognition in VR/AR Applications, *Adv. Sci.* 7 (2020) 2000261.
 140. F. Wen, Z. Zhang, T. He, C. Lee, AI enabled sign language recognition and VR space bidirectional communication using triboelectric smart glove, *Nat. Commun.* 12 (2021) 5378.
 141. F. Li, H. Xue, X. Lin, H. Zhao, T. Zhang, Wearable temperature sensor with high

resolution for skin temperature monitoring, ACS Appl. Mater. Interfaces. 14 (2022) 43844-43852.

142. Y. Fang, Y. Zou, J. Xu, G. Chen, Y. Zhou, W. Deng, X. Zhao, M. Roustaei, T.K. Hsiai, J. Chen, Ambulatory Cardiovascular Monitoring Via a Machine-Learning-Assisted Textile Triboelectric Sensor, Adv. Mater. 33 (2021) 2104178.

Chapter 3: Conductive Chenille Yarn-based Triboelectric Carpet Fabrics for Smart Home Monitoring

3.1 Introduction

In recent years, the smart home industry has rapidly advanced due to innovations in computer technology and shifts in lifestyle. Smart homes encompass various functions such as appliance control, environmental monitoring, energy efficiency, emission reduction, and security alarms [1,2]. These features not only safeguard residents' lives and property but also enhance convenience and comfort. Currently, the most prevalent residential security measure is the installation of camera systems, which can identify unusual intruders and activities to preemptively address potential dangers [3,4]. However, camera surveillance is more suited to public areas than private homes, as they are vulnerable to hacking and can infringe on personal privacy [5]. Additionally, these systems may not quickly and accurately detect abnormal physical states of occupants, potentially leading to tragedies. Given the unique nature of individual behavior, smart home products with automatic sensing capabilities are better suited for monitoring indoor anomalies.

With advancements in textile technology, household fabrics like curtains and rugs can enhance both home aesthetics and safety [6,7]. Integrating sensors into these textiles allows for precise and secure monitoring without disrupting the environment [8]. In the realm of sensors, a diverse array exists, encompassing those with distinct mechanisms such as resistive [9,10], piezoresistive [11,12], capacitive [13,14], piezoelectric [15,16], and triboelectric [17,18]. Among these, flexible sensors founded on triboelectric nanogenerators (TENGs) are particularly notable for their simple structure and ease of production in smart home systems [19,20]. Research has explored textile TENGs (t-TENGs) for energy harvesting, motion monitoring, and hazard alerting in smart homes. Applications include sustainable power sources [21,22], self-powered switches [23],

motion-tracking smart floor arrays [24-28], anti-theft carpets [29], and fall detection carpets [30-32]. However, several challenges remain for practical implementation. Large-area polymer films or coatings can compromise the softness and breathability of sensing fabrics, making them unsuitable for daily use [25,26]. Xu's team developed coated core-spun strips with high triboelectric properties, assembling them into a smart monitoring carpet through manual interweaving [24,30], enhancing softness and durability. Unfortunately, this manual method is not scalable. While traditional textile techniques like weaving [28] and braiding [29] have improved production efficiency, current methods remain cumbersome. Thus, more efficient production strategies are needed for smart fabrics.

In this study, weft knitting technology was utilized to create a comfortable, warm, and intelligent sensory carpet fabric. By integrating machine learning, the carpet can recognize personal behavior and monitor home security. A special conductive chenille yarn was produced using fancy spinning technology as the primary raw material. Weft insertion technology was then employed to develop the chenille TENG (C-TENG). The TENG fabric consists of a high-elastic 1×1 rib base with chenille weft insertion, where the rib stitches securely encase the chenille yarn, and the short fibers form a comfortable suede texture. Lightweight, warm, and comfortable, this smart carpet fabric is both aesthetically pleasing and practical for indoor use. Crucially, it functions as a sensor for human motion and identity recognition, offering an effective strategy for smart home security systems.

3.2 Experimental Section

3.2.1 Materials

The silver (Ag)-plated nylon yarn, with a specification of 280D (indicating 280 grams per 9000 meters), was obtained from Qingdao Tianyin Textile Technology Co., Ltd.,

China. The 24S/2 acrylic yarn, which consists of two twisted single yarns where each is 24 times the length of 840 yards when the weight is one pound, was sourced from Dongguan Zhengyu Textile Co., Ltd., China. The high elastic nylon yarn (420D) was acquired from Dongguan Dalang Chen Shengli Yarn Shop, China. The coral velvet fabric was purchased from Ruixi Home Textiles, and the striped felt fabric was obtained from Dezhou Xinxiang Carpet Factory, both in China. The tufted fabric was provided by Jinmao Textile Co., Ltd., China.

3.2.2 Fabrication methods

Fabrication of the conductive chenille carpet fabric involved a sequential two-stage process: preparation of specialized conductive chenille yarn, followed by its integration into a knitted weft-inlay structure. The conductive chenille yarn was manufactured using a chenille spinning machine (SFM-A7, Kunshan Shun Feng Textile Co., Ltd., China), wherein two 280D Ag-plated nylon yarns functioned as lock yarns, while a 24S/2 acrylic yarn served as the pile yarn. During production, the acrylic yarn was first cut into short fibers and then sandwiched between two twisted conductive lock yarns to form the final chenille structure. Subsequently, the fabricated conductive chenille yarn was knitted together with a 420D nylon/spandex elastic yarn into a weft-inlay structure using a 7-gauge flat knitting machine. For electrical characterization, small samples were produced on a hand-operated knitting machine to accommodate testing requirements, whereas larger C-TENG carpet fabric specimens were manufactured using a computerized flat knitting machine (Stoll CMS 530) to achieve high efficiency. Structurally, the elastic yarn constituted a 1×1 rib stitch base layer, while the conductive chenille yarn was precisely inserted as a weft inlay-oriented linearly once per course and encapsulated between the rib loops within the fabric's medial layer. The high elasticity of the base yarn ensured the secure positioning of the chenille yarn. The protrusion of chenille feather yarn through the fabric pores created a hairiness effect on both sides of the fabric.

3.2.3 Physical and electrical characterization

A Leica microscope was utilized to capture enlarged images of the chenille yarn and fabric. SEM images of the yarns were obtained using a Tescan VEGA3 scanning electron microscope. The comfort properties of the fabric were tested using KES instruments (Kato Tech Co., Ltd., Japan) under the guidance of the KES operating manual. Specifically, the tactile properties were assessed with a KES-FB3 automatic compression tester and a KES-FB4 automatic surface tester, air permeability was measured using a KES-FB-AP1 air permeability tester, while warmth retention was evaluated with a KES-F7 THERMO LABO II. The electrical output of the C-TENG fabric was tested using a Keithley 6514 electrometer (USA), and a keyboard life tester (ZX-A03) manufactured by Shenzhen Zhongxingda Testing Equipment Co., Ltd. was employed to apply compression movements.

3.3 Results and Discussion

3.3.1 Design and fabrication of the C-TENG carpet fabric

Acrylic fiber is an ideal material for producing blankets or carpets due to its softness, bulkiness, lightweight nature, warmth retention, ease of washing and drying, and affordability. As depicted in Figure 3.1a, a specialized conductive chenille yarn is crafted using acrylic fiber to create the C-TENG carpet fabric. This chenille yarn is composed of conductive lock yarn and acrylic fiber. Two Ag-plated nylon yarns with low resistance (approximately $2 \Omega \text{ cm}^{-1}$) serve as the lock yarns, while bundles of short acrylic fibers are positioned in the middle in a cross shape by twisting the two lock yarns, forming the conductive chenille yarn. These chenille yarns are then inserted as weft inlay yarns into a 1×1 rib stitch made from high-elastic nylon yarn to construct the carpet fabric.

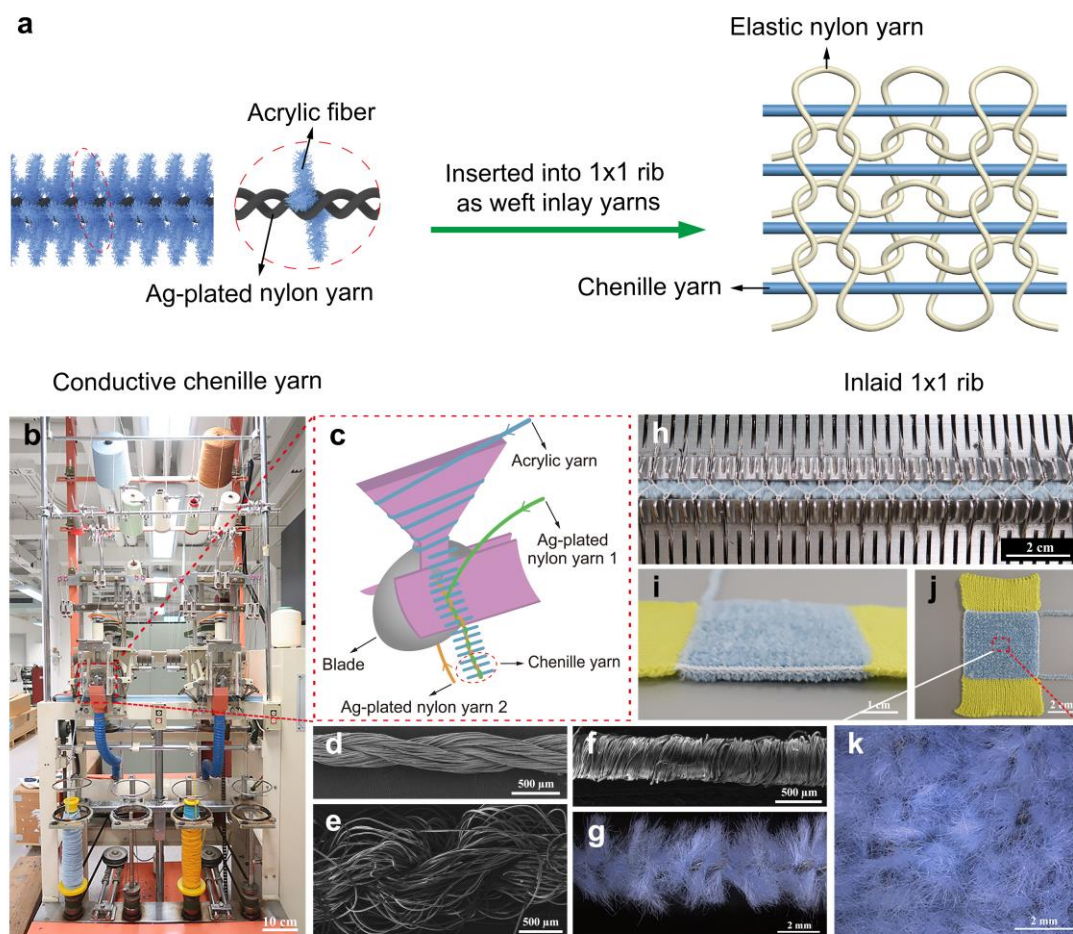


Figure 3.1 Preparation of the conductive chenille yarn and C-TENG. (a) Schematic diagram of the fabrication process. (b) Picture of the chenille spinning machine. (c) Schematic diagram of the blade device. SEM images of (d) Ag-plated nylon yarn, (e) acrylic yarn, and (f) elastic nylon yarn. (g) Enlarged photo of the conductive chenille yarn. (h) Photo of the C-TENG carpet fabric being knitted on the flat knitting machine. (i) Side view and (j) top view of the C-TENG fabric. (k) Enlarged photo of the fabric surface.

The chenille yarn was produced using a chenille spinning machine, as shown in Figure 3.1b. The blade device, illustrated in Figure 3.1c, played a crucial role in forming the chenille yarn. Initially, the acrylic yarn was cut into fiber bundles approximately 4 mm in length using the blade. Subsequently, two Ag-plated nylon yarns acted as lock yarns, twisting around the acrylic fiber bundles to create the chenille yarn, which was then

wound onto a bobbin. Figures 3.1d, e, and f present SEM images of the Ag-plated nylon yarn, acrylic yarn, and elastic nylon yarn, respectively. The acrylic yarn, made by twisting short fibers, tended to become hairy after cutting. In contrast, the Ag-plated yarn, composed of filaments, had a smooth surface and tight structure, effectively binding the acrylic staple fibers. The microscope image of the conductive chenille yarn (Figure 3.1g) clearly shows the secure clamping of acrylic fibers. The C-TENG carpet fabric sample was produced using a hand-operated weft knitting machine with a gauge of seven. Figure 3.1h illustrates the fabric being knitted on the machine. A complete course consisted of a row of 1×1 rib and a row of weft inlay. The white nylon elastic yarn formed the rib stitch by creating loops on the front and back needle beds sequentially, while the conductive chenille yarn was introduced as the weft inlay yarn in a straight line between the two needle beds until it was secured by the rib in the subsequent course unit. Through the repetition of multiple courses, the fabric gradually extended longitudinally, forming a complete fabric. Due to the high elastic shrinkage of the base stitch, the chenille yarn was tightly bound by the loops, allowing the short fibers to protrude from the loop gaps, resulting in a fluffy surface. Side-view and top-view photographs of the carpet fabric are shown in Figures 3.1i and j (the blue part in the middle). The enlarged photo in Figure 3.1k highlights the excellent surface hairiness coverage of the C-TENG carpet fabric.

3.3.2 Comfort performance of the C-TENG fabric

The C-TENG fabric was found to offer excellent comfort. For comparison, three conventional carpet fabrics-coral velvet, striped felt, and tufted fabric-were selected, as shown in Figure 3.2. The Kawabata Evaluation System (KES) was employed to evaluate the tactility, breathability, and warmth retention properties of these fabrics. Table 3.1 details the thickness, weight, air resistance, and warmth retention ratio for each fabric. The C-TENG fabric had the greatest thickness and weight, measuring approximately 6.87 mm and 997.63 g/m², respectively. The high elastic rib in the C-

TENG sensor fabric reduced porosity, resulting in an increased air resistance of 1.105 KPa·s/m. The Ag-plated core within the chenille yarn, known for its excellent thermal conductivity, was integrated into every loop course of the fabric, ensuring even distribution across the fabric's surface. This feature could have compromised the warmth retention of the C-TENG fabric. However, its substantial thickness and low air permeability allowed it to achieve a thermal retention rate of 56.57%, comparable to the other three fabrics. Overall, all fabrics demonstrated commendable thermal insulation, with warmth retention ratios exceeding 50%.

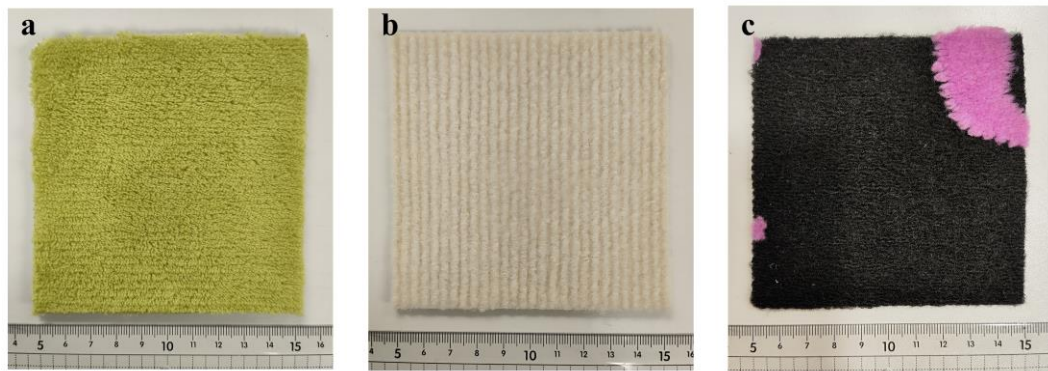


Figure 3.2 Photos of three conventional carpet fabrics. (a) Coral velvet fabric. (b) Striped felt fabric. (c) Tufted fabric.

Table 3.1 Basic parameters and physical properties of the C-TENG fabric and three conventional carpet fabrics.

Sample	Thickness (mm)	Weight (g/m ²)	Air resistance (KPa·s/m)	Warmth retention ratio
C-TENG	6.87 ± 0.10	997.63 ± 0.60	1.105 ± 0.006	56.57%
Coral velvet	3.44 ± 0.14	165.81 ± 0.75	0.080 ± 0.002	60.61%
Striped felt	5.66 ± 0.02	462.82 ± 0.92	0.060 ± 0.002	63.92%
Tufted	4.36 ± 0.05	307.38 ± 1.55	0.072 ± 0.003	64.95%

The KES test provided valuable insights into the fabric's tactile properties. Table 3.2 illustrates the output indicators of the four fabrics under compression and dynamic

friction tests, reflecting their hand feel. The compression test yielded three key indicators: LC, WC, and RC. LC, or compression linearity, indicates the softness of the fabric. WC, the specific work of compression, serves as a measure of fluffiness. RC, or compression resilience, reflects the fullness of the fabric. In dynamic friction testing, the indicators MIU, MMD, and SMD were measured. MIU represents the average coefficient of dynamic friction, with lower values indicating a smoother surface. MMD is the average deviation of the friction coefficient, where smaller values indicate better friction uniformity. SMD measures surface roughness, with smaller values indicating a more even surface. A comprehensive evaluation of subjective feel characteristics, quantified using these objective metrics, is displayed in Figure 3.3. Compared to the reference fabrics, the C-TENG fabric showed slightly lower softness and fullness due to the tightly bundled high-elastic ribbed base, which made it relatively rigid and harder to compress. Nevertheless, it maintained the second-highest level of fluffiness among the tested carpet fabrics. The striped felt fabric had the poorest surface uniformity and flatness due to its raised stripes. Although the C-TENG fabric exhibited a high dynamic friction coefficient due to the anisotropic arrangement of acrylic short fibers in the chenille yarn, it demonstrated excellent surface uniformity and flatness. In summary, the C-TENG fabric was both comfortable and warm, making it ideal for use as a light-duty thermal carpet in autumn and winter. When used on indoor floors, it could enhance aesthetics, provide practical daily functions, and offer sensing capabilities.

Table 3.2 Comparison of comfort parameters of four fabrics.

Sample	Compression			Friction (warp)			Friction (weft)		
	LC	WC (gf·cm/cm ²)	RC (%)	MIU	MMD	SMD (um)	MIU	MMD	SMD (um)
C-TENG	1.044	4.690	37.080	0.389	0.008	4.950	0.404	0.008	4.538
Coral velvet	0.663	3.819	54.920	0.345	0.006	7.448	0.323	0.006	7.937
Striped felt	0.920	4.830	54.213	0.345	0.015	8.913	0.297	0.011	11.283
Tufted	0.949	4.353	45.837	0.301	0.009	4.990	0.308	0.009	3.358

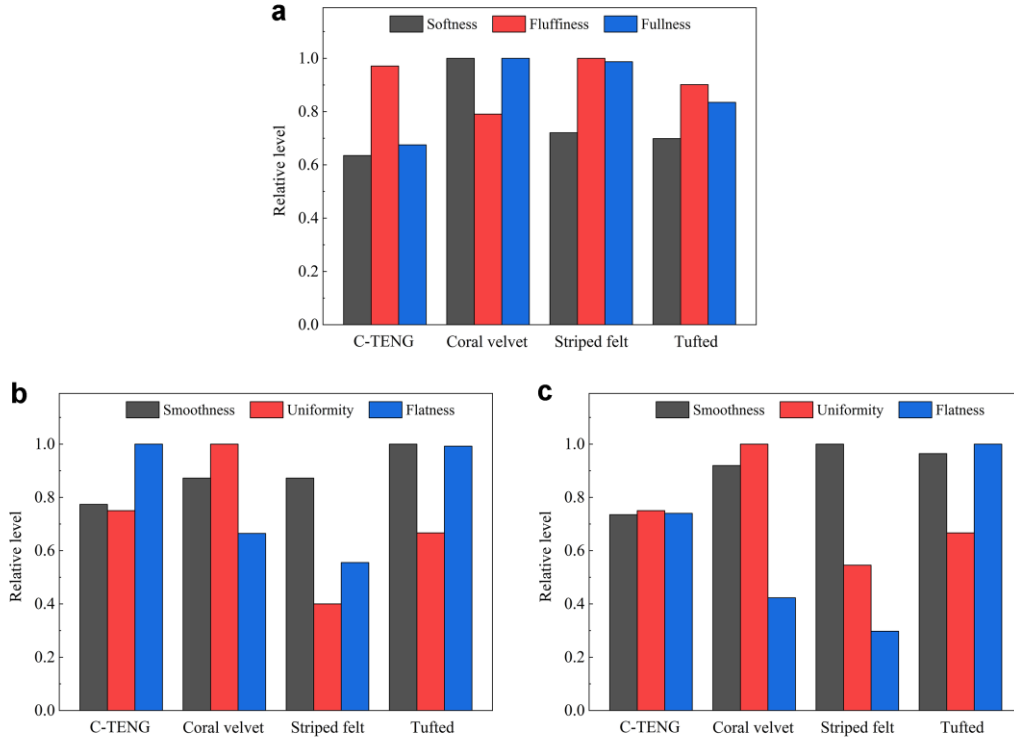


Figure 3.3 Comparison of the hand feel properties of four fabrics. (a) Softness, fluffiness, and fullness. (b) Warp surface characteristics. (c) Weft surface characteristics.

3.3.3 Working mechanism of the C-TENG fabric

Figure 3.4 illustrates the working mechanism of the chenille carpet fabric. Using common cotton material as an example, when a cotton object comes into contact with the surface of the carpet fabric (step I), electron transfer occurs between the surfaces of cotton and the acrylic fiber. In accordance with the triboelectric series, cotton loses electrons and accumulates positive charges on its surface, while acrylic gains electrons, resulting in an equal amount of negative charge on its surface. As the cotton object moves away from the carpet fabric, the increasing distance creates a potential difference between the upper and lower surfaces. To neutralize this potential difference, electrons are induced to flow between the conductor embedded in the TENG fabric and the reference ground, generating a current (step II). The circuit reaches a potential equilibrium when the cotton object is separated by a critical distance (step III). As the upper and lower surfaces move closer again, the decreasing distance reduces the

potential difference between them. To restore balance, a reverse flow of electrons, or reverse current, occurs between the electrode and the reference ground (step IV).

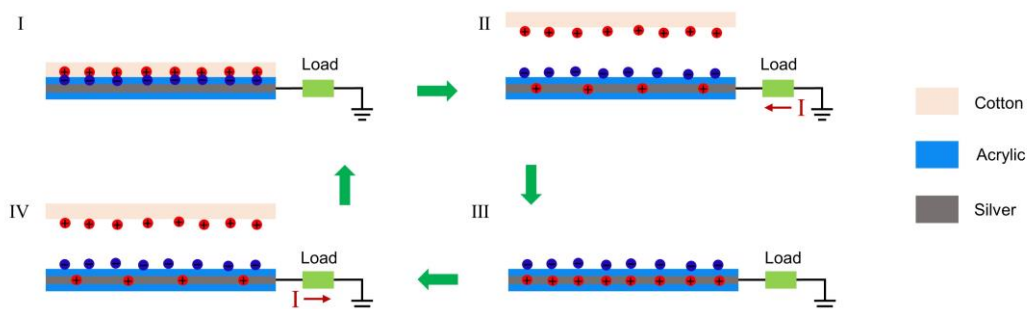


Figure 3.4 Working mechanism of the C-TENG.

3.3.4 Electrical performance of the C-TENG fabric

The electrical outputs generated by the contact-separation with various materials, including knitted cotton fabric, knitted polyethylene (PE) fabric, Kapton film, and PET film were evaluated. Each material was tested with a contact area of $5\text{ cm} \times 5\text{ cm}$ and a maximum separation distance of 1 cm. The tests varied in compression frequency (1 Hz, 2 Hz, and 3 Hz) and compression force (50 N, 100 N, and 200 N). Among these materials, PE fabric and PET film exhibited superior electrical output performance. Figures 3.5a and 3.5b display the voltage and current outputs at different frequencies under a 200 N force for the PE fabric and chenille fabric in contact-separation mode. Figures 3.5c and 3.5d illustrate the outputs at various forces with a frequency of 3 Hz. The electrical output increased with both force and frequency, achieving a peak voltage of approximately 39 V and a maximum current of about 375 nA at 200 N and 3 Hz. As the force increased, the contact between the two dielectric surfaces improved, leading to a higher surface charge density and enhanced output voltage and current. Although ideally, a faster frequency does not necessarily result in higher output voltage, in practice, the increased impact frequency of the pressing plate led to greater extrusion force at the contact moment, thereby increasing the induced charge density.

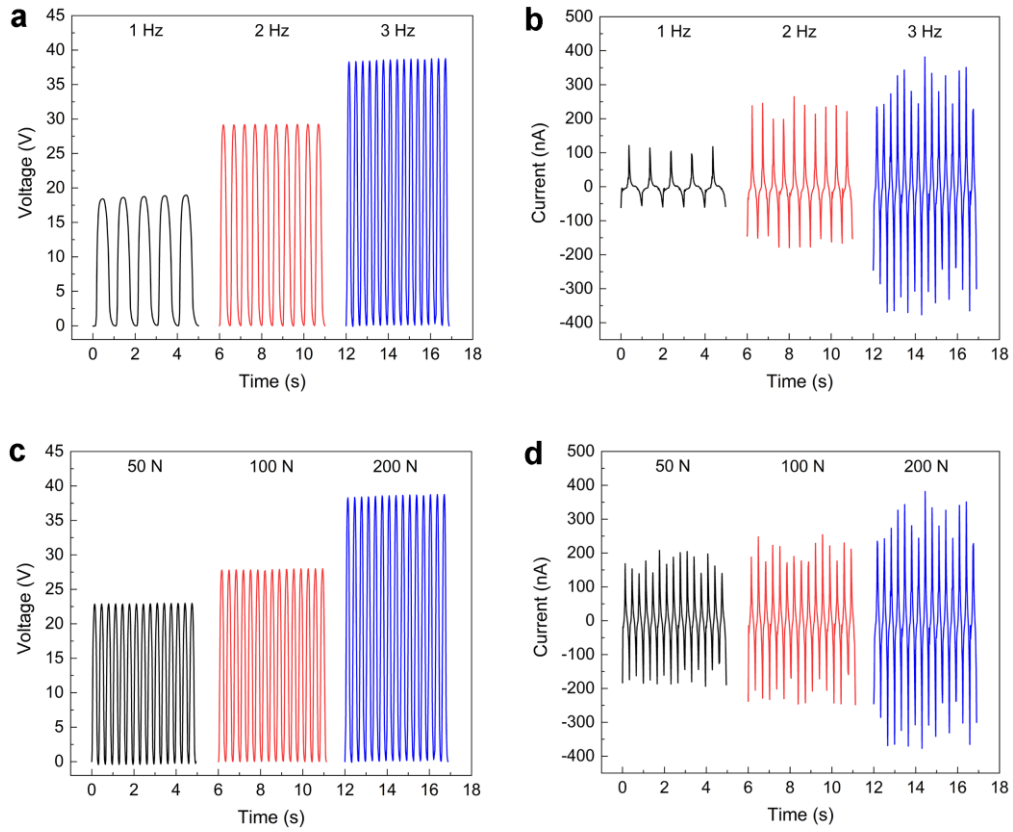


Figure 3.5 Electrical Output of the C-TENG rubbed against a PE fabric. (a) Output voltage and (b) current at different frequencies under the force of 200N. (c) Output voltage and (d) current with different forces at a frequency of 3 Hz.

Under a force of 200 N and a frequency of 3 Hz, the trend of output voltage and power density as load resistance increased is shown in Figure 3.6a, reaching a maximum power density of approximately $2942 \mu\text{W}/\text{m}^2$ at a resistance of $100 \text{ M}\Omega$. By connecting a simple circuit with a bridge rectifier and a capacitor ($10 \mu\text{F}$), this C-TENG was capable of powering small electronic devices, such as a calculator. Additionally, Figure 3.6b shows the voltage output generated by different contact materials under 200 N and 3 Hz. The triboelectric sequence and surface characteristics of the materials jointly determined the output intensity. For instance, although PET's triboelectric negative ordering is closer to that of acrylic fiber compared to PE, the dense micro-nano structure on the film's surface resulted in higher electrical output.

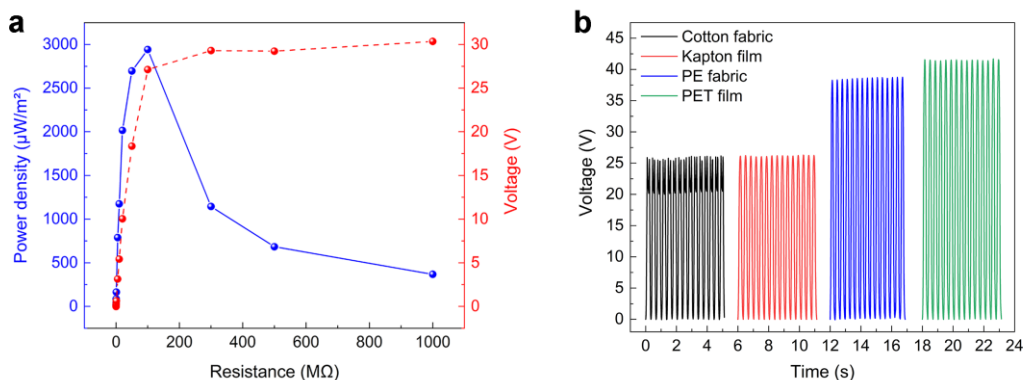


Figure 3.6 Electrical performance of the C-TENG. (a) Output voltage and power density of the C-TENG under different external resistances under 200N and 3 Hz. (b) Output voltage of the C-TENG with different contact materials under 200N and 3Hz.

Regarding stability, the long-term current output at 200 N and 3 Hz was tested using PE fabric as the contact material (Figure 3.7a). After approximately 5400 contact-separation cycles, the current output remained stable and even increased slightly compared to the initial stage. To assess the impact of washing on C-TENG's performance, the fabric sample was washed multiple times with clean water using the quick mode of a household washing machine. As shown in Figure 3.7b, washing affected the C-TENG fabric's output voltage, with the amplitude of output attenuation gradually decreasing with each wash. The performance degradation was about 19% after the first wash, followed by an additional 11.5% decrease after the third wash, and a further 5.8% decline after the fifth wash. Nonetheless, the overall performance remained substantial. Considering that routine cleaning of carpet fabrics primarily involves vacuuming and spot cleaning, with washing typically limited to once or twice a year, the current performance post-washing is adequate for practical use.

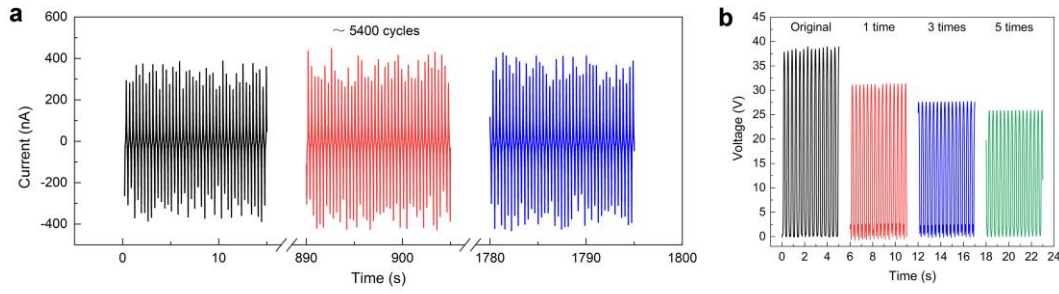


Figure 3.7 Stability and durability of the C-TENG. (a) Long-term current output of the C-TENG under 200 N and 3 Hz. (b) Output voltage of the C-TENG under 200N and 3 Hz after washing.

3.3.5 Sensing carpet for home security systems

A C-TENG carpet fabric measuring 23 cm \times 46 cm was produced using a computerized flat knitting machine. Like a traditional carpet, this fabric can be rolled and folded (Figure 3.8a). As illustrated in Figure 3.8b, when a person moves across the carpet, such as by walking, it generates electrical signals. These signals vary with different movements, allowing the sensory carpet to identify user behavior. For instance, Figure 3.8c displays the output signals from a volunteer performing various activities on the carpet, including slow walking, normal walking, jogging, and jumping. The current curves for each activity show significant differences in fluctuation period, amplitude, and slope, which are crucial for accurate behavior recognition. The potential for using this sensory carpet for individual identification was also investigated. Four participants, comprising two males and two females, participated in walking trials on the carpet fabric (Figure 3.8d). Variations in the electrical signals were influenced by factors such as foot size, weight, and walking habits. Details about the participants are provided in Table 3.3. However, the output data showed fewer distinguishing features between different users compared to the signals generated by different movements, making individual identification more challenging. Additionally, the study explored how various sole and sock materials affect signal identification, given the diverse range of footwear materials in everyday life. Specifically, two sole materials-rubber and

polyurethane (PU), and two sock materials-cotton and nylon, were tested. As shown in Figure 3.8e, the material primarily influenced the magnitude of the output current. For example, rubber generated a significantly higher current than the other materials due to its superior triboelectric properties and density.

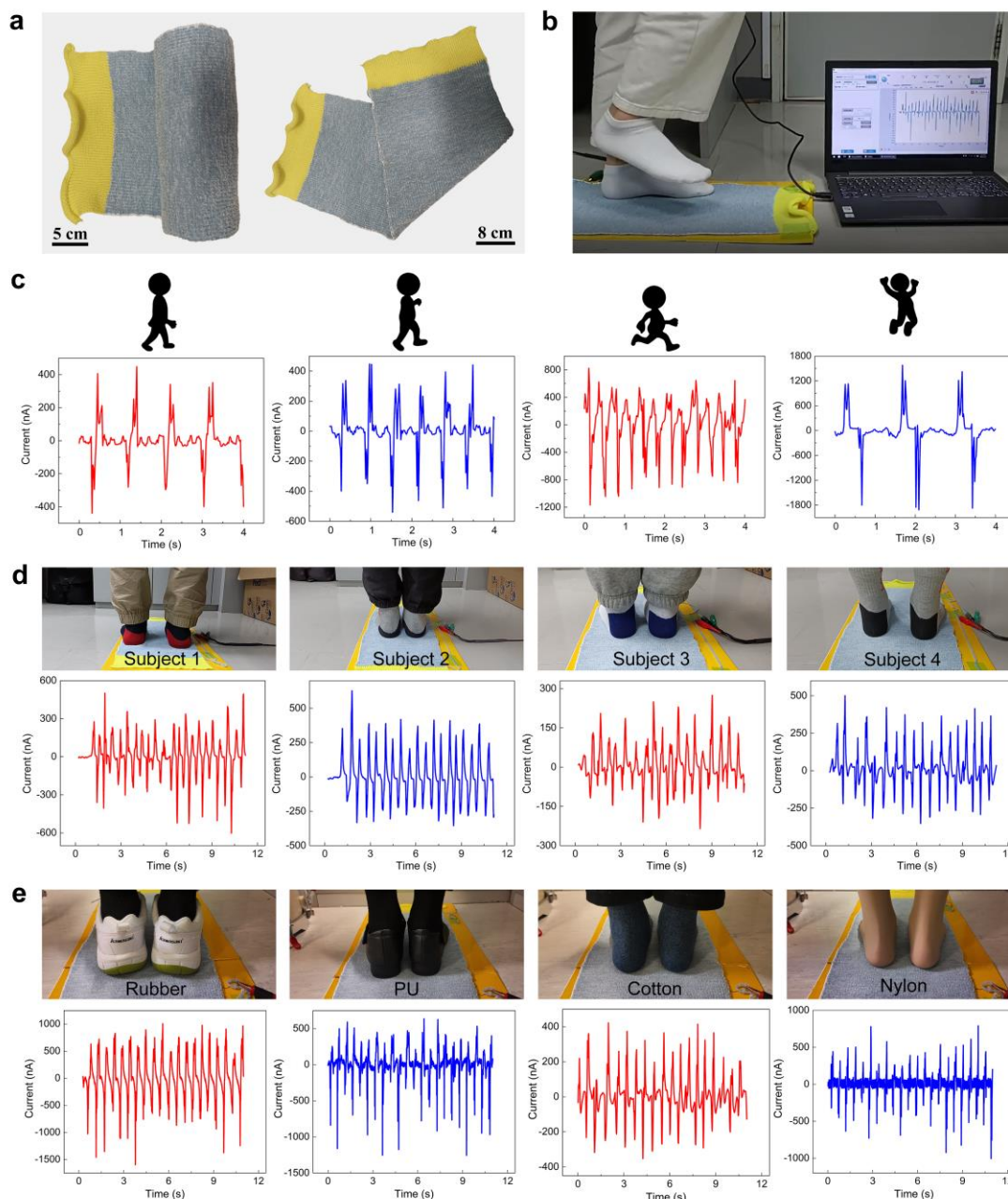


Figure 3.8 The C-TENG carpet fabric and its output under different motions and subjects. (a) Photos of the carpet fabric being rolled and folded. (b) Electrical signals produced when walking on the carpet. (c) Characteristics of the current signals under four behaviors (slow walking, walking, jogging, and jumping). (d) Photos of four

subjects standing on the carpet and the current signals generated by them. (e) Photos of soles and socks made of different materials and the current signals they generate.

Table 3.3 Information about four subjects involved in individual identification.

No.	Gender	Weight (kg)	Foot length (cm)
Subject 1	Male	64	26.0
Subject 2	Male	83	25.5
Subject 3	Female	56	23.5
Subject 4	Female	45	22.5

The deep learning-based time series data classification method effectively categorizes different signal data to enable the recognition of motion behaviors and user identities. Figure 3.9a presents a schematic flow chart of the employed method. Initially, the input time-correlated data is divided into multiple segments. Feature extraction and parameter reduction are then achieved through convolutional and pooling layers, respectively. Finally, classification is conducted using fully connected layers. The durations of the current-time signal data for four motions were recorded as follows: 373 seconds for slow walking, 500 seconds for normal walking, 335 seconds for jogging, and 145 seconds for jumping. For model training and testing, 80% of the data was allocated for training, while the remaining 20% was reserved for testing. The max-voting method was applied to predict the behavior of the input data by selecting the predominant class from all segments of the same time series data, yielding the final prediction result. Figure 3.9b illustrates the segment classification results for the four time series data. The correct classification rates for data segments were 83.3% for slow walking (U1), 81.8% for normal walking (U2), 96.7% for jogging (U3), and 55.6% for jumping (U4), achieving 100% recognition for the four behaviors. Regarding user identification, each subject's walking data was collected for 580 seconds, with 80% used for training and 20% for testing. Employing the same method as behavior

recognition, the segment classification results for four users are depicted in Figure 3.9c. The correct classification percentages were 50.0%, 41.7%, 50.0%, and 83.3%, respectively, which were sufficient to accurately identify the four subjects. Additionally, the C-TENG carpet successfully distinguished four different underfoot materials, as shown in Figure 3.9d. Real-world scenarios are more complex, with various factors such as behavior, user, and footwear materials often influencing the sensing output simultaneously. By controlling variables, the C-TENG carpet demonstrated significant potential for personal behavior recognition and individual identification, suggesting its applicability in home monitoring systems.

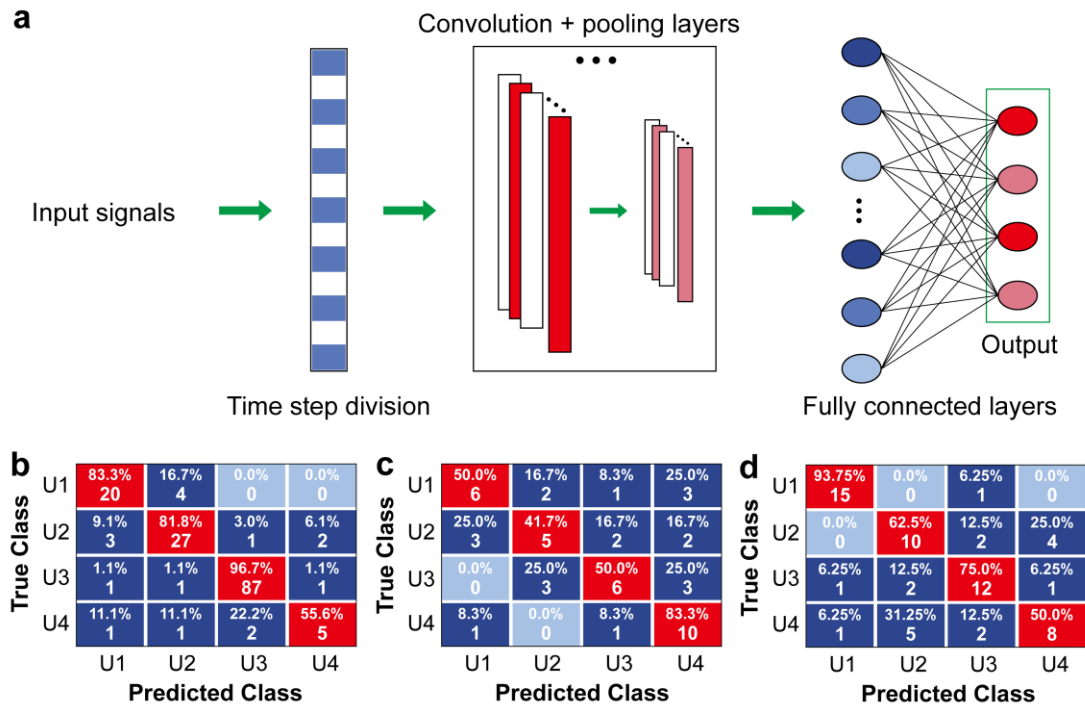


Figure 3.9 Motion behavior recognition and individual identification. (a) Schematic flowchart of the machine learning method. (b) Classification results of motion behavior recognition. (c) Classification results of individual identification. (d) Classification results for different sole and sock materials.

The C-TENG carpet fabric holds significant promise for integration into smart home monitoring systems. Future research should focus on enhancing its recognition capabilities to be more accurate and comprehensive. This can be achieved by gathering

extensive sample data and refining machine learning algorithms. By integrating wireless transmission and network technology, residents can receive real-time alerts about abnormalities through communication devices. As illustrated in Figure 3.10, the smart carpet, when placed on the floor, can be seamlessly integrated into a flexible home security system. It can perform functions such as intrusion detection, motion recognition, and safety monitoring, all while maintaining the comfort and aesthetics of the living environment.



Figure 3.10 Applications of the C-TENG carpet in smart home security systems.

3.4 Conclusion

In conclusion, this study presents the successful development of a sensor-integrated carpet system for ground motion monitoring, achieved through two key technological innovations: 1) the fabrication of conductive chenille yarn via fancy spinning and 2) the production of warm C-TENG carpet fabric using weft inlay technology. The resulting C-TENG fabric combines exceptional tactile comfort and soft texture with remarkable electrical performance, demonstrating a maximum power density of about $2942 \mu\text{W}/\text{m}^2$ under contact with PE fabric while maintaining stable output during extended operational periods. When integrated with machine learning algorithms, the system demonstrates robust capabilities for multimodal detection and recognition, including differentiation of human actions, individual identification, and material

characterization. These advanced functionalities, coupled with the fabric's inherent aesthetic qualities, position it as an ideal candidate for next-generation smart home surveillance and security applications.

Future research directions should focus on three key areas to advance this technology. First, material optimization represents a critical pathway for commercialization, as the current reliance on Ag-plated nylon yarn imposes significant cost constraints. Exploring alternative conductive materials, such as carbon-based fibers or conductive polymers, could substantially reduce production expenses while maintaining performance. Second, enhancing sensing accuracy through large-scale dataset acquisition and refinement of machine learning algorithms would improve the system's capability to discriminate between similar signals. Finally, comprehensive evaluation of environmental adaptability is essential, as real-world deployment exposes carpet fabrics to diverse conditions including humidity fluctuations, particulate contamination, thermal variations, soiling, and mechanical wear. Systematic investigation of these factors will be crucial to ensure reliable performance across various application scenarios and facilitate practical implementation.

References

1. R.J. Robles, T. Kim, Applications, systems and methods in smart home technology: A, *Int. J. Adv. Sci. Technol.* 15 (2010) 37-48.
2. B.L.R. Stojkoska, K.V. Trivodaliev, A review of Internet of Things for smart home: Challenges and solutions, *J. Cleaner Prod.* 140 (2017) 1454-1464.
3. T.D. Rätty, Survey on contemporary remote surveillance systems for public safety, *IEEE Trans. Syst. Man Cybern. Syst., C.* 40 (2010) 493-515.
4. A.B. Mabrouk, E. Zagrouba, Abnormal behavior recognition for intelligent video surveillance systems: A review, *Expert Syst. Appl.* 91 (2018) 480-491.
5. N. Kalbo, Y. Mirsky, A. Shabtai, Y. Elovici, The security of ip-based video surveillance systems, *Sensors* 20 (2020) 4806.
6. A.R. Horrocks, B.K. Kandola, P.J. Davies, S. Zhang, S.A. Padbury, Developments in flame retardant textiles-a review, *Polym. Degrad. Stab.* 88 (2005) 3-12.
7. C. Byrne, Technical textiles market—an overview, *Handb. Tech. Text.* (2000) 1-23.
8. S. Majumder, E. Aghayi, M. Noferesti, H.M. Tehran, T. Mondal, Z. Pang, M.J. Deen, Smart homes for elderly healthcare-Recent advances and research challenges, *Sensors* 17 (2017) 2496.
9. K.H. Kim, S.K. Hong, N.S. Jang, S.H. Ha, H.W. Lee, J.M. Kim, Wearable resistive pressure sensor based on highly flexible carbon composite conductors with irregular surface morphology, *ACS Appl. Mater. Interfaces.* 9 (2017) 17499-17507.
10. Y. Wang, J. Hao, Z. Huang, G. Zheng, K. Dai, C. Liu, C. Shen, Flexible electrically resistive-type strain sensors based on reduced graphene oxide-decorated electrospun polymer fibrous mats for human motion monitoring, *Carbon* 126 (2018) 360-371.
11. Z. Wang, S. Wang, J. Zeng, X. Ren, A.J.Y. Chee, B.Y.S. Yiu, W.C. Chung, Y. Yang, A.C.H. Yu, R.C. Roberts, A.C.O. Tsang, K.W. Chow, P.K.L. Chan, High sensitivity, wearable, piezoresistive pressure sensors based on irregular microhump structures and its applications in body motion sensing, *Small* 12 (2016) 3827-3836.
12. F. Ji, Z. Sun, T. Hang, J. Zheng, X. Li, G. Duan, C. Zhang, Y. Chen, Flexible

- piezoresistive pressure sensors based on nanocellulose aerogels for human motion monitoring: A review, *Compos. Commun.* 35 (2022) 101351.
13. L. Chen, M. Lu, H. Yang, J.R.S. Avila, B. Shi, L. Ren, G. Wei, X. Liu, W. Yin, Textile-based capacitive sensor for physical rehabilitation via surface topological modification, *ACS Nano* 14 (2020) 8191-8201.
 14. Y. Xiong, Y. Shen, L. Tian, Y. Hu, P. Zhu, R. Sun, C.P. Wong, A flexible, ultra-highly sensitive and stable capacitive pressure sensor with convex microarrays for motion and health monitoring, *Nano Energy* 70 (2020) 104436.
 15. Y. Yang, H. Pan, G. Xie, Y. Jiang, C. Chen, Y. Su, Y. Wang, H. Tai, Flexible piezoelectric pressure sensor based on polydopamine-modified BaTiO₃/PVDF composite film for human motion monitoring, *Sens. Actuators, A* 301 (2020) 111789.
 16. Y. Wang, Y. Yu, X. Wei, F. Narita, Self-powered wearable piezoelectric monitoring of human motion and physiological signals for the postpandemic era: a review, *Adv. Mater. Technol.* 7 (2022) 2200318.
 17. J. Luo, W. Gao, Z.L. Wang, The triboelectric nanogenerator as an innovative technology toward intelligent sports, *Adv. Mater.* 33 (2021) 2004178.
 18. Z.L. Wang, Triboelectric nanogenerator (TENG)—sparking an energy and sensor revolution, *Adv. Energy Mater.* 10 (2020) 2000137.
 19. W. Wang, A. Yu, X. Liu, Y. Liu, Y. Zhang, Y. Zhu, Y. Lei, M. Jia, J. Zhai, Z.L. Wang, Large-scale fabrication of robust textile triboelectric nanogenerators, *Nano Energy* 71 (2020) 104605.
 20. F. Xu, S. Dong, G. Liu, C. Pan, Z.H. Guo, W. Guo, L. Li, Y. Liu, C. Zhang, X. Pu, Z.L. Wang, Scalable fabrication of stretchable and washable textile triboelectric nanogenerators as constant power sources for wearable electronics, *Nano Energy* 88 (2021) 106247.
 21. S.A. Graham, S.C. Chandrarathna, H. Patnam, P. Manchi, J.W. Lee, J.S. Yu, Harsh environment-tolerant and robust triboelectric nanogenerators for mechanical-energy harvesting, sensing, and energy storage in a smart home, *Nano Energy* 80

- (2021) 105547.
22. M. Salauddin, S.M.S. Rana, M. Sharifuzzaman, M.T. Rahman, C. Park, H. Cho, P. Maharjan, T. Bhatta, J.Y. Park, A novel MXene/Ecoflex nanocomposite-coated fabric as a highly negative and stable friction layer for high-output triboelectric nanogenerators, *Adv. Energy Mater.* 11 (2021) 2002832.
 23. S.M.S. Rana, M.T. Rahman, M. Salauddin, S. Sharma, P. Maharjan, T. Bhatta, H. Cho, C. Park, J.Y. Park, Electrospun PVDF-TrFE/MXene nanofiber mat-based triboelectric nanogenerator for smart home appliances, *ACS Appl. Mater. Interfaces.* 13 (2021) 4955-4967.
 24. C. Jiang, C.L. Lai, B. Xu, M.Y. So, Z. Li, Fabric-rebound triboelectric nanogenerators with loops and layered structures for energy harvesting and intelligent wireless monitoring of human motions, *Nano Energy* 93 (2022) 106807.
 25. Q. Shi, Z. Zhang, Y. Yang, X. Shan, B. Salam, C. Lee, Artificial intelligence of things (AIoT) enabled floor monitoring system for smart home applications, *ACS Nano* 15 (2021) 18312-18326.
 26. Q. Shi, Z. Zhang, T. He, Z. Sun, B. Wang, Y. Feng, X. Shan, B. Salam, C. Lee, Deep learning enabled smart mats as a scalable floor monitoring system, *Nat. Commun.* 11 (2020) 4609.
 27. Y. Wang, Z. Hu, J. Wang, X. Liu, Q. Shi, Y. Wang, L. Qiao, Y. Li, H. Yang, J. Liu, L. Zhou, Z. Yang, C. Lee, M. Xu, Deep Learning-Assisted Triboelectric Smart Mats for Personnel Comprehensive Monitoring toward Maritime Safety, *ACS Appl. Mater. Interfaces.* 14 (2022) 24832-24839.
 28. L. Ma, R. Wu, S. Liu, A. Patil, H. Gong, J. Yi, F. Sheng, Y. Zhang, J. Wang, J. Wang, W. Guo, Z.L. Wang, A machine-fabricated 3D honeycomb-structured flame-retardant triboelectric fabric for fire escape and rescue, *Adv. Mater.* 32 (2020) 2003897.
 29. Y. Gao, Z. Li, B. Xu, M. Li, C. Jiang, X. Guan, Y. Yang, Scalable core-spun coating yarn-based triboelectric nanogenerators with hierarchical structure for wearable energy harvesting and sensing via continuous manufacturing, *Nano*

Energy 91 (2022) 106672.

30. M.Y. So, B. Xu, Z. Li, C.L. Lai, C. Jiang, Flexible corrugated triboelectric nanogenerators for efficient biomechanical energy harvesting and human motion monitoring, Nano Energy 106 (2023) 108033.
31. S.B. Jeon, Y.H. Nho, S.J. Park, W.G. Kim, I.W. Tcho, D. Kim, D.S. Kwon, Y.K. Choi, Self-powered fall detection system using pressure sensing triboelectric nanogenerators, Nano Energy 41 (2017) 139-147.
32. A. Yu, W. Wang, Z. Li, X. Liu, Y. Zhang, J. Zhai, Large-scale smart carpet for self-powered fall detection, Adv. Mater. Technol. 5 (2020) 1900978.

Chapter 4: Flexible and Freely Cuttable Fleecy Triboelectric Fabrics for Ultra-High Scalability in Self-Powered Sensing Applications

4.1 Introduction

Driven by the remarkable progress in materials science and computer technologies, flexible sensors have witnessed widespread applications in diverse sectors, such as wearable technology, medical health monitoring, robotic systems, and human-computer interfaces [1,2]. These sensing devices are usually fabricated by integrating conductive elements onto flexible substrates like polymer films [3-5], gels [6-8], and textiles (either fibers or fabrics) [9-12], thus endowing them with flexibility. Among these, textile-based flexible sensors hold great promise for market growth. Firstly, textile-material-based sensors can be smoothly integrated into products including apparel [13,14], upholstery fabrics [15,16], and bedding fabrics [17,18]. This unobtrusive integration not only enhances the user experience through a more natural and aesthetically appealing combination but also allows for a seamless presence. Secondly, the innate softness and breathability of textile materials enable these sensors to reduce skin irritation to a minimum and maximize comfort, which is especially beneficial for long-term use. Thirdly, certain designs of textile flexible sensors are designed to endure laundering, a vital characteristic for regular use and maintenance. Finally, compared with traditional silicon-based sensors, the manufacturing costs of textile flexible sensors are substantially lower, rendering them more viable for large-scale production and broader distribution.

At present, a wide variety of textile-based flexible sensors have been reported, encompassing resistive [19-21], capacitive [22-24], triboelectric [25-27], and piezoelectric [28-30] types. These sensors are predominantly manufactured by affixing

conductive functional materials to fibers or fabrics through techniques like coating [31,32], dipping [33,34], chemical vapor deposition [35,36], and printing [37,38]. The fabrication processes of these methods can be complex, and the incorporation of conductive layers might have an adverse effect on the softness and breathability of the textiles. Some approaches form functional structures by compounding with conductive polymer layers or metal layers [39,40], which severely impairs the inherent comfort of textiles, rendering them less suitable for practical usage. Additionally, certain research has employed established textile industry techniques, such as core-sheath wrapping or core-spinning, to produce conductive core-shell yarns for sensor applications [41-43]. Although these methods are highly viable for mass production, their production efficiency is still relatively restricted. A fur-like knitted triboelectric nanogenerator fabric, manufactured using well-established industrial production methods, can be efficiently produced on a large scale [44]. Nevertheless, the applications of such thick, fur-like textiles are significantly constrained. Consequently, there is an urgent requirement to develop thin sensor fabrics that are not only amenable to efficient, large-scale production but also have a wider range of applications.

In this work, we have devised a mass-production approach for fleecy TENG fabrics by leveraging commercially accessible raw materials and three-thread fleecy knitting technology. This technique enables an extraordinarily high production rate of around 11.53 m²/h. The resultant fabric retains a bulky and comfortable tactile property, along with excellent flexibility, adaptability, and permeability. It is designed to harvest energy from compressive frictional interactions, attaining a maximum power density of approximately 2446 $\mu\text{W}/\text{m}^2$ when rubbed against a cotton fabric. This textile can be freely cut into any shape and utilized as a self-powered flexible sensor in numerous applications. For example, it can be used as an insole for monitoring motion patterns and energy capture and a carpet for tracking movement postures. When integrated with deep-learning algorithms, the fleecy TENG fabric is capable of performing a broad range of sensing and identification tasks, thereby paving the way for the development

of cost-effective, highly adaptable, and extremely comfortable flexible sensors.

4.2 Experimental Section

4.2.1 Materials

The 100D Ag-plated nylon yarn was procured from Qingdao Tianyin Textile Technology Co., Ltd., located in China. The 24S/2 acrylic yarn was acquired from Dongguan Zhengyu Textile Co., Ltd., China. Additionally, the 32S cotton yarn was obtained from Weifang Qimian Spinning Co., Ltd.

4.2.2 Fabrication methods

The fleecy TENG fabric was directly fabricated in a single step using an 18-gauge three-thread fleecy knitting machine (Jumberca, Spain), employing exclusively commercially available yarns without post-processing. The 24S/2 acrylic yarn was selected as the material for the fleecy component. The 100D Ag-plated nylon yarn was chosen to serve as the tie-in yarn, while the 32S cotton yarn was utilized as the face yarn. At regular intervals, the fleecy yarn was held in place by the tie-in yarn and the face yarn, thereby generating a thick and compact fleecy appearance on one side of the fabric.

4.2.3 Characterization and testing

For the determination of fabric weight, an electronic balance (SHIMADZU BX 300) was implemented. The thickness of the fabric was gauged by means of a RME5 thickness tester. To obtain enlarged photographic images of the fleecy TENG fabric, a Leica microscope was employed. The scanning electron microscope (Tescan VEGA3) was used to acquire SEM images of the yarns. The hand feel of the fabric was evaluated using the KES-FB2 pure bending tester and the KES-FB3 automatic compression tester.

The air permeability was examined with the KES-FB-AP1 air permeability tester. The electrical output of the fleecy TENG fabric was tested by an electrometer (Keithley 6514, USA). Compression movements were provided by a keyboard life tester (ZX-A03). Additionally, the washing tests were carried out with the utilization of a home washing machine (Whirlpool 6th sense).

4.3 Results and Discussion

4.3.1 Structural features and fabrication process of the fleecy TENG fabric

The structure of the fleecy TENG fabric is presented in Figure 4.1a. The acrylic yarn (fleecy yarn) is clamped at regular intervals (a space of three needles) by the Ag-plated nylon yarn (tie-in yarn) and the cotton yarn (face yarn), creating a fleecy effect on one side of the fabric. As depicted in Figure 4.1b, it was manufactured on a three-thread fleecy knitting machine. The operational principle of this machine is grounded in single-face circular knitting, where the interaction between the needles in the needle cylinder and the yarns leads to the formation of the fabric. In the fabrication process, three main feeders were utilized: the fleecy yarn feeder, the tie-in yarn feeder, and the face yarn feeder. By passing the selected yarn materials through these three feeders, the fleecy TENG fabric was successfully produced. Operating at a standard production speed of 43 rpm, the machine can generate approximately 11.53 square meters of fleecy TENG fabric per hour. An enlarged photograph of the fleecy side (Figure 4.1c) shows that the acrylic fleecy fully covers the fabric surface. The acrylic yarn demonstrates a relatively fluffy and disordered spatial arrangement of fibers (Figure 4.1d). This arrangement is more effective in enhancing friction compared to a neat, parallel structure. Moreover, as shown in Figure 4.1e, each acrylic fiber exhibits a diameter of merely a dozen microns and is characterized by rough surface grooves. Such traits augment the specific surface area of the fleecy yarn, consequently bolstering both the frictional and electrification phenomena. In the fabric structure, the cotton yarn and the

Ag-plated nylon yarn collaboratively constitute the substrate loops, with the cotton yarn positioned on the face side (Figure 4.1f). A cross-sectional view presented in Figure 4.1g uncovers the internal arrangement of the three yarns, manifesting a sandwich-like configuration where the conductive material lies in the middle. Notably, the fleecy yarn assumes a wavy, arched contour. Through measurement of ten adjacent fleecy yarns, it has been ascertained that their average length expands by around 1.38 times in comparison to their straightened state. This expansion further amplifies the effective surface area of the entire fleecy surface. As a result, this structural idiosyncrasy substantially augments the output efficiency. To assess whether the fluffy fleecy surface alone contributes to the triboelectric output without the influence of other factors, a plain-knitted fabric made from the same acrylic yarn was prepared. Additionally, a simple TENG with an area of $5\text{ cm} \times 5\text{ cm}$ was fabricated using conductive copper tape and polyester tape. This generator was then subjected to compressive friction with the two fabrics. It was observed that the voltage output for the fleecy surface was approximately 29 V, while the plain-knitted surface yielded about 25.2 V. The current outputs were approximately 154 nA and 140 nA, respectively. The fleecy surface demonstrated a 10% to 15% improvement in triboelectric output performance compared to the common flat plain-knitted surface. In addition, as shown in Figure 4.1h, the conductive yarn used is a twisted assembly of multiple Ag - plated nylon filaments. This configuration ensures excellent flexibility and conductivity, with a resistance of around $2\ \Omega/\text{cm}$.

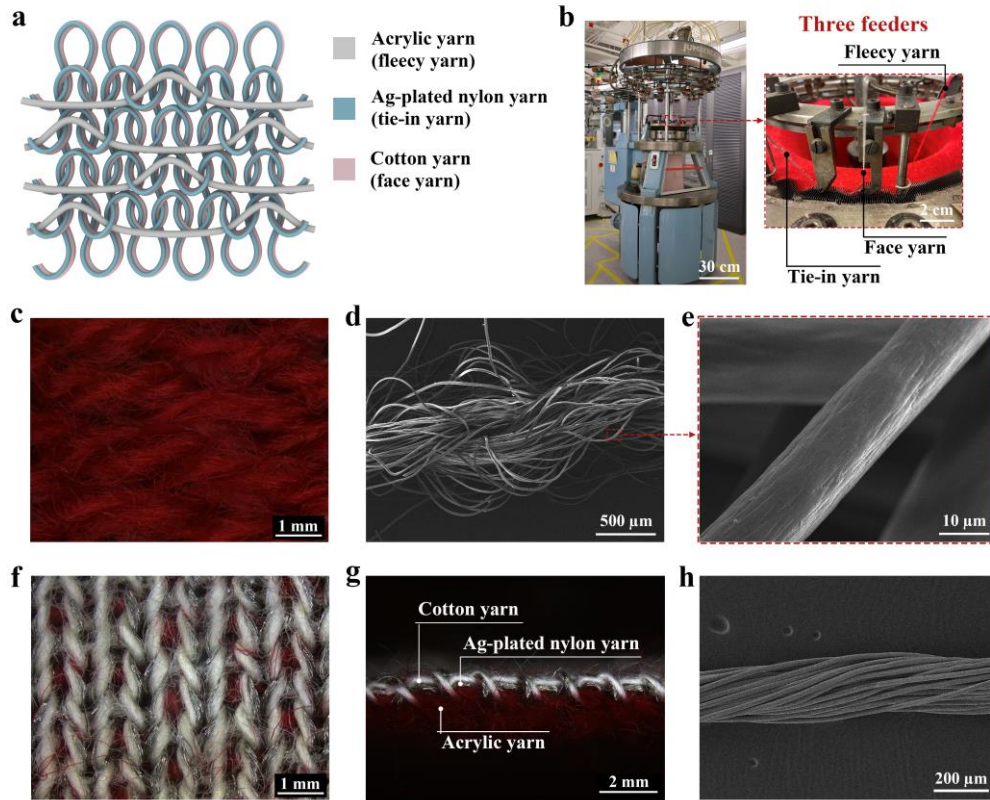


Figure 4.1 Fabrication of the fleecy TENG fabric. (a) Schematic diagram of the fleecy fabric structure. (b) Photos of the three-thread fleecy machine and its knitting work area. (c) Enlarged photo of the fleecy side. SEM images of (d) acrylic yarn and (e) single fiber. Enlarged photos of (f) substrate side surface and (g) cross side. (h) SEM image of Ag-plated nylon multifilament.

4.3.2 Basic parameters and physical properties

The fundamental parameters and physical properties of the fleecy TENG fabric were analyzed and evaluated, and the results are presented in Table 4.1. In the horizontal (course) direction, the fleecy TENG fabric showed a loop density of 20 wales/inch, while in the vertical (wale) direction, it was 38 courses/inch. The fabric had a thickness of 1.96 mm, and its weight and air resistance were measured as 263.89 g/m² and 0.054 kPa·s/m, respectively. Additionally, the TENG fabric was contrasted with two commercially available fleecy fabrics for sweatshirts (the photos of the three fabrics are

illustrated in Figure 4.2). Due to its sparser gauge, the fleecy TENG fabric presented the lowest loop density, which indicated better breathability. However, it also had the largest thickness and a moderate weight, because of the application of thicker yarns.

Table 4.1 Basic parameters and breathability properties of three fabrics.

Sample	Course density (wales/inch)	Wale density (courses/inch)	Thickness (mm)	Weight (g/m ²)	Air resistance (kPa·s/m)
Fleecy TENG	20	38	1.96 ± 0.01	263.89 ± 1.20	0.054 ± 0.001
Commercial fabric 1	28	45	1.06 ± 0.01	252.47 ± 3.39	0.174 ± 0.007
Commercial fabric 2	29	43	1.36 ± 0.01	295.67 ± 3.01	0.221 ± 0.007

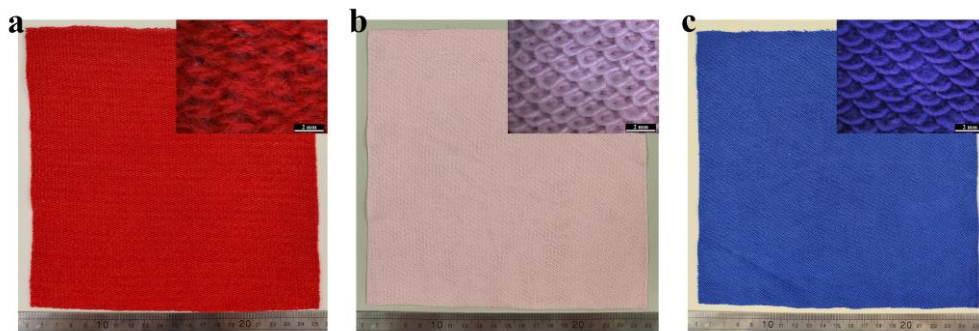


Figure 4.2 Photos of three fleecy fabrics. (a) Fleecy TENG fabric. (b) Commercial fabric 1. (c) Commercial fabric.

The tactile qualities of the TENG fabric underwent evaluation through bending and compression tests with the utilization of the Kawabata Evaluation System (KES). For each of these tests, measurements were taken in three separate areas. In the bending tests carried out in the wale direction (as shown in Figure 4.3a) and the course direction (depicted in Figure 4.3b), it became apparent that, in contrast to the other two fabrics,

the fleecy TENG fabric manifested a stronger resistance to bending. This was evidenced by the necessity for a greater force. The existence of the course fleecy yarns notably augmented the stiffness of all three fabrics during course bending (wherein the fleecy yarn was bent), in comparison to wale bending (where the fleecy yarn remained unbent). Moreover, when the fabric was bent in the wale direction, the load required for bending toward the loop side (represented by the upper right curve) was substantially smaller than that for bending toward the fleecy side (indicated by the lower left curve). This disparity was due to the lack of obstruction from the fleecy yarns. The bending test furnished two principal evaluation parameters: bending stiffness B and bending hysteresis moment $2HB$ (with the specific values provided in Table 4.2). A diminished bending stiffness implies a fabric that is softer and more malleable, whereas a lower bending hysteresis moment suggests an easier restoration from bending distortion. The compression curves are illustrated in Figure 4.3c, and the test generated three indices: LC, RC, and WC, which respectively mirror the softness, fullness, and fluffiness of the fabric (the specific values are presented in Table 4.2). A thorough comparison of the hand-feel characteristics of the three fabrics was achieved by dissecting each evaluation metric (as demonstrated in Figure 4.3d). In general, the fleecy TENG fabric exhibited enhanced fullness and fluffiness, along with an augmented resistance to bending attributable to its thickness. Concurrently, it still retained a gentle tactile perception.

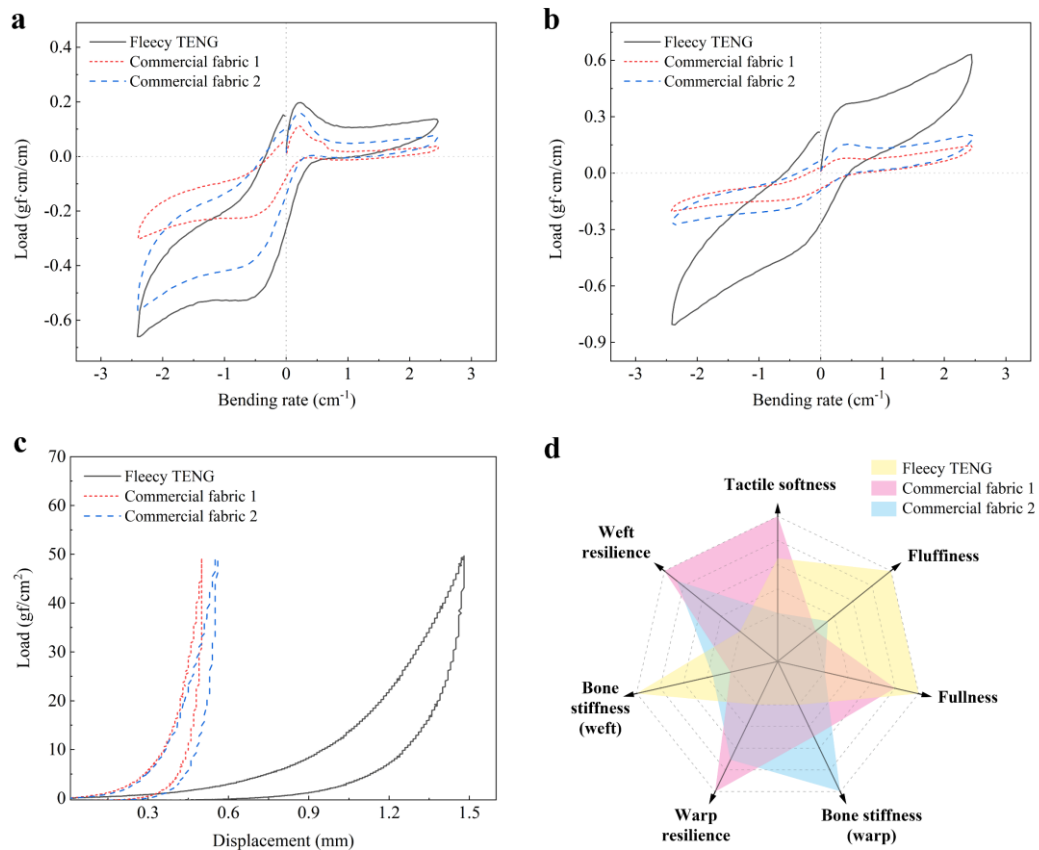


Figure 4.3 Results of KES compression and bending tests. (a) Wale bending curves and (b) course bending curves. (c) Load-displacement curves under compression. (d) Capability comparison radar chart of the hand-feel attributes of the three fabrics.

Table 4.2 Comparison of comfort parameters of three fabrics.

Sample	Compression			Wale bending		Course bending	
	LC	WC (gf·cm/cm ²)	RC (%)	B	2HB	B	2HB
Fleecy TENG	0.616	1.953	42.893	0.011	0.241	0.063	0.329
Commercial fabric 1	0.530	0.590	40.937	0.015	0.079	0.015	0.072
Commercial fabric 2	0.729	0.814	35.133	0.022	0.139	0.024	0.114

4.3.3 Working mechanism of the fleecy TENG fabric

The generation of triboelectric energy by the fleecy TENG fabric principally occurs through its contact with other materials. The fundamental mechanism underlying the production of electrical energy via compressive contact between a cotton fabric and the fleecy TENG fabric is illustrated in Figure 4.4. In the initial stage of interaction, when the cotton fabric comes into contact with the acrylic fleecy yarns of the TENG fabric (Step I), static charges of opposite polarities are acquired on the surfaces of these disparate materials. In accordance with the triboelectric series, cotton discharges electrons, leading to the presence of positive charges on its surface. Conversely, acrylic absorbs electrons, thus obtaining an equal quantity of negative charge. As the cotton and the fleecy TENG fabric start to separate, an increasing distance between them gives rise to a potential difference. To counterbalance this potential difference, electrons flow between the Ag conductive layer of the fleecy TENG fabric and a reference ground (with zero potential), thereby generating an electric current (Step II). Once the cotton and the fleecy TENG fabric have been separated to a specific distance, the circuit attains electrostatic equilibrium (Step III). Subsequently, when the two fabrics move closer to each other again, the diminishing distance lessens the potential difference. To adapt to this new potential difference, electrons flow in the reverse direction between the electrode and the reference ground, resulting in a reverse current (Step IV).

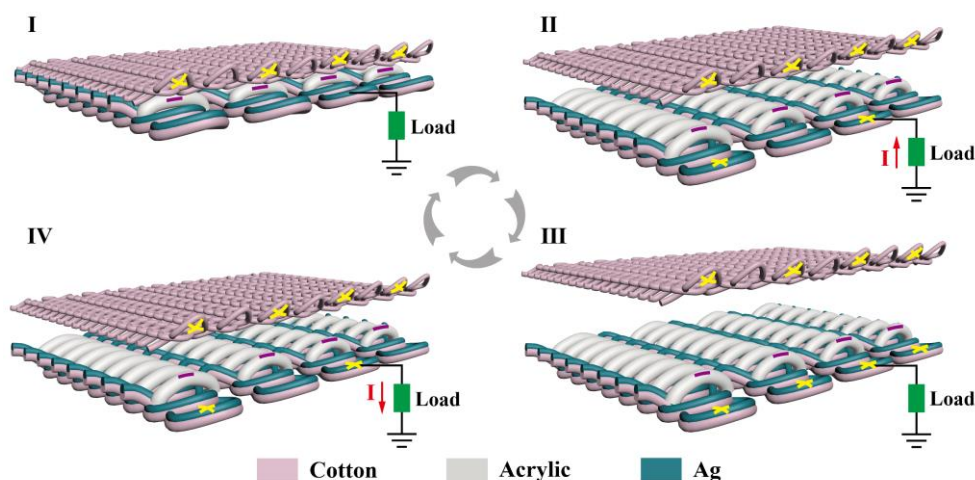


Figure 4.4 Working mechanism of the fleecy TENG fabric. (I) Initial Contact. (II)

Separation in Progress. (III) Equilibrium State of Separation. (IV) Reapproaching Phase.

4.3.4 Output performance of the fleecy TENG fabric

The electrical output of the fleecy TENG fabric operating in the contact-separation mode was evaluated, with a cotton fabric serving as the triboelectric counterpart. The evaluation was carried out under six distinct frequencies ranging from 0.5 Hz to 3 Hz and three compression forces varying from 50 N to 200 N. Throughout the tests, a constant contact area of 5 cm \times 5 cm was maintained, along with a maximum separation distance of 1 cm. Figures 4.5a and b present the voltage and current outputs at different frequencies when a 200 N force was applied. It was observed that, generally, the electrical output augmented with increasing frequency. Nevertheless, beyond 2 Hz, the voltage either plateaued or exhibited a slight decline. Contrary to the ideal assumption that frequency has no impact on electrical output, practical tests revealed that alterations in frequency could trigger instantaneous pressure fluctuations upon impact with the fleecy TENG fabric, subsequently influencing the electrical output. Moreover, the electrical output was found to rise with increasing pressure. Specifically, the voltage climbed from 5.5 V at 50 N to 10.2 V at 200 N (as shown in Figure 4.5c), and the current doubled from 100 nA to 200 nA (depicted in Figure 4.5d).

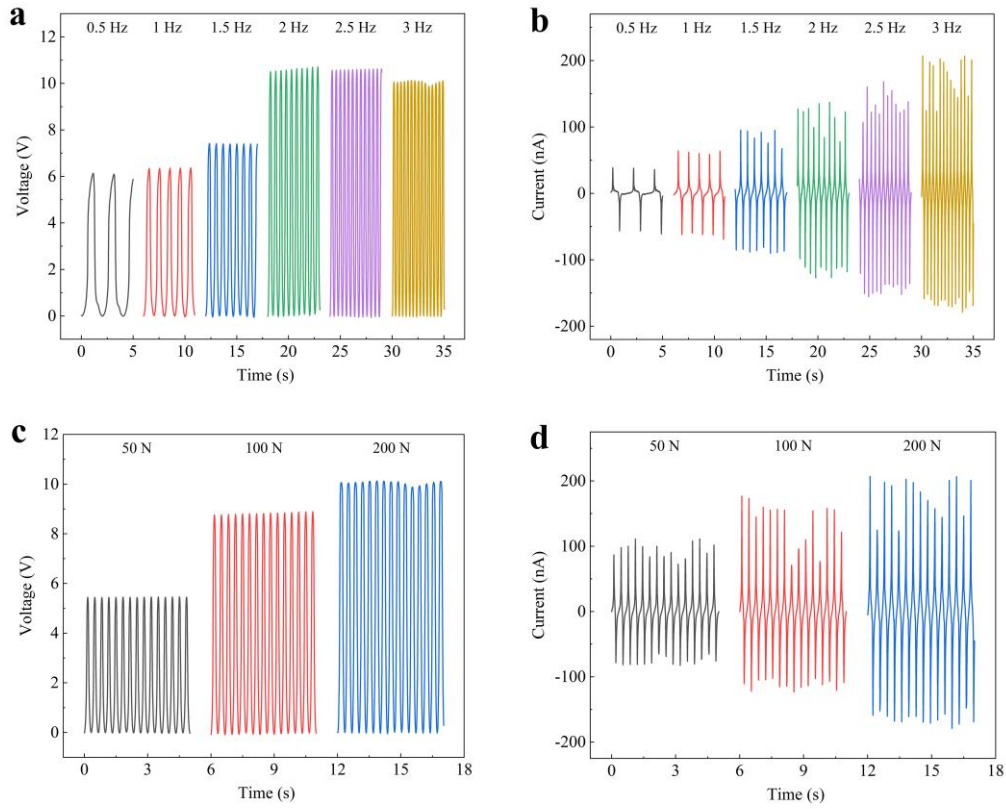


Figure 4.5 Electrical output of the fleecy TENG fabric rubbed against a cotton fabric. (a) Output voltage and (b) current at different frequencies under a compression force of 200 N. (c) Output voltage and (d) current under different compression forces at a frequency of 3 Hz.

The variation trends of output voltage and power density with the escalation of load resistance are illustrated in Figure 4.6a, peaking at a power density of around 2446 $\mu\text{W}/\text{m}^2$ when the resistance was 50 $\text{M}\Omega$. In addition, the electrical output of knitted fabrics crafted from diverse materials, namely cotton, polyethylene (PE), polyester (PET), and nylon, during contact-separation with the fleecy TENG fabric was also examined (Figure 4.7). Among them, nylon fabric exhibited the highest electrical output, attaining a voltage of approximately 30 V under the conditions of 200 N and 3 Hz (as demonstrated in Figure 4.6b), which was in line with the triboelectric series.

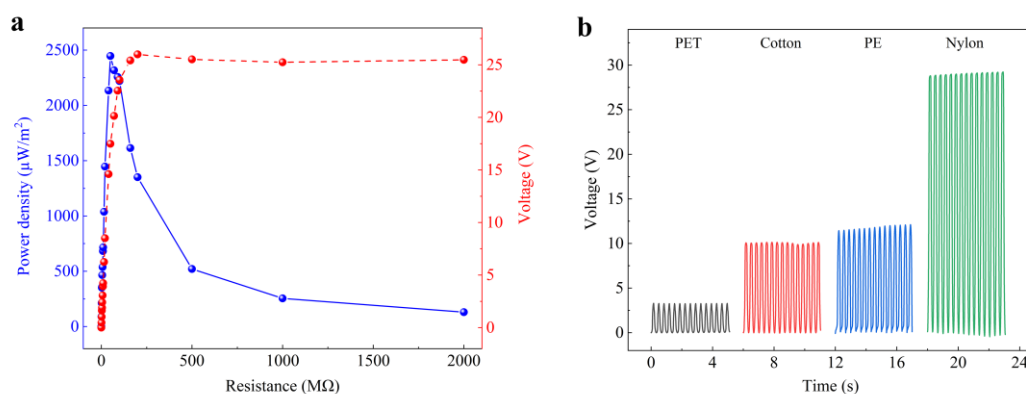


Figure 4.6 Electrical performance of the fleecy TENG fabric. (a) Output voltage and power density under different external resistances under 200 N and 3 Hz. (b) Output voltage with different contact materials under 200 N and 3Hz.

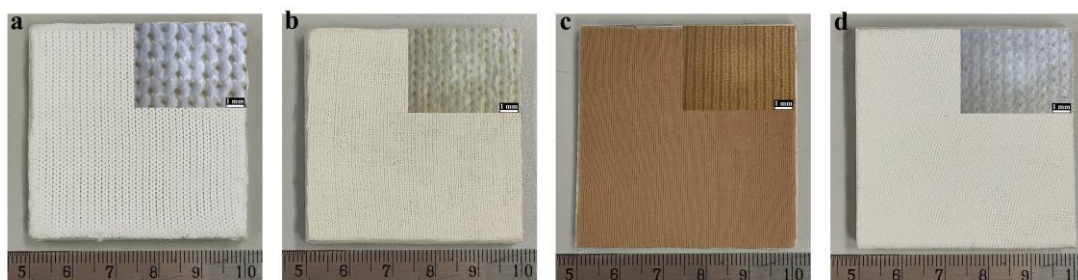


Figure 4.7 Photos of different knitted fabrics used for rubbing against the fleecy TENG fabric. (a) Polyethylene fabric. (b) Cotton fabric. (c) Nylon fabric. (d) Polyester fabric.

To gauge the stability and durability of the power-generating fabric, its output was tested after extended operation and multiple washing cycles. Figure 4.8a reveals that upon approximately 10,000 contact-separation cycles, the current output exhibited not only stability but also a progressive increment. This augmentation is presumably attributable to the accumulation of charges and the formation of a denser surface structure consequent to repeated compression, which promotes more efficacious contact. Six identically sized samples were excised from the fleecy fabric and subjected to a varying number of washing cycles. The washing regimen adhered to the ISO 6330:2021 standard, and each sample was thoroughly desiccated subsequent to the final wash. The outcomes demonstrated that the output voltage augmented with successive

wash cycles, initially escalating from approximately 10 V to around 30 V after three washes (as depicted in Figure 4.8b), which suggested that the washing process does not impair the structural integrity and functionality of the fabric. Instead, washing may have enhanced the fabric's performance through several mechanisms. First, mechanical friction during the washing process likely induced micro-scratches on the fiber surfaces, increasing their roughness. Second, washing removed residual additives (e.g., spinning oil) from the fabric production process, resulting in softer fibers that facilitated closer contact during friction (as evidenced by the SEM images before and after washing in Figure 4.9). Finally, physical damage from water washing may have generated additional charge traps (e.g., lattice defects and vacancies) within the material, delaying charge recombination and thereby enhancing the output. However, after the fourth wash cycle, the output voltage showed a slight decrease, likely due to the detachment of acrylic staple fibers from the fabric surface and enhanced fiber hydrophilicity caused by repeated washing and oil removal, which promoted moisture absorption from the surrounding environment. Overall, the net effect of water washing on electrical output was determined by the interplay of these competing factors, with the dominant mechanism dictating the final performance. In general, standard washing procedures do not seem to substantially compromise the structural integrity or functionality of this fleecy fabric. Such findings hold great promise for the practical application of this type of power-generating fabric.

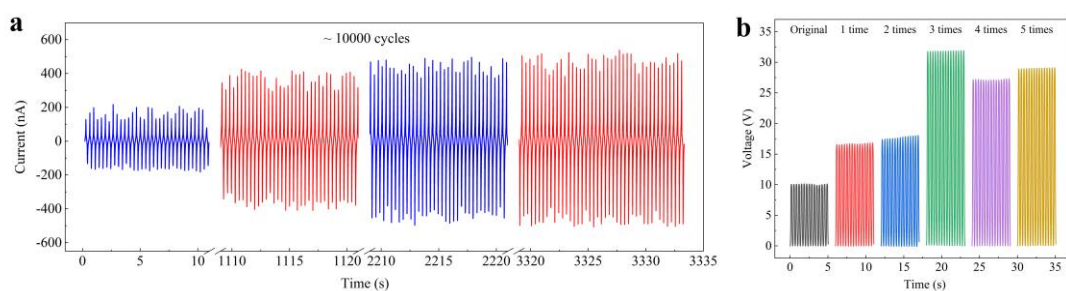


Figure 4.8 Stability and durability of the fleecy TENG fabric. (a) Current output under 10,000 contact-separation cycles at 200 N and 3 Hz. (b) Output voltage under 200 N and 3 Hz after different washing times.

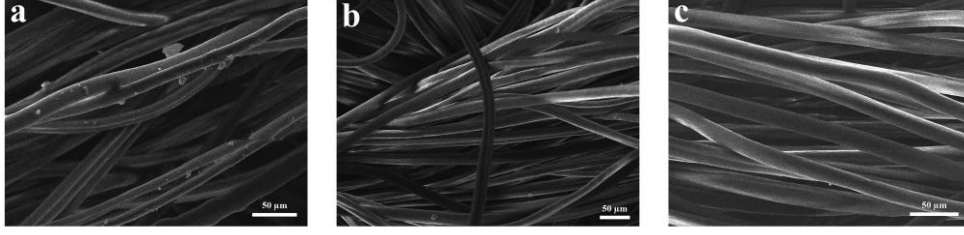


Figure 4.9 SEM images of fleecy TENG fabric before and after washing. (a) Unwashed. (b) Washed once. (c) Washed three times.

4.3.5 Applications of the fleecy TENG fabric

The fleecy TENG fabric possesses the capacity to harvest mechanical energy, which can then be utilized to power small electronic devices. By employing a simple rectifier circuit (depicted in Figure 4.10a), the harvested energy is transformed into practical electrical power. Figure 4.10b showcases the charging performance of capacitors with diverse specifications when the $5\text{ cm} \times 5\text{ cm}$ fleecy TENG fabric is rubbed against cotton fabric under the conditions of 200 N and 3 Hz. Commercial capacitors having capacitances of 0.47, 1, 3.3, 4.7, and $10\text{ }\mu\text{F}$ can be charged to 3 V within 44, 90, 304, 584, and 998 seconds, respectively. Furthermore, this fabric can function as a self-powered sensor for monitoring a variety of activities. It notably presents the benefit of high customizability, enabling it to be cut into any preferred shape to fulfill specific requirements. As an illustration, through cutting and hemming processes, the fabric was fabricated into a pair of insoles (as shown in Figure 4.10c). When inserted into sports shoes (Figure 4.10d), these sensing insoles are capable of generating electrical output signals with distinctive characteristics corresponding to different sports modalities. Figure 4.10e presents the output voltage signals under three types of movement: tiptoeing, walking, and jumping, each of which displays clearly distinguishable signal traits, such as amplitude, frequency, and the morphology of peaks and troughs. A convolutional neural network (CNN), which was specifically designed for time-series classification, was adopted as the deep learning model to conduct a more profound analysis of the signals generated by three distinct behaviors. These behaviors included

tiptoeing, walking, and jumping, and the dataset was composed of voltage readings corresponding to these activity classes. To prepare the data, a sliding window technique was employed. With a window size of 3 seconds and a step size of 1 second, each data sample was processed to generate sequences of a fixed length, aiming for 30 samples per window. In total, 600 seconds of data were collected for each behavior and then divided into 600 data segments (where the interval step = 1 s and the segment length = 3 s). The CNN model was structured with three convolutional layers. After each convolutional layer, ReLU activation and max-pooling were applied. Eventually, it concluded with a fully connected layer for classifying the data into the three aforementioned categories. The training process was carried out using the Adam optimizer. The learning rate was set at 0.005, the batch size was 64, and the cross-entropy loss function was utilized as the objective function. The dataset was partitioned such that 80% was allocated for training and 20% for testing. The model underwent training over 5 epochs. During this process, the loss was recorded, and at the end of each epoch, the accuracy was evaluated on the test set. All the experiments were implemented by leveraging Python and PyTorch. The results as well as the model weights were saved to facilitate further analysis and ensure reproducibility. The recognition results, as depicted in Figure 4.10f, demonstrated classification accuracies of up to 99.2% for tiptoeing (U1), 100% for walking (U2), and 99.2% for jumping (U3). Moreover, the fleecy TENG fabric demonstrates significant potential in home security monitoring applications, like smart carpets and bed sheets. It can also achieve an aesthetically pleasing appearance through careful yarn color matching and fabric shaping. This versatility highlights its broad applicability across a multitude of fields.

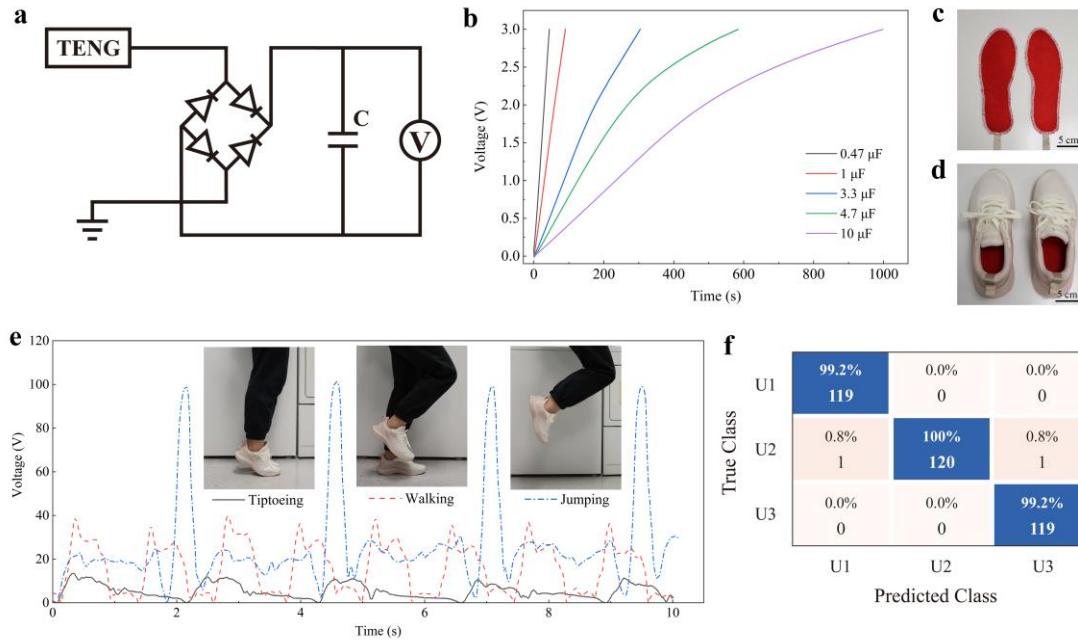


Figure 4.10 Application demonstration of the fleecy TENG fabric. (a) Circuit diagram for charging a capacitor. (b) Curves for charging commercial capacitors of various specifications. (c) A pair of insoles made from fleecy TENG fabric and (d) sports shoes with smart insoles placed. (e) Differential signals output under three motions: tiptoeing, walking, and jumping. (f) Recognition and classification results of three motions based on deep learning.

4.4 Conclusion

This study presents a novel one-step fabrication method for three-thread fleecy TENG fabric using industrial-scale fleecy knitting technology, achieving a remarkable production efficiency of 11.53 m^2/h . The as-developed fabric exhibits exceptional characteristics: 1) superior physical properties including high breathability, excellent flexibility, outstanding washability, and optimal tactile comfort; 2) outstanding electrical performance with a peak power density of 2446 $\mu\text{W}/\text{m}^2$ when interfaced with cotton, sufficient to power various microelectronic devices; and 3) remarkable design flexibility enables arbitrary cutting and shaping into diverse products without compromising functionality, significantly expanding its potential for customized sensing applications.

The practical applicability of the fabric was experimentally validated through its fabrication into functional insole prototypes. When coupled with a deep learning algorithm, this product effectively served as a self-powered motion sensor capable of precise footstep recognition and gait pattern identification. Beyond this proof-of-concept demonstration, the developed fleecy TENG fabric demonstrates significant potential for diverse applications, ranging from sports science and healthcare monitoring to smart home systems and virtual/augmented reality interfaces. These diverse application possibilities highlight the technology's significant potential to bridge the gap between wearable electronics and practical real-world implementations.

Future research should pursue three avenues to advance this technology: 1) investigation of more cost-effective alternative materials to enhance economic viability, 2) comprehensive evaluation of performance under complex environmental conditions to ensure operational reliability, and 3) development of diversified product derivatives tailored to specific application scenarios. These efforts will collectively expand the practical utility of fleecy TENG fabric technology.

References

1. T. Sun, B. Feng, J. Huo, Y. Xiao, W. Wang, J. Peng, Z. Li, C. Du, W. Wang, G. Zou, L. Liu, Artificial intelligence meets flexible sensors: emerging smart flexible sensing systems driven by machine learning and artificial synapses, *Nanomicro Lett.* 16 (2024) 14.
2. W.D. Li, K. Ke, J. Jia, J.H. Pu, X. Zhao, R.Y. Bao, Z.Y. Liu, L. Bai, K. Zhang, M.B. Yang, W. Yang, Recent advances in multiresponsive flexible sensors towards E-skin: a delicate design for versatile sensing, *Small*. 18 (2022) 2103734.
3. K. Zhou, K. Dai, C. Liu, C. Shen, Flexible conductive polymer composites for smart wearable strain sensors, *SmartMat*. 1 (2020) e1010.
4. M. Gong, L. Zhang, P. Wan, Polymer nanocomposite meshes for flexible electronic devices, *Prog. Polym. Sci.* 107 (2020) 101279.
5. J. Ouyang, Application of intrinsically conducting polymers in flexible electronics, *SmartMat*. 2 (2021) 263-285.
6. P. Lu, X. Liao, X. Guo, C. Cai, Y. Liu, M. Chi, G. Du, Z. Wei, X. Meng, S. Nie, Gel-Based Triboelectric Nanogenerators for Flexible Sensing: Principles, Properties, and Applications, *Nanomicro Lett.* 16 (2024) 1-47.
7. K.X. Hou, S.P. Zhao, D.P. Wang, P.C. Zhao, C.H. Li, J.L. Zuo, A puncture-resistant and self-healing conductive gel for multifunctional electronic skin, *Adv. Funct. Mater.* 31 (2021) 2107006.
8. F. Pinelli, L. Magagnin, F. Rossi, Progress in hydrogels for sensing applications: A review, *Mater. Today Chem.* 17 (2020) 100317.
9. G.M.N. Islam, A. Ali, S. Collie, Textile sensors for wearable applications: A comprehensive review, *Cellulose*. 27 (2020) 6103-6131.
10. X. Liu, J. Miao, Q. Fan, W. Zhang, X. Zuo, M. Tian, S. Zhu, X. Zhang, L. Qu, Recent progress on smart fiber and textile based wearable strain sensors: materials, fabrications and applications, *Adv. Fiber Mater.* 4 (2022) 361-389.
11. Z. Gao, X. Xiao, A.D. Carlo, J. Yin, Y. Wang, L. Huang, J. Tang, J. Chen, *Advances*

- in wearable strain sensors based on electrospun fibers, *Adv. Funct. Mater.* 33 (2023) 2214265.
12. K. Dong, X. Peng, R. Cheng, C. Ning, Y. Jiang, Y. Zhang, Z.L. Wang, Advances in high-performance autonomous energy and self-powered sensing textiles with novel 3D fabric structures, *Adv. Mater.* 34 (2022) 2109355.
 13. Y. Luo, C. Liu, Y.J. Lee, J. DelPreto, K. Wu, M. Foshey, D. Rus, T. Palacios, Y. Li, A. Torralba, W. Matusik, Adaptive tactile interaction transfer via digitally embroidered smart gloves, *Nat. Commun.* 15 (2024) 868.
 14. C. Fan, Y. Liu, Y. Zhang, A Universal, Highly Sensitive and Seamlessly Integratable Textile Resistive Strain Sensor, *Adv. Fiber Mater.* 6 (2024) 1152-1161.
 15. S. Honda, Q. Zhu, S. Satoh, T. Arie, S. Akita, K. Takei, Textile-based flexible tactile force sensor sheet, *Adv. Funct. Mater.* 29 (2019) 1807957.
 16. C. Jiang, C.L. Lai, B. Xu, M.Y. So, Z. Li, Fabric-rebound triboelectric nanogenerators with loops and layered structures for energy harvesting and intelligent wireless monitoring of human motions, *Nano Energy.* 93 (2022) 106807.
 17. Z. Zhou, S. Padgett, Z. Cai, G. Conta, Y. Wu, Q. He, S. Zhang, C. Sun, J. Liu, E. Fan, K. Meng, Z. Lin, C. Uy, J. Yang, J. Chen, Single-layered ultra-soft washable smart textiles for all-around ballistocardiograph, respiration, and posture monitoring during sleep, *Biosens. Bioelectron.* 155 (2020) 112064.
 18. Z. Lin, J. Yang, X. Li, Y. Wu, W. Wei, J. Liu, J. Chen, J. Yang, Large-scale and washable smart textiles based on triboelectric nanogenerator arrays for self-powered sleeping monitoring, *Adv. Funct. Mater.* 28 (2018) 1704112.
 19. Y. Wang, J. Hao, Z. Huang, G. Zheng, K. Dai, C. Liu, C. Shen, Flexible electrically resistive-type strain sensors based on reduced graphene oxide-decorated electrospun polymer fibrous mats for human motion monitoring, *Carbon.* 126 (2018) 360-371.
 20. J. Lee, S. Shin, S. Lee, J. Song, S. Kang, H. Han, S. Kim, S. Kim, J. Seo, D. Kim, T. Lee, Highly sensitive multifilament fiber strain sensors with ultrabroad sensing range for textile electronics, *ACS nano.* 12 (2018) 4259-4268.

21. F. Huang, J. Hu, X. Yan, A wide-linear-range and low-hysteresis resistive strain sensor made of double-threaded conductive yarn for human movement detection, *J. Mater. Sci. Technol.* 172 (2024) 202-212.
22. L. Chen, M. Lu, H. Yang, J.R.S. Avila, B. Shi, L. Ren, G. Wei, X. Liu, W. Yin, Textile-based capacitive sensor for physical rehabilitation via surface topological modification, *ACS nano.* 14 (2020) 8191-8201.
23. Q. Zhang, Y.L. Wang, Y. Xia, P.F. Zhang, T.V. Kirk, X.D. Chen, Textile-only capacitive sensors for facile fabric integration without compromise of wearability, *Adv. Mater. Technol.* 4 (2019) 1900485.
24. P. Kateb, A. Fornaciari, C. Ahmadizadeh, A. Shokurov, F. Cicoira, C. Menon, High-Performance Textile-Based Capacitive Strain Sensors via Enhanced Vapor Phase Polymerization of Pyrrole and Their Application to Machine Learning-Assisted Hand Gesture Recognition, *Adv. Intell. Syst.* (2024) 2400292.
25. W. Wang, A. Yu, J. Zhai, Z.L. Wang, Recent progress of functional fiber and textile triboelectric nanogenerators: towards electricity power generation and intelligent sensing, *Adv. Fiber Mater.* 3 (2021) 394-412.
26. Y. Fang, Y. Zou, J. Xu, G. Chen, Y. Zhou, W. Deng, X. Zhao, M. Roustaei, T.K. Hsiai, J. Chen, Ambulatory cardiovascular monitoring via a machine-learning-assisted textile triboelectric sensor, *Adv. Mater.* 33 (2021) 2104178.
27. H. Jiao, X. Lin, Y. Xiong, J. Han, Y. Liu, J. Yang, S. Wu, T. Jiang, Z.L. Wang, Q. Sun, Thermal insulating textile based triboelectric nanogenerator for outdoor wearable sensing and interaction, *Nano Energy.* 120 (2024) 109134.
28. S. Ahn, Y. Cho, S. Park, J. Kim, J. Sun, D. Ahn, M. Lee, D. Kim, T. Kim, H. Shin, J.J. Park, Wearable multimode sensors with amplified piezoelectricity due to the multi local strain using 3D textile structure for detecting human body signals, *Nano Energy.* 74 (2020) 104932.
29. Y. Wu, Y. Ma, H. Zheng, S. Ramakrishna, Piezoelectric materials for flexible and wearable electronics: A review, *Mater. Des.* 211 (2021) 110164.
30. Z. Feng, Z. Zhao, Y. Liu, Y. Liu, X. Cao, D.G. Yu, K. Wang, Piezoelectric effect

- polyvinylidene fluoride (PVDF): from energy harvester to smart skin and electronic textiles, *Adv. Mater. Technol.* 8 (2023) 2300021.
31. A. Rashid, U. Zubair, M. Ashraf, A. Javid, H.A. Abid, S. Akram, Flexible piezoelectric coatings on textiles for energy harvesting and autonomous sensing applications: a review, *J Coat Technol Res.* 20 (2023) 141-172.
 32. Z. Ouyang, D. Xu, H.Y. Yu, S. Li, Y. Song, K.C. Tam, Novel ultrasonic-coating technology to design robust, highly sensitive and wearable textile sensors with conductive nanocelluloses, *Chem. Eng. J.* 428 (2022) 131289.
 33. N. Yang, X. Yin, H. Liu, X. Yan, X. Zhou, F. Wang, X. Zhang, Y. Zhao, T. Cheng, Dual-Layer All-Textile Flexible Pressure Sensor Coupled by Silver Nanowires with Ti3C2-Mxene for Monitoring Athletic Motion during Sports and Transmitting Information, *ACS Appl. Mater. Interfaces.* 15 (2023) 42992-43002.
 34. Y. Zhao, L. Liu, Z. Li, F. Wang, X. Chen, J. Liu, C. Song, J. Yao, Facile fabrication of highly sensitive and durable cotton fabric-based pressure sensors for motion and pulse monitoring, *J. Mater. Chem. C.* 9 (2021) 12605-12614.
 35. T.L. Andrew, L. Zhang, N. Cheng, M. Baima, J.J. Kim, L. Allison, S. Hoxie, Melding vapor-phase organic chemistry and textile manufacturing to produce wearable electronics, *Acc. Chem. Res.* 51 (2018) 850-859.
 36. M. Clevenger, H. Kim, H.W. Song, K. No, S. Lee, Binder-free printed PEDOT wearable sensors on everyday fabrics using oxidative chemical vapor deposition, *Sci. Adv.* 7 (2021) eabj8958.
 37. B. Ju, I. Kim, B.M. Li, C.G. Knowles, A. Mills, L. Grace, J.S. Jur, Inkjet printed textile force sensitive resistors for wearable and healthcare devices, *Adv. Healthc. Mater.* 10 (2021) 2100893.
 38. X. Wang, M. Zhang, L. Zhang, J. Xu, X. Xiao, X. Zhang, Inkjet-printed flexible sensors: From function materials, manufacture process, and applications perspective, *Mater. Today Commun.* 31 (2022) 103263.
 39. J. Peng, B. Wang, H. Cheng, R. Yang, Y. Yin, S. Xu, C. Wang, Highly sensitive and superhydrophobic fabric sensor based on AgNPs/Polypyrrole composite conductive

- networks for body movement monitoring, *Compos Sci Technol.* 227 (2022) 109561.
40. A.M. Eagleton, M. Ko, R.M. Stolz, N. Vereshchuk, Z. Meng, L. Mendecki, A.M. Levenson, C. Huang, K.C. MacVeagh, A. Mahdavi-Shakib, J.J. Mahle, G.W. Peterson, B.G. Frederick, K.A. Mirica, Fabrication of multifunctional electronic textiles using oxidative restructuring of copper into a Cu-based metal–organic framework, *J. Am. Chem. Soc.* 144 (2022) 23297-23312.
 41. Y. Wu, X. Dai, Z. Sun, S. Zhu, L. Xiong, Q. Liang, M.C. Wong, L.B. Huang, Q. Qin, J. Hao, Highly integrated, scalable manufacturing and stretchable conductive core/shell fibers for strain sensing and self-powered smart textiles, *Nano Energy.* 98 (2022) 107240.
 42. R. Wu, S. Seo, L. Ma, J. Bae, T. Kim, Full-fiber auxetic-interlaced yarn sensor for sign-language translation glove assisted by artificial neural network, *Nanomicro Lett.* 14 (2022) 139.
 43. D. Xu, Y. Liu, C. Ge, C. Gao, Z. Chen, Z. Su, H. Gong, W. Xu, J. Fang, Chemical Resistant Yarn with Hierarchical Core–Shell Structure for Safety Monitoring and Tunable Thermal Management in High-Risk Environments, *Engineering.* 32 (2024) 217-225.
 44. Y. Shen, C. Chen, L. Chen, L. Shang, T. Wang, K. Wang, Y. Zhao, R. Hou, H. Cong, G. Jiang, A. Zhang, P. Ma, Z.L. Wang, Mass-production of biomimetic fur knitted triboelectric fabric for smart home and healthcare, *Nano Energy.* 125 (2024) 109510.

Chapter 5: Highly Stretchable and Structurally Stable Auxetic Braided Yarn based Sensor for Motion Monitoring

5.1 Introduction

Flexible and stretchable strain sensors are essential components in the development of smart wearables. Strain sensors include resistive sensors [1-5], capacitive sensors [6-8], piezoelectric sensors [9-12], and triboelectric sensors [13-15]. Among them, yarn-based ones have garnered attention for their uncomplicated design, ease of manufacturing, and exceptional flexibility [16]. These sensors can be integrated into various textile products, such as clothing, using physical methods like sewing, pasting, and seamless insertion, without compromising the comfort of the product. Consequently, they hold great promise for applications in sports and health monitoring, human-computer interaction, robotics, and other fields.

A strain yarn sensor usually consists of a highly elastic linear substrate and a conductive material. Various structures are employed in yarn sensors, including mosaic [17,18], core-shell [19-21], helical [22-24], and braided structures [5,25]. In the mosaic structure, conductive materials are embedded within the elastic substrate, commonly with carbon-based nanoparticles and metal nanoparticles commonly utilized as conductive particles to achieve an exceptionally high sensing threshold [17,18]. However, nanoparticles may experience peeling and detachment through repeated mechanical friction and washing during daily use. The core-shell structure is formed by coaxially extending two or more materials in a fully covered form. Typically, either the core or shell layer exhibits high elasticity to facilitate tensile deformation, while the other layer serves as an electrical conductor, providing a responsive change in resistance. Nevertheless, the extrusion of core-shell filaments from the nozzle necessitates precise spinning solution ratios, making the preparation process cumbersome [20]. Another approach for core-shell yarn sensors involves coating the surface of highly elastic core yarns with

conductive materials such as ink [21], metals [26], and conductive polymers [27] using various electrochemical techniques. Microscopic cracks in the conductive coating occur during stretching, resulting in resistance changes. This unpredictable and disruptive working mechanism renders the sensing yarns unstable for prolonged use. Helical yarn sensors, created through winding or twisting methods, offer effective protection for the conductive components against damage caused by direct stretching and coaxial forces [24,28-31]. Additionally, auxetic helical yarn sensors exhibit enhanced sensitivity to small changes due to their relatively larger force-sensitive deformations. This characteristic makes them a promising choice for accurate and precise sensing in demanding applications such as high tensile strain sensing and motion monitoring [32-34]. For instance, a strain-sensitive optical fiber with a negative Poisson's ratio has been developed by interlocking two silver-coated nylon yarns in opposite directions onto a core-spun polyurethane elastic yarn [33]. During the stretching process, the torsional expansion of the core yarn increases the contact change between the two conductive yarns, resulting in high strain sensitivity and fast response [33]. Furthermore, a capacitive auxetic yarn sensor has surpassed the sensitivity limit of traditional capacitive sensors. This breakthrough is achieved by leveraging the auxetic effect, which leads to a greater increase in the electrode area relative to the applied strain. However, despite the potential of auxetic yarn sensors, there are still several challenges that need to be addressed. Firstly, the stability of auxetic yarn sensors with only one or two winding yarns is not sufficient when subjected to multiple stretches. The slip effect can cause uneven and loose spirals, thereby affecting the overall performance of the auxetic yarn sensor. Secondly, the elastic durability of the sensor, which refers to its ability to recover elasticity after undergoing tens of thousands of stretches, remains a significant concern. Lastly, seamless integration of sensors into textile products has not yet been achieved, with current methods relying on pasting or sewing techniques [32, 33]. Braided structures offer superior stability compared to other configurations due to the inclusion of multiple sets of interlaced wrapped yarns. However, these structures have certain limitations, including restricted stretchability and increased thickness

resulting from the presence of multiple wraps.

To tackle these challenges, we initially developed an innovative auxetic braided strain yarn sensor (ABSYS) that merges the benefits of auxetic helical and braided structures. The ABSYS is characterized by its reliable structural stability, extensive stretch range, durability, and seamless integration capabilities. A specially designed braided high-elastic interlaced covering layer maintains structural stability throughout multiple stretch-recovery cycles without affecting the sensor's resistive sensing performance. Subsequently, we created a performance-optimized sensing fabric by seamlessly incorporating ABSYS into ribbed fabrics using knitted weft inlay technology. The fabric strain sensor exhibits a notable wide sensing range of 2% to 60%, coupled with a rapid response time of 0.018 s, reliable stability, and high comfort. The sensor has been successfully integrated into finger and elbow sleeves to effectively capture the movements of finger and elbow joints, underscoring its potential in motion monitoring applications.

5.2 Experimental Section

5.2.1 Materials

280D Ag-plated nylon yarn was obtained from Qingdao Tianyin Textile Technology Co., Ltd., China. High elastic nylon/spandex yarn (30D) was purchased from Zhuji Mingyun Chemical Fiber Co., Ltd., China. Core-spun elastic yarns (0.8 mm, 1 mm, 1.2 mm, and 1.5 mm) were bought from Min Shang Xiang Zhi Yuan Store, China. 420D elastic nylon yarn was bought from Dongguan Dalang Chen Shengli Yarn Shop, China.

5.2.2 Fabrication methods

The fabrication process began with the preparation of auxetic sensing yarn (ABSYS),

which was produced on an industrial 16-spindle circular braiding machine. To ensure continuous machine operation, the tension control components for the high-elastic wrap yarn were replaced with lighter 3D-printed parts. Subsequently, the knitted sensor fabric was manufactured using a manual flat knitting machine with a gauge of 7. The fabric's base structure consisted of a rib knit formed with 420D elastic nylon yarn, into which the ABSYS was strategically incorporated through weft inlay technology. This integration resulted in a highly elastic sensor fabric.

5.2.3 Characterization and testing

Enlarged photos of different yarn materials and ABSYSs under various tensile strains were taken using a Leica microscope (M165 C). Tensile tests were completed on the Instron 5566 Universal Testing Machine. And an LCR digital bridge (TH2830) was employed to test the resistance change.

5.3 Results and Discussion

5.3.1 Structure design and working mechanism of the ABSYS

As shown in Figure 5.1a, the designed ABSYS structure comprises three components: a thick elastic core yarn, a conductive multifilament, and a braided layer formed with multiple fine elastic wrap yarns. The elastic core yarn provides good stretch and recovery properties and requires sufficient elastic stability. The conductive multifilament spirally wound around the core yarn is responsible for resistance sensing and requires good conductivity and relative rigidity to form a tensile expansion effect. The elastic wrap yarn is mainly used for fixation, improving structural stability, and enhancing the tensile recovery ability of the sensor without restricting deformation behavior, requiring good elasticity and low modulus. The sensing mechanism of the structure lies in the electric resistance changes due to the extruded contact changes

among the conductive monofilaments during the first stage of deformation when they are stretched from a helical shape to a straight form (Figure 5.1b) and the changes in length and cross-sectional area during the second stage of deformation when the conductive monofilaments are extended (Figure 5.1c). Compared with existing helical yarn sensors, the most significant innovation of this structure is the addition of a braided layer formed with elastic wrap yarns. By interlocking with the conductive multifilament, the elastic wrap yarns can avoid undesired slippage of the conductive multifilament along the core yarn, which can considerably enhance the stability of the yarn sensor structure. The ABSYS has several improvements compared with nonauxetic yarn sensors. First, in applications such as joint activity monitoring, the expanded elastic yarns can minimize stress concentration on the sensing fibers, ensuring better wearing comfort. Second, the unique deformation mechanism of auxetic yarns allows for a wider sensing strain range and higher sensitivity. Furthermore, the full-fiber structure makes the sensor soft enough to be seamlessly embedded in clothing and the preparation process simple enough to achieve large-scale production.

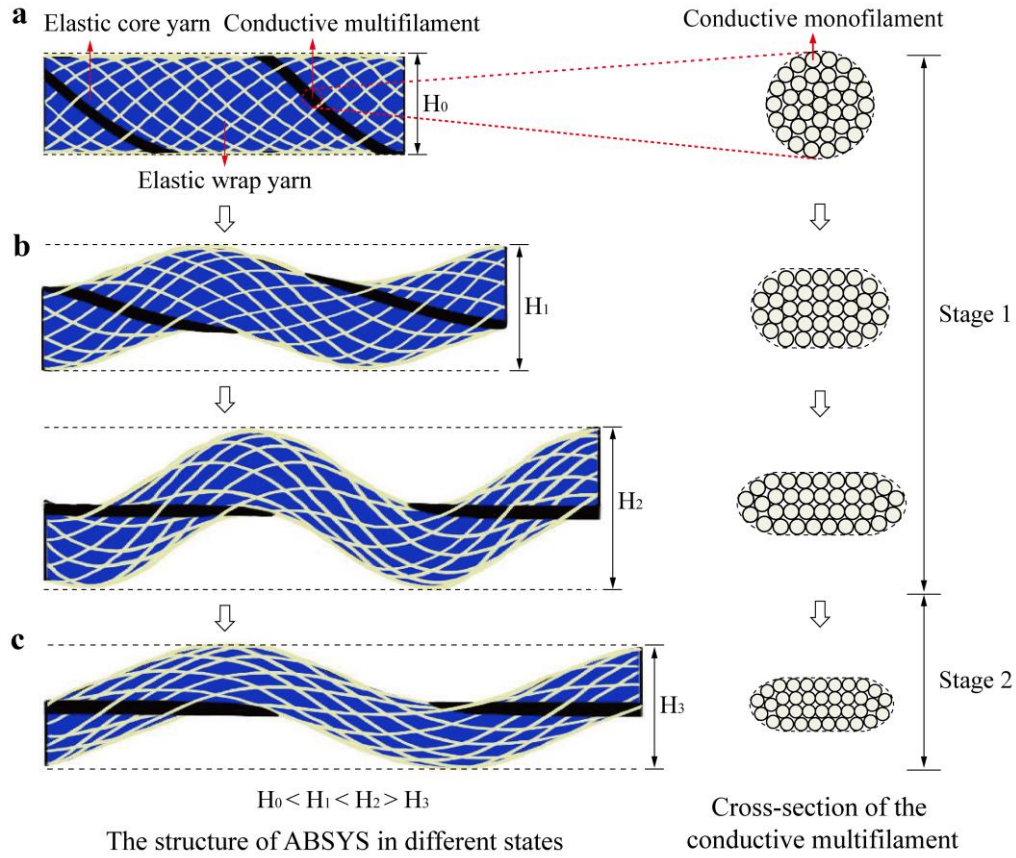


Figure 5.1 Structure of the ABSYS and cross-section of the conductive multifilament: (a) at the initial state; (b) under extrusion in the first stage; (c) under extension in the second stage.

5.3.2 Fabrication of the ABSYS

As shown in Figure 5.2a, a circular braiding machine was employed to fabricate various ABSYS samples with different structural parameters and raw material properties. The elastic core yarn was erected in the middle of the platform and the conductive multifilament and multiple elastic wrap yarns were placed on the spindles of the disc with bobbins. Due to the low modulus of the elastic wrap yarn, the industrial steel tension device could not be adjusted to a suitable small tension. PLA tension devices were specially manufactured by 3D printing to provide suitable and uniform tension for the elastic wrap yarns during the braiding process. The operational mechanism of the braiding machine is illustrated in Figure 5.2b, using a 16-spindle configuration as an

example. The process begins with the elastic core yarn being threaded through a central circular aperture on the braiding machine platform. A simple tension disk is employed to apply tension to the core yarn, ensuring it remains straight. Two sets of yarn bobbins, equal in number but moving in opposite directions—one set moves clockwise, while the other moves counterclockwise—are placed on the spindles and follow a wavy circular path along the spindle track. Among the sixteen bobbins, one is wound with conductive multifilament, while the rest are wound with elastic wrap yarn. As the two sets of yarn bobbins move along the track, the sixteen peripheral yarns interlace with each other and merge with the core yarn along the platform's central axis. This intricate interweaving process results in the formation of the final braided yarn. Subsequently, the braided yarn is collected by a collection device.

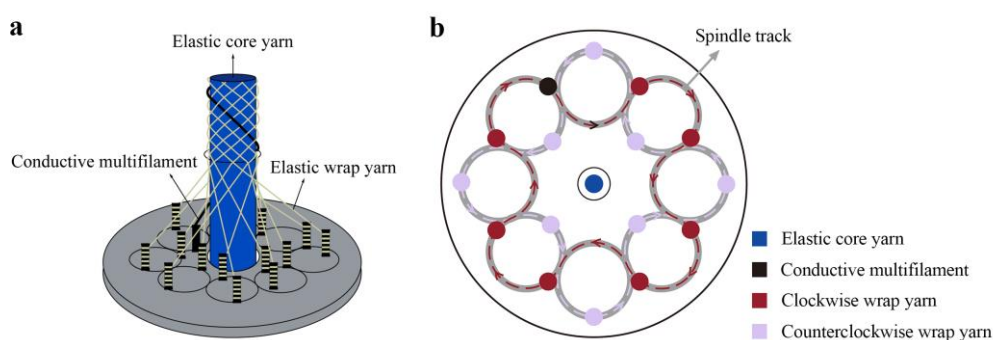

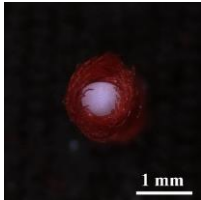

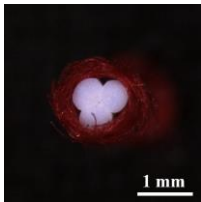
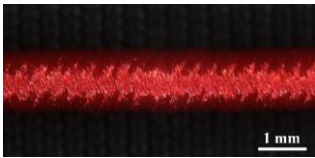
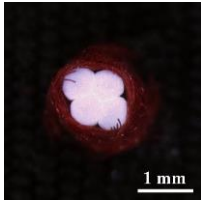
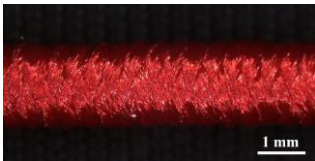
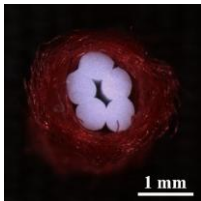
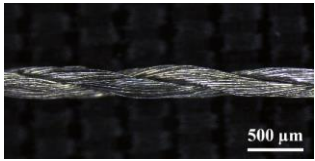
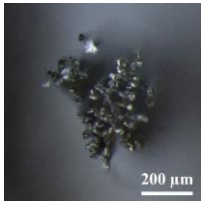
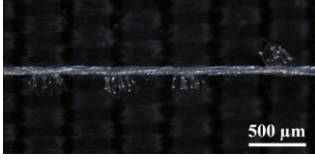


Figure 5.2 Fabrication process of the ABSYS. (a) Yarn configuration on the circular braiding machine. (b) Schematic diagram of the mechanism responsible for forming the braided structure.

To prepare the ABSYS samples, four core yarns of varying diameters, one conductive multifilament, and one wrap yarn were utilized. Table 5.1 details the specific specifications of these yarn materials. The elastic core yarn used is polyester-latex covered yarn available in four diameters: 0.8 mm, 1 mm, 1.2 mm, and 1.5 mm. Cross-sectional photos show that they contain different numbers of latex cores, specifically 1, 3, 4, and 5, respectively. The conductive multifilament employed is 280D Ag-plated nylon multifilament, created by twisting two strands of multifilaments composed of multiple Ag-plated nylon monofilaments together (each strand has a measured diameter

of approximately 195 μm). This commercially prevalent multifilament is noted for its low toxicity and excellent conductivity, with a resistivity of approximately 2 Ω/cm . The elastic wrap yarn is 30D nylon-spandex covered yarn with a very small diameter of about 75 μm .

Table 5.1 Details of three composing yarns.

Yarn type	Property	Code	Spec	Photograph	
				Side view	Cross section
Elastic core yarn	Polyester-latex core-spun yarn	C 1	0.8 mm		
		C 2	1 mm		
		C 3	1.2 mm		
		C 4	1.5 mm		
Conductive multifilament	Ag-plated nylon multifilament	Ag	280 D		
Elastic wrap yarn	Nylon-spandex covered yarn	W	30 D		-

The tensile properties of the three component yarns were evaluated, with their stress-

strain curves depicted in Figure 5.3. The elastic moduli of the core yarns, measured at 1% strain, were 11.60 MPa, 12.34 MPa, 10.27 MPa, and 12.69 MPa, corresponding to increasing diameters. The stress of the 0.8 mm core yarn was the lowest within 50% strain but then increased rapidly, surpassing the other three at 75% strain, indicating poor elastic elongation. In contrast, the core yarns of the other three diameters exhibited excellent elastic elongation, with significant stress increases occurring after approximately 100% strain. The conductive multifilament and wrap yarn exhibited elastic moduli of 882.26 MPa and 20.97 MPa, respectively. The conductive multifilament, possessing the highest elastic modulus, fractured at a tensile strain of approximately 25%. The elastic wrap yarn required the least force to stretch, yet it exhibited an intermediate tensile modulus due to its extremely small diameter. At approximately 45% strain, the outer nylon yarn began to break randomly, causing fluctuations in the curve, and it completely fractured at about 60% strain. In contrast, the conductive multifilament was relatively rigid, meeting the structural requirements for the helical auxetic yarn.

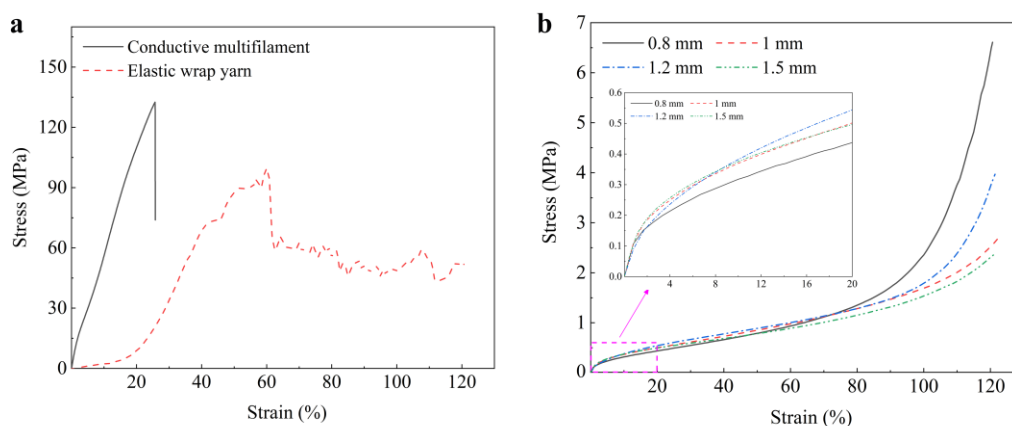

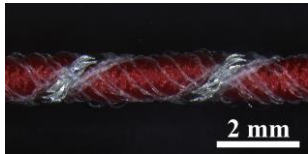
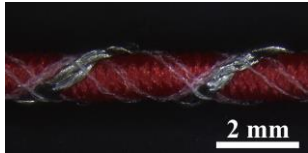
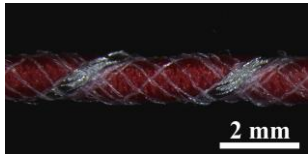




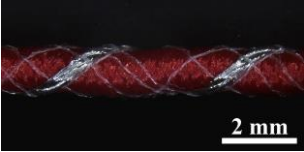
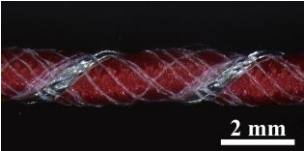
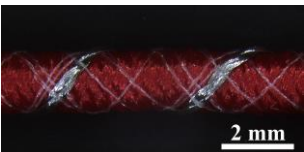
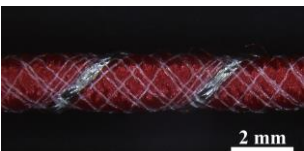
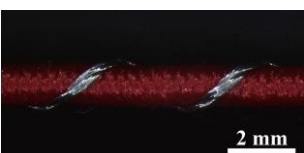
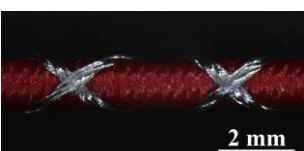
Figure 5.3 Tensile properties of three component yarns. (a) Stress-strain curves of conductive yarn and wrap yarn. (b) Stress-strain curves of elastic core yarns with different diameters.

Ten distinct ABSYS samples were prepared, as detailed in Table 5.2, with variations in material parameters including core yarn diameter, and quantities of conductive multifilament and elastic wrap yarn. Machine parameters such as core yarn tension disc

setting (spring-controlled maintain vertical of the core yarn during braiding), spindle movement speed, and collection speed were held constant. Theoretically, under these conditions, the braiding angle (the angle between the conductive multifilament and the central axis of ABSYS) will increase with larger core yarn diameters. However, variations in core yarn shrinkage post-braiding affect the braiding angle, with the significant shrinkage of C1 resulting in a larger angle. Additionally, two helical auxetic yarn samples without elastic wrap yarn, labeled H-A and H-B, were prepared for comparative analysis.

Table 5.2 Details of various ABSYS samples.

Code	Description	Braiding angle (degree)	Photograph
C 1-A	1 C 1 + 1 Ag + 7 W	50.1	
C 1-B	1 C 1 + 1 Ag + 15 W	50.1	
C 2-A	1 C 2 + 1 Ag + 7 W	39.0	
C 2-B	1 C 2 + 1 Ag + 15 W	39.0	
C 2-C	1 C 2 + 2 Ag + 6 W	39.0	
C 2-D	1 C 2 + 2 Ag + 14 W	39.0	

C 3-A	1 C 3 + 1 Ag + 7 W	39.8	
C 3-B	1 C 3 + 1 Ag + 15 W	39.8	
C 4-A	1 C 4 + 1 Ag + 7 W	50.2	
C 4-B	1 C 4 + 1 Ag + 15 W	50.2	
H-A	1 C 3 + 1 Ag	39.8	
H-B	1 C 3 + 2 Ag	39.8	

5.3.3 Auxetic performance of ABSYSs

The tensile Poisson's ratio for each sample was determined by capturing images at 5% increments of tensile strain. Figure 5.4 illustrates the changes observed in a sample during the stretching process. During tensile deformation, two concurrent phenomena were observed: progressive straightening of the rigid yarn and helical twisting of the elastic core yarn. The sample gradually exhibited visual expansion within 40% strain elongation, followed by contraction resulting from elastomeric thinning of the core yarn. Experimental results indicated that the rigid yarn became fully straightened at approximately 60% strain, suggesting that the optimal working range for ABSYS should be limited to the 0-60% strain interval in future applications. Poisson's ratio ν of the ABSYS can be determined using the following equation:

$$\nu = -\frac{(H-H_0)/H_0}{\varepsilon} \quad \text{Equation 5.1}$$

where H_0 is the initial diameter of the cross section, H is the diameter of the cross section under tensile conditions, and ε is the axial strain.

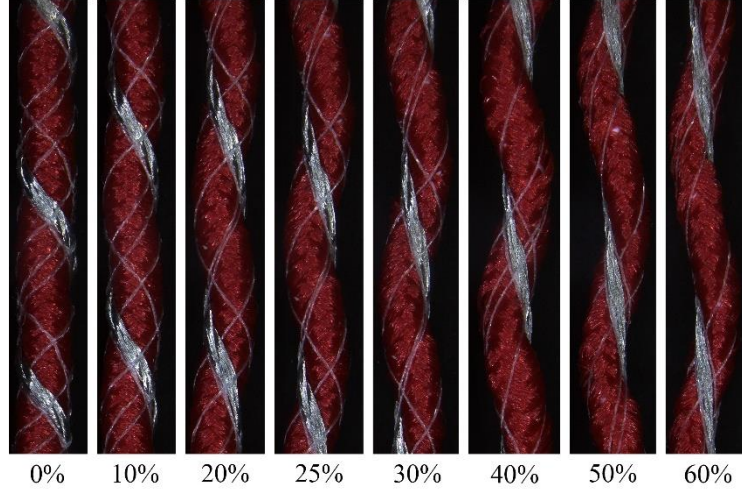


Figure 5.4 Photos of a sample at different strains during stretching.

Figure 5.5 presents the tensile Poisson's ratio of all samples across various strains. As shown in Figure 5.5a, both excessively large and small core yarn diameters adversely affected the auxetic effect. Samples with the C1 core exhibited limited auxetic capability, particularly C1-A, which demonstrated a negligible negative Poisson's ratio throughout the stretching process. This was likely because the core yarn's diameter of 0.8 mm was too thin, resulting in minimal visual expansion despite twisting. Similarly, samples with the C4 core showed a weak auxetic effect, probably due to the 1.5 mm diameter core yarn's relatively high modulus, which made it more difficult to achieve the necessary twisting for expansion compared to other core yarns. Conversely, samples with C2 and C3 cores exhibited favorable auxetic effects. Notably, C2-B and C3-A maintained a negative Poisson's ratio throughout the entire stretching process. Specifically, C2-A achieved a maximum negative Poisson's ratio of approximately -0.66 at 50% strain, C2-B reached about -0.58 at 30% strain, C3-A attained about -0.62 at 25% strain, and C3-B reached about -0.36 at 35% strain. Figure 5.5b examined the impact of the number of helical conductive yarns oriented in the same direction. C2-C

demonstrated a significantly enhanced auxetic effect, achieving a maximum negative Poisson's ratio of approximately -1.26 at 25% strain. This enhancement was likely due to the increased presence of rigid components, which facilitated easier twisting of the core yarn during stretching, resulting in greater visual expansion. However, C2-D did not exhibit a noticeable auxetic effect, possibly due to the increased number of peripheral elastic wrap yarns, which may have impeded further expansion. Additionally, the two rigid yarns reached a straightened state at about 40% strain, reducing the auxetic range of the sensing yarn. As a control, the auxetic capacity of H-A and H-B structures, which lacked the outer elastic network, was also evaluated. As depicted in Figure 5.5c, H-B, featuring outer rigid yarn crossing, demonstrated the most pronounced auxetic effect, achieving a maximum negative Poisson's ratio of approximately -1.47 at 20% strain, consistent with previous research [33].

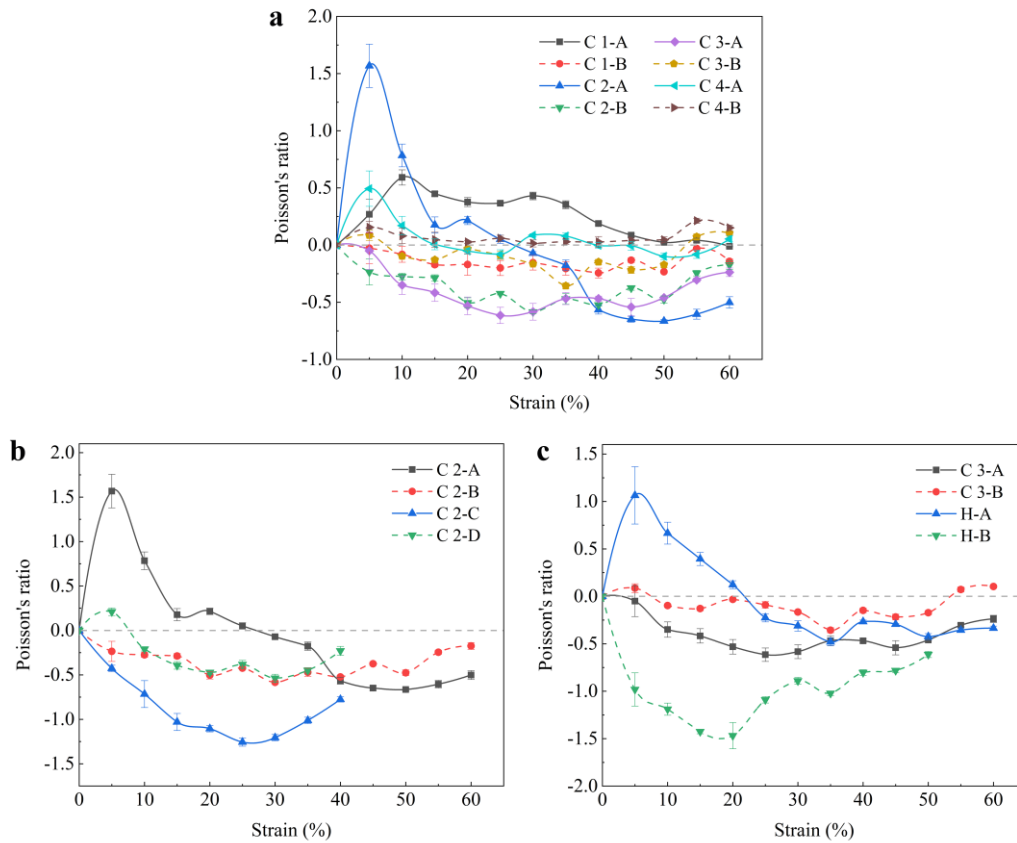


Figure 5.5 Tensile Poisson's ratio of all samples at different strains. (a) Strain-Poisson's ratio curves of ABSYS samples with one conductive yarn. (b) Comparison with ABSYS samples with two conductive yarns. (c) Comparison with samples without wrap

network.

5.3.4 Strain sensing capabilities of ABSYSs

Initially, the resistance change rate of all samples was tested over a large strain range of 60%, with the results presented in Figure 5.6. Generally, improved auxetic performance enhances sensing sensitivity. As illustrated in Figure 5.6a, the C2-B and C3-A structures, which exhibit more stable tensile negative Poisson's ratios, demonstrated more sensitive resistance change responses. Additionally, compared to structures with two conductive rigid yarns and unwrapped networks, C2-B and C3-A showed superior performance in large-range sensing. Considering both the auxetic effect and sensing performance, the C3-A structure was preferred for subsequent development of sensing fabrics and application demonstration.

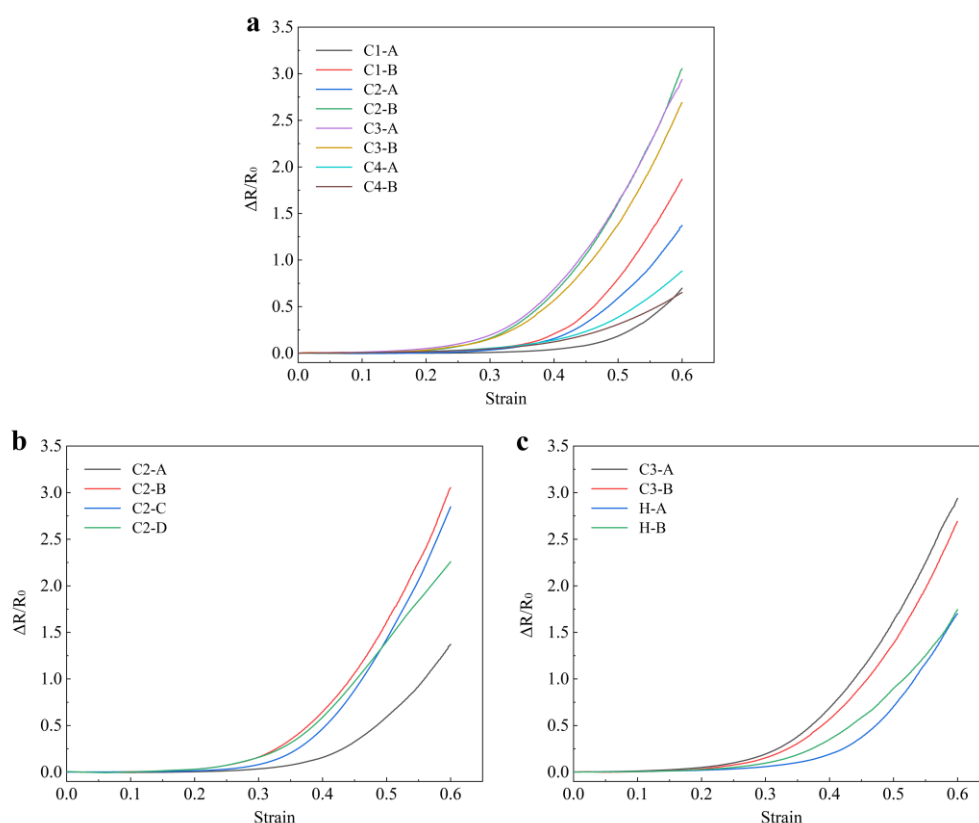


Figure 5.6 $\Delta R/R_0$ -strain curves of all samples within a large strain range of 60%. (a) ABSYS samples with one conductive yarn. (b) Comparison with ABSYS samples with

two conductive yarns. (c) Comparison with samples without wrap network.

The resistance response of C3-A under various tensile strains was evaluated. The sensitivity to tensile strain is quantified by the GF, which is defined as the ratio of the change in resistance to the applied strain ε . The formula for calculating the GF is given by:

$$GF = \frac{\Delta R/R_0}{\varepsilon} \quad \text{Equation 5.2}$$

Typically, a larger absolute value of the GF indicates a higher sensitivity of the sensor to strain. As illustrated in Figure 5.7a, C3-A demonstrated distinct average GFs across different strain ranges. Specifically, the average GFs were 0.25, 1.43, 4.97, 9.34, and 13.15 for strain ranges of 0-20%, 20-30%, 30-40%, 40-50%, and 50-60%, respectively. This indicates that the response sensitivity of C3-A increased with the strain range. And the overall average GF within the 60% strain range was about 4.90. At a cyclic stretching speed of 200 mm/min, the resistance changes of the sensing yarn under varying strains were examined. Figures 5.7b and 5.7c reveal that the sensing yarn maintained a relatively constant $\Delta R/R_0$ from a small strain of 2% to a large strain of 60%. Furthermore, the impact of stretching speed on resistance response was investigated. As depicted in Figure 5.7d, at a 40% strain, $\Delta R/R_0$ slightly increased with higher stretching speeds. This increase might be attributed to the greater elongation of C3-A due to inertia at the maximum strain value during high-speed stretching. Furthermore, it is noteworthy that during the cyclic stretching process, the baseline of the resistance versus time curve exhibits a gradual and subtle upward shift. This behavior is most likely attributable to the inherent recovery hysteresis characteristic of the elastic material. To mitigate this phenomenon and enhance the practical applicability of ABSYS, it will be integrated into the fabric through knitting technology to make a fabric sensor.

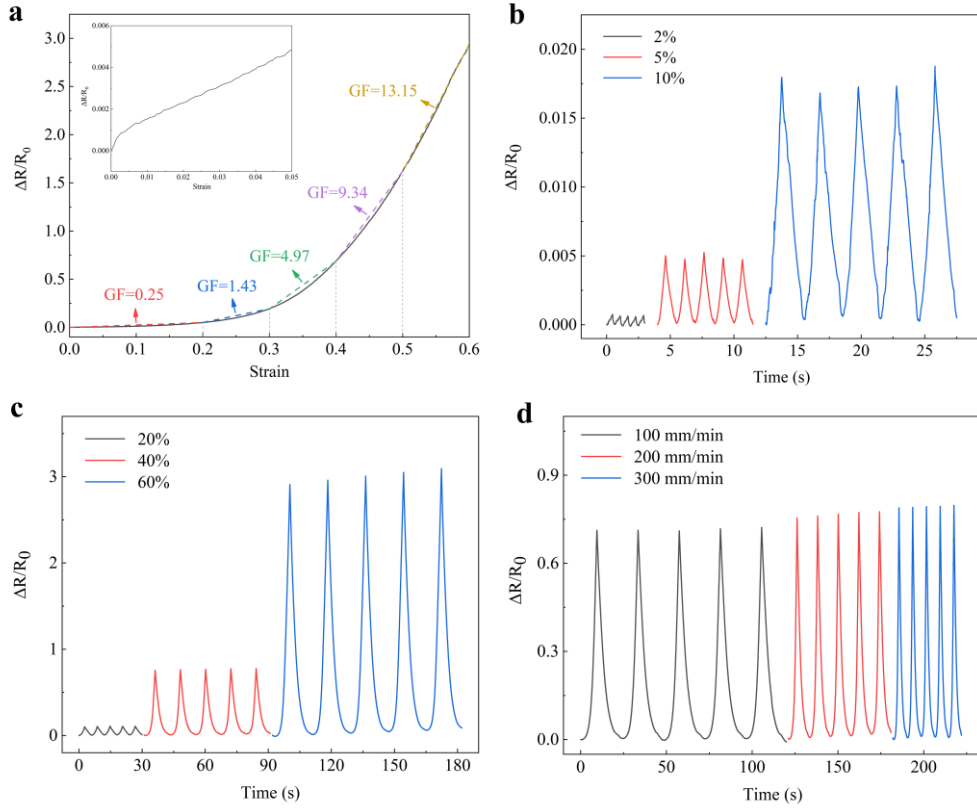


Figure 5.7 Sensing Performance of the C3-A Sample. (a) Gauge factor at different strains. (b) $\Delta R/R_0$ -time curves at 2%, 5%, 10% strains with 200 mm/min tensile speed. (c) $\Delta R/R_0$ -time curves at 20%, 40%, 60% strains with 200 mm/min tensile speed. (d) $\Delta R/R_0$ -time curves at different tensile speeds with 40% strain.

5.3.5 Fabrication and characterization of ABSYS-based knitted sensors

Fabric sensors with seamless ABSYS embedding were developed using weft inlay technology on a hand-operated knitting machine. The support structure was a 1×1 rib stitch composed of high-elastic nylon yarn, into which ABSYS (C3-A) was linearly inserted within the rib's interlayer to form a highly elastic fabric sensor. The ABSYS insertion measured 5 cm in length, while the fabric width was 3.3 cm, as shown in Figure 5.8a. The sensitivity and resistance changes of the fabric sensor were evaluated under various strains (Figure 5.8b and c). When exploring the minimum detection limit, it was found that the sensing signal within the small strain range of 1% showed fluctuations, which was problematic for accurate strain sensing. Consequently, the

effective sensing range of the fabric sensor was determined to be 2%-60% strain, which is sufficient for joint motion monitoring. Similar to ABSYS, the sensitivity of the fabric increased with strain. However, its overall sensitivity was lower than that of the yarn sensor. The fabric exhibited an average GF of approximately 2.06 within the 60% strain range. The integration of an elastic fabric substrate contributed to the decrease in sensitivity, which can be primarily attributed to two factors. Firstly, the insulated nylon yarn in close contact with the ABSYS increased the overall contact resistance. Since the resistance change originated solely from the sensing yarn, this led to a lower overall resistance change rate. Secondly, the compression of ABSYS by the elastic fabric substrate may have impeded the contact changes among the fibers within the conductive yarn.

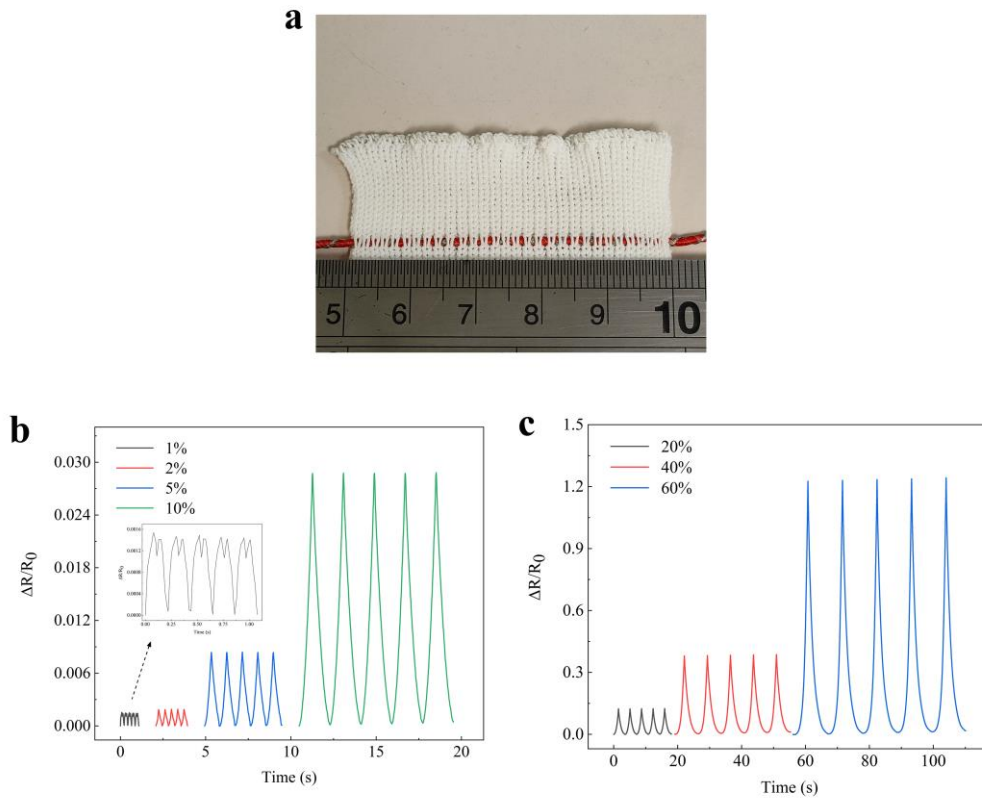


Figure 5.8 Sensing Performance of the ABSYS-based knitted sensor. (a) Photograph of the knitted sensor. (b) $\Delta R/R_0$ -time curves for the knitted sensor under strain levels of 1%, 2%, 5%, and 10% at a tensile speed of 200 mm/min. (c) $\Delta R/R_0$ -time curves for the knitted sensor under strain levels of 20%, 40%, and 60% at a tensile speed of 200

mm/min.

A notable advantage was that the inclusion of the elastic fabric substrate significantly reduced the response hysteresis of the sensor, resulting in a more stable output response curve. Furthermore, the response speed to stimuli was a crucial evaluation metric. The response time was assessed by applying a small strain of 2% to the sensing fabric at a relatively rapid rate of 500 mm/min, maintaining it briefly, and then unloading it at the same rate. The loading duration was 0.072 seconds, and the resistance response curve indicated that the resistance completed its response in 0.09 seconds, yielding a response time of 0.018 seconds, which demonstrated excellent response speed (Figure 5.9).

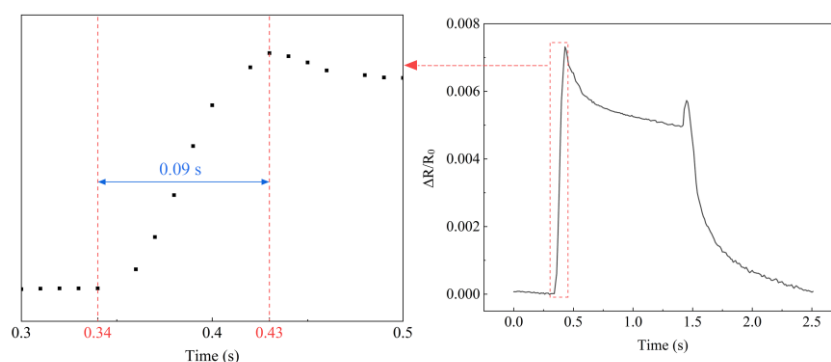


Figure 5.9 Response time measurement of the ABSYS-based knitted sensor.

The resistance change response of the sensing fabric was evaluated under both 1% small strain (Figure 5.10a) and 60% large strain (Figure 5.10b) conditions, both before and after washing. Washing did not significantly alter the sensitivity of the fabric under large strain conditions. However, it notably enhanced both the sensitivity and stability of the fabric under small strain conditions. This improvement was primarily due to the slight shrinkage of the fabric base caused by washing, which resulted in a more compact structure and more stable tensile recovery under small strain. Figure 5.10c presents the resistance response change of the sensing fabric over 3,000 cycles of 40% strain. Although $\Delta R/R_0$ exhibited a slight upward shift over time during these cycles, it generally remained within an acceptable range for motion sensing applications. Furthermore, the upward trend of the baseline tended to flatten as the number of cycles

increased.

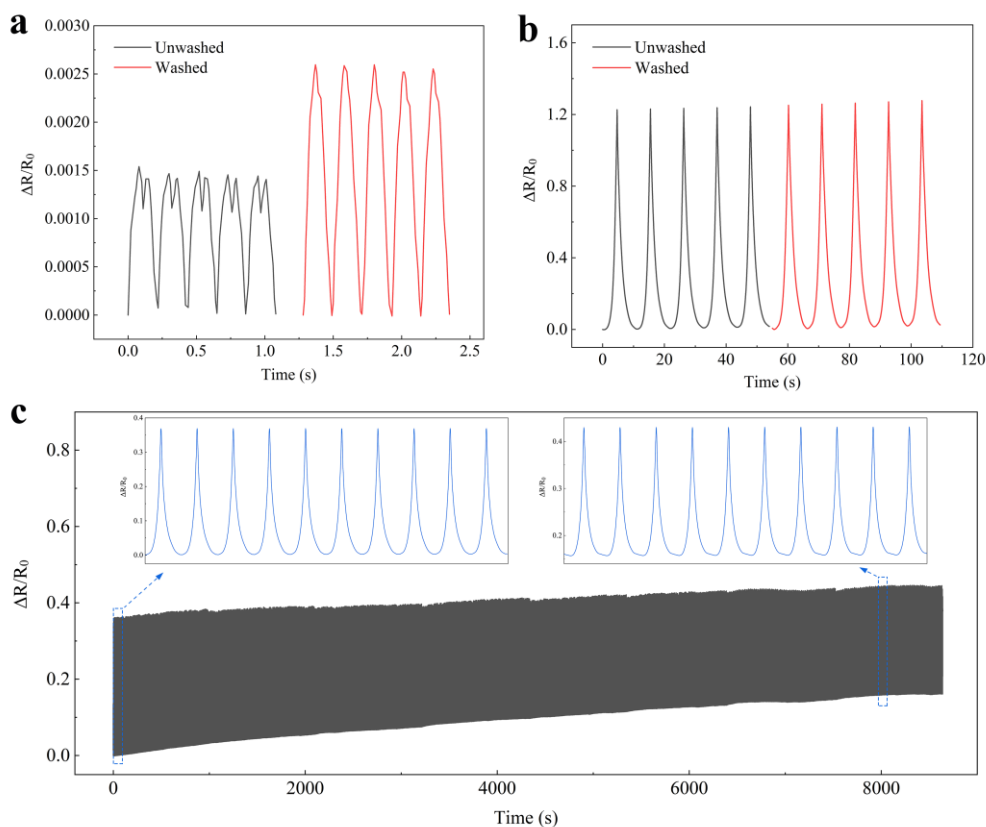


Figure 5.10 Durability of the ABSYS-based knitted sensor. (a) Comparison of the resistance response of the knitted sensor at 1% strain before and after washing. (b) Comparison of the resistance response at 60% strain before and after washing. (c) Resistance response at 40% strain over 3000 stretch-recovery cycles.

5.3.6 Application demonstration of motion monitoring

To demonstrate the feasibility of detecting various human motions, ABSYSs were seamlessly integrated into an elbow sleeve (Figure 5.11a) and a finger sleeve (Figure 5.11c) to capture responses to different gestures and movements. As demonstrated in Figure 5.11b and d, the tube fabrics produced sensitive and distinct response signals corresponding to finger and arm movements at various bending angles. Furthermore, the bending speed influenced the signal waveform, as depicted in Figure 5.11e and f. These characteristics could be utilized as capture features for motion recognition. This

kind of sensor, when applied to multiple joints and combined with deep learning algorithms, has the potential to detect a wide range of complex body movements. Furthermore, compared to traditional yarns, the auxetic structure of ABSYS applies less pressure on the skin during stretching, thereby enhancing user comfort. This sensing strategy demonstrates significant potential in the field of wearable motion monitoring.

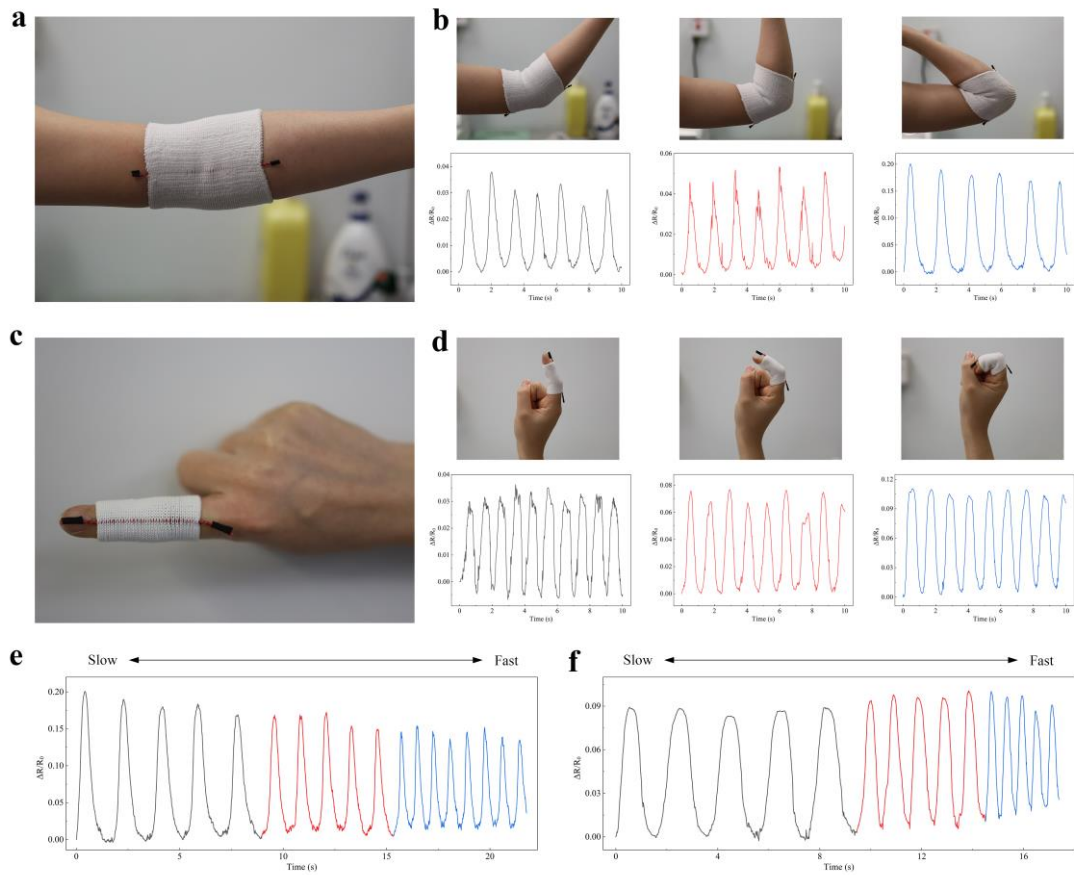


Figure 5.11 Elbow and finger sleeves responding to various joint bending movements. (a) Photograph of the elbow sleeve. (b) Resistance response signals of the elbow joint at different bending degrees. (c) Photograph of the finger sleeve. (d) Resistance response signals of the finger at different bending degrees. (e) Resistance response signals of the elbow joint at varying bending speeds. (f) Resistance response signals of the finger at varying bending speeds.

5.4 Conclusion

In summary, this study presents a novel strategy for fabricating flexible and stable strain-sensing textiles by integrating auxetic braided yarn with elastic knitted structures. The key innovation lies in the development of an auxetic braided sensing yarn manufactured via circular braiding technology, which exhibits a distinct negative Poisson's ratio and exceptional structural stability. Leveraging this yarn, a highly elastic knitted sensor was fabricated using weft inlay technology, demonstrating a broad working strain range (2%-60%), rapid response time (0.018 s), and reliable cyclic stability-critical attributes for practical wearable applications. The sensor's performance was further validated through human joint and motion detection, confirming its high sensitivity and durability under dynamic conditions. Moreover, the fabric's seamless integration into clothing minimizes aesthetic and comfort compromises, offering a significant advantage over conventional rigid or bulky sensing devices.

Despite these advancements, several limitations warrant further investigation. First, the current material selection limited to specific conductive multifilament and elastic yarns could be expanded to explore alternative functional materials (e.g., conductive polymers or hybrid nanocomposites) to enhance sensing performance and multifunctionality. Second, while the sensor achieves a high gauge factor, its nonlinear response may complicate signal interpretation in precision-demanding applications; future work should optimize the braiding architecture or material combinations to linearize the electromechanical response. Finally, although the sensor excels in joint motion monitoring, its potential in broader applications, such as smart textiles for healthcare (e.g., respiratory monitoring or posture correction) and human-machine interfaces remains underexplored and warrants systematic investigation.

References

1. A. Qiu, P. Li, Z. Yang, Y. Yao, I. Lee, J. Ma, A path beyond metal and silicon: polymer/nanomaterial composites for stretchable strain sensors, *Adv. Funct. Mater.* 29 (2019) 1806306.
2. Z. Shen, Z. Zhang, N. Zhang, J. Li, P. Zhou, F. Hu, Y. Rong, B. Lu, G. Gu, High-stretchability, ultralow-hysteresis conducting polymer hydrogel strain sensors for soft machines, *Adv. Mater.* 34 (2022) 2203650.
3. Z. Yang, Y. Pang, X. Han, Y. Yang, J. Ling, M. Jian, Y. Zhang, Y. Yang, T.L. Ren, Graphene textile strain sensor with negative resistance variation for human motion detection, *ACS nano.* 12 (2018) 9134-9141.
4. D. Lu, S. Liao, Y. Chu, Y. Cai, Q. Wei, K. Chen, Q. Wang, Highly durable and fast response fabric strain sensor for movement monitoring under extreme conditions, *Adv. Fiber Mater.* 5 (2023) 223-234.
5. J. Pan, M. Yang, L. Luo, A. Xu, B. Tang, D. Cheng, G. Cai, X. Wang, Stretchable and highly sensitive braided composite yarn@ polydopamine@ polypyrrole for wearable applications, *ACS Appl. Mater. Interfaces.* 11 (2019) 7338-7348.
6. J. Qin, L.J. Yin, Y.N. Hao, S.L. Zhong, D.L. Zhang, K. Bi, Y.X. Zhang, Y. Zhao, Z.M. Dang, Flexible and stretchable capacitive sensors with different microstructures, *Adv. Mater.* 33 (2021) 2008267.
7. T.J. Cuthbert, B.C. Hannigan, P. Roberjot, A.V. Shokurov, C. Menon, HACS: Helical Auxetic Yarn Capacitive Strain Sensors with Sensitivity Beyond the Theoretical Limit, *Adv. Mater.* 35 (2023) 2209321.
8. X. Hu, F. Yang, M. Wu, Y. Sui, D. Guo, M. Li, Z. Kang, J. Sun, J. Liu, A Super-Stretchable and Highly Sensitive Carbon Nanotube Capacitive Strain Sensor for Wearable Applications and Soft Robotics, *Adv. Mater. Technol.* 7 (2022) 2100769.
9. Q. Sun, W. Seung, B.J. Kim, S. Seo, S.W. Kim, J.H. Cho, Active matrix electronic skin strain sensor based on piezopotential-powered graphene transistors, *Adv. Mater.* 27 (2015) 3411-3417.

10. Y. Wu, Y. Ma, H. Zheng, S. Ramakrishna, Piezoelectric materials for flexible and wearable electronics: A review, *Mater. Des.* 211 (2021) 110164.
11. Y.G. Kim, J.H. Song, S. Hong, S.H. Ahn, Piezoelectric strain sensor with high sensitivity and high stretchability based on kirigami design cutting, *npj Flex. Electron.* 6 (2022) 52.
12. J. Ryu, J. Kim, J. Oh, S. Lim, J.Y. Sim, J.S. Jeon, K. No, S. Park, S. Hong, Intrinsically stretchable multi-functional fiber with energy harvesting and strain sensing capability, *Nano Energy.* 55 (2019) 348-353.
13. C. Ning, K. Dong, R. Cheng, J. Yi, C. Ye, X. Peng, F. Sheng, Y. Jiang, Z.L. Wang, Flexible and stretchable fiber-shaped triboelectric nanogenerators for biomechanical monitoring and human-interactive sensing, *Adv. Funct. Mater.* 31 (2021) 2006679.
14. F. Xu, X. Jin, C. Lan, Z.H. Guo, R. Zhou, H. Sun, Y. Shao, J. Meng, Y. Liu, X. Pu, 3D Arch-Structured and Machine-Knitted Triboelectric Fabrics as Self-Powered Strain Sensors of Smart Textiles, *Nano Energy.* 109 (2023) 108312.
15. T. Bu, T. Xiao, Z. Yang, G. Liu, X. Fu, J. Nie, T. Guo, Y. Pang, J. Zhao, F. Xi, C. Zhang, Z.L. Wang, Stretchable triboelectric–photonic smart skin for tactile and gesture sensing, *Adv. Mater.* 30 (2018) 1800066.
16. X. Tang, D. Cheng, J. Ran, D. Li, C. He, S. Bi, G. Cai, X. Wang, Recent advances on the fabrication methods of nanocomposite yarn-based strain sensor, *Nanotechnol. Rev.* 10 (2021) 221-236.
17. J. Lee, S. Shin, S. Lee, J. Song, S. Kang, H. Han, S.G. Kim, S. Kim, J. Seo, D.E. Kim, T. Lee, Highly sensitive multifilament fiber strain sensors with ultrabroad sensing range for textile electronics, *ACS nano.* 12 (2018) 4259-4268.
18. X. Wang, H. Sun, X. Yue, Y. Yu, G. Zheng, K. Dai, C. Liu, C. Shen, A highly stretchable carbon nanotubes/thermoplastic polyurethane fiber-shaped strain sensor with porous structure for human motion monitoring, *Compos Sci Technol.* 168 (2018) 126-132.

19. H. Wang, Z. Liu, J. Ding, X. Lepro, S. Fang, N. Jiang, N. Yuan, R. Wang, Q. Yin, W. Lv, Z. Liu, M. Zhang, R.O. Robles, K. Inoue, S. Yin, R.H. Baughman, Downsized sheath-core conducting fibers for weavable superelastic wires, biosensors, supercapacitors, and strain sensors, *Adv. Mater.* 28 (2016) 4998-5007.
20. W. Li, Y. Zhou, Y. Wang, L. Jiang, J. Ma, S. Chen, F.L. Zhou, Core-Sheath Fiber-Based Wearable Strain Sensor with High Stretchability and Sensitivity for Detecting Human Motion, *Adv. Electron. Mater.* 7 (2021) 2000865.
21. H. Souri, D. Bhattacharyya, Highly stretchable and wearable strain sensors using conductive wool yarns with controllable sensitivity, *Sens. Actuator A-Phys.* 285 (2019) 142-148.
22. J. Zhou, X. Xu, Y. Xin, G. Lubineau, Coaxial thermoplastic elastomer-wrapped carbon nanotube fibers for deformable and wearable strain sensors, *Adv. Funct. Mater.* 28 (2018) 1705591.
23. T. Yan, Y. Wu, J. Tang, Z. Pan, Highly sensitive strain sensor with wide strain range fabricated using carbonized natural wrapping yarns, *Mater. Res. Bull.* 143 (2021) 111452.
24. L. Lu, Y. Zhou, J. Pan, T. Chen, Y. Hu, G. Zheng, K. Dai, C. Liu, C. Sheng, X. Sun, H. Peng, Design of helically double-leveled gaps for stretchable fiber strain sensor with ultralow detection limit, broad sensing range, and high repeatability, *ACS Appl. Mater. Interfaces.* 11 (2019) 4345-4352.
25. S. Park, H. Choi, Y. Cho, J. Jeong, J. Sun, S. Cha, M. Choi, J. Bae, J.J. Park, Wearable strain sensors with aligned macro carbon cracks using a two-dimensional triaxial-braided fabric structure for monitoring human health, *ACS Appl. Mater. Interfaces.* 13 (2021) 22926-22934.
26. Y. Lu, J. Jiang, S. Yoon, K.S. Kim, J.H. Kim, S. Park, S.H. Kim, L. Piao, High-performance stretchable conductive composite fibers from surface-modified silver nanowires and thermoplastic polyurethane by wet spinning, *ACS Appl. Mater. Interfaces.* 10 (2018) 2093-2104.

27. W. Shi, G. Han, Y. Chang, H. Song, W. Hou, Q. Chen, Using stretchable PPy@PVA composites as a high-sensitivity strain sensor to monitor minute motion, *ACS Appl. Mater. Interfaces*. 12 (2020) 45373-45382.
28. J. Zhong, Q. Zhong, Q. Hu, N. Wu, W. Li, B. Wang, B. Hu, J. Zhou, Stretchable self-powered fiber-based strain sensor, *Adv. Funct. Mater.* 25 (2015) 1798-1803.
29. T. Yan, H. Zhou, H. Niu, H. Shao, H. Wang, Z. Pan, T. Lin, Highly sensitive detection of subtle movement using a flexible strain sensor from helically wrapped carbon yarns, *J. Mater. Chem. C*. 7 (2019) 10049-10058.
30. T. Yan, Y. Wu, J. Tang, Z. Pan, Highly sensitive strain sensor with wide strain range fabricated using carbonized natural wrapping yarns, *Mater. Res. Bull.* 143 (2021) 111452.
31. H. Li, J. Cao, J. Chen, X. Liu, Y. Shao, Z. Du, Highly sensitive MXene helical yarn/fabric tactile sensors enabling full scale movement detection of human motions, *Adv. Electron. Mater.* 8 (2022) 2100890.
32. L. Chen, C. Chen, L. Jin, H. Guo, A.C. Wang, F. Ning, Q. Xu, Z. Du, F. Wang, Z. L. Wang, Stretchable negative Poisson's ratio yarn for triboelectric nanogenerator for environmental energy harvesting and self-powered sensor, *Energy Environ. Sci.* 14 (2021) 955-964.
33. R. Wu, S. Seo, L. Ma, J. Bae, T. Kim, Full-Fiber Auxetic-Interlaced Yarn Sensor for Sign-Language Translation Glove Assisted by Artificial Neural Network, *Nanomicro Lett.* 14 (2022) 1-14.
34. T.J. Cuthbert, B.C. Hannigan, P. Roberjot, A.V. Shokurov, C. Menon, HACS: Helical Auxetic Yarn Capacitive Strain Sensors with Sensitivity Beyond the Theoretical Limit, *Adv. Mater.* 35 (2023) 2209321.

Chapter 6: Conclusions and Outlook

6.1 Conclusions

This thesis presents the development of comfortable and scalable textile sensors for motion monitoring by leveraging yarn materials, knitting structures, and textile technologies. Three distinct knit-based sensors have been developed to monitor specific human motion modes: ground motion, contact-motion, and joint motion. This study systematically evaluates the fabricated sensing fabrics through comprehensive characterization of their electrical output performance, sensing sensitivity, mechanical properties, and comfort levels. The developed fabric sensors maintain the tactile experience and comfort of conventional fabrics while exhibiting superior durability and washability. Importantly, they achieve high recognition accuracy and sensitivity in practical motion monitoring applications.

In Chapter 3, the research focuses on the development of triboelectric carpet fabrics using chenille yarns. Core-conductive chenille yarns are initially created through fancy spinning technology. These yarns are then integrated into a highly elastic 1×1 rib structure using knitting weft inlay technology, resulting in a carpet fabric with a shaggy surface. This process is fully industrializable, eliminating the need for additional pretreatment steps. The resulting carpet fabric exhibits promising triboelectric output performance, achieving a maximum power density of approximately 2942 $\mu\text{W}/\text{m}^2$ in contact-separation mode. Energy harvested can power small electronic devices through simple circuit management. Furthermore, with machine learning support, the carpet fabric is capable of behavior recognition and user identification. After training with time-current data, it successfully classifies four behaviors-slow walking, walking, jogging, and jumping-and identifies four different subjects. The fabric retains the appearance and comfort of traditional textiles, is warm, cost-effective, easy to manufacture, and demonstrates electrical stability and durability, showing significant

potential for smart home security monitoring systems.

Chapter 4 introduces triboelectric fleecy fabrics developed using three-thread fleecy knitting technology. Commercial yarn materials, including Ag-plated conductive yarn, are directly transformed into triboelectric fleecy fabrics through a one-step knitting process that is both convenient and cost-effective. This method boasts ultra-high production efficiency, with a capacity of approximately 11.53 square meters per hour. The resulting fleecy sensing fabric functions as a triboelectric nanogenerator, producing electrical signals when rubbed with cotton fabrics and achieving a peak power density of about 2446 $\mu\text{W}/\text{m}^2$. Made entirely from commercially available yarns, the fabric offers excellent flexibility, fullness, and breathability, maintaining consistent output performance even after multiple machine wash cycles. Importantly, this fabric can be freely cut and customized into self-powered flexible sensors for various applications, such as insoles and carpets for sports monitoring. Enhanced by deep learning algorithms, the fabric exhibits strong recognition capabilities, paving the way for the development of cost-effective, comfortable, and widely applicable flexible sensors, thereby expanding their potential for practical applications across different scenarios.

In Chapter 5, the study develops a sensing fabric based on auxetic sensing yarn. Auxetic strain sensing yarns are prepared using circular braiding technology. Unlike previously reported auxetic helical yarns, these yarns incorporate a highly elastic network layer, enhancing structural stability during repeated stretching cycles. The auxetic braided yarn demonstrates high sensitivity to strain, particularly large strains, achieving a maximum GF of 13.15 within the 50%-60% strain range. A highly elastic fabric sensor, seamlessly embedded with this auxetic sensing yarn, is created using knitting weft inlay technology. It exhibits high response sensitivity in the strain range of 2% to 60%, with a high response speed of 0.018s, and shows reliable stability in long-term stretching cycles. The sensor is seamlessly integrated into elbow and finger sleeves, displaying distinct resistance change responses to various joint bending activities. The sensor

maintains comfort and aesthetics while maintaining high sensitivity, providing a promising strategy for future wearable motion monitoring.

In conclusion, this study explores the feasibility of preparing flexible sensors using pure textile materials and technologies. The findings indicate that industrialized fiber/yarn materials and textile technologies, including spinning, braiding, and knitting, are well-suited for creating flexible, comfortable, and durable fabric sensors. Advanced knitting technology, in particular, enables variable fabric structures and complex yarn combinations, offering unique advantages and prospects in the development of textile sensors.

6.1 Outlook

This study utilized a range of textile technologies, with a primary focus on knitting, to successfully develop various pure textile flexible sensors for motion monitoring. The results highlight the significant potential of knitting technology in the fabrication of flexible sensors. However, the current research has certain limitations that necessitate further investigation and development. Key areas for future exploration include:

1. Diverse knitted-cased sensing fabrics: While this study developed several sensitive sensing fabrics, it primarily explored triboelectric and resistive mechanisms. The potential of knitting technology for other sensing mechanisms, such as capacitive and piezoelectric sensors, remains largely unexplored and warrants further investigation.
2. Expansion of textile raw materials: The yarn materials used in this study were relatively limited, with conductive properties primarily derived from Ag-plated fibers. The applicability of alternative conductive materials, such as carbon-based fibers, in knitting technology should be further explored. Expanding the range of raw materials will enhance the library of knitted sensors, contributing significantly to the diversified

development of flexible sensing technologies.

3. Development of Protective Strategies: To ensure reliable performance in real-world applications, future work must systematically evaluate the effects of key environmental stressors, including hygrothermal variations, particulate contamination, surface fouling, and mechanical wear. This investigation will establish optimized material design rules and protective strategies (e.g., hydrophobic coatings, self-cleaning interfaces) that enhance environmental resilience without compromising textile comfort.

4. Complexity in signal recognition: This study achieved basic action and user recognition with the support of machine learning. However, real-world signal sources are complex and often subject to interference. Achieving more accurate recognition will require larger datasets and optimized machine learning algorithms, presenting a promising avenue for future improvement.

5. Development of a comprehensive monitoring system: The study has yet to explore a complete monitoring system based on knitted sensors, which would integrate sensors, data acquisition and processing devices, data transmission modules, user interfaces, and power management systems. Numerous challenges remain in the practical application of these sensors, such as packaging methods and integration with other devices. Addressing these issues is crucial for the future commercial application of sensor fabrics.